A Study of the Material Properties of Silicone Nanocomposites Developed by Electrospinning

by

Shanshan Bian

A thesis

presented to the University of Waterloo

in fulfillment of the

thesis requirement for the degree of

Doctor of Philosophy

in

Electrical and Computer Engineering

Waterloo, Ontario, Canada, 2013

Author’s Declaration

I hereby declare that I am the sole author of this thesis. This is a true copy of the thesis, including any required final revisions, as accepted by my examiners. I understand that my thesis may be made electronically available to the public.

Abstract

The current thrust towards the compaction of electrical power equipment, resulting in increased insulation electrical stress levels, necessitates new electrical insulating materials. In the last few decades, polymeric materials that exhibit light weight, excellent mechanical properties, low cost, and some with unique non-wetting surface characteristics, have surpassed the use of the conventional porcelain and glass insulating materials. Despite these advantages, polymeric materials are incapable of withstanding the high heat from surface arcing that is instigated by the synergism of pollution, moisture, and voltage. Surface arcing results in material loss due to heat ablation and/or the electrical tracking of polymeric materials. To overcome such issues, inorganic fillers are added to the base polymers to enhance their resistance to surface discharge activities and other performances. Since their addition can significantly reduce material costs, their use is compelling.

Micron-sized fillers, here after defined as microfillers, have been used to acquire these desirable properties, but due to limitations in material processability, the further application of such fillers is limited. Consequently, nano-sized fillers, here after defined as nanofillers, have been viewed as replacements or assistant combinations to microfillers. Nanofillers are characterized by large surface areas, resulting in increased bond strengths that yield significant improvements in the various properties at fill levels well below that of microfillers. However, the primary problem of using nanofillers is their characteristic property of agglomeration due to their physical size and the forces between the fillers. Conventional mechanical mixing of nanofillers does not adequately separate the nanofillers, leading to behaviour similarly to that of microfillers. Therefore, the implementation of nanofillers is not completely effective. In chemical dispersion techniques, for example, the use of surfactants, are normally very elaborate and complicated. Due to the negative impact of agglomeration, the successful dispersion of nanofillers is pivotal in the further development of nanodielectrics for various insulation applications.

In this thesis, electrospinning is proposed and realized as a new dispersal method for nanofillers in polymeric materials. This novel technique facilitates polymeric

nanocomposites with improved properties due to the uniform distribution of fillers. Scanning electron microscopy (SEM) images and energy dispersive X-ray analysis (EDX) clearly indicate that electrospun nanocomposites demonstrate a better filler distribution than nanocomposites, produced by conventional mechanical mixing. Also electrospinning introduces the possibility of separating different nanofillers in different base polymers.

The mechanical properties: tensile strength and hardness; the electrical properties: permittivity, tracking, and erosion resistance; and the thermal properties: thermal conductivity, thermal degradation, and heat erosion resistance of electrospun nanocomposites are compared to those of conventional nanocomposites for silicone rubber and cycloaliphatic epoxy-based polymers. All the experimental studies in this thesis confirm that electrospun nanocomposites exhibit better thermal performances than the conventional composites which are attributed to the improved distribution of the nanofillers by the newly developed electrospinning process.

Also in this investigation, a two-dimensional thermal model is developed in COMSOL Multiphysics^{TM} by using the finite element method (FEM) to theoretically address the benefits of using nanofillers and the effects of filler dispersion. The model confirms that electrospun nanocomposites have much more uniform temperature distribution than conventional nanocomposites.

This thesis presents the possible mechanisms by which nanofillers improve the heat and erosion resistance of silicone rubber nanocomposites, and also addresses the possible mechanism by which electrospinning improves nanofiller dispersion.

Acknowledgements

First I would like to express my profound gratitude, and thanks to my supervisors, Professors Shesha Jayaram and Edward Cherney for their constant guidance throughout the duration of this work, continuous financial support, and invaluable advice.

I also like to thank Dr. Mario Gauthier, Dr Loong Tak Lim, and Dr. Chitral Angammana for their valuable discussion. I also extend my thanks to my friends in the high voltage engineering laboratory at the University of Waterloo: namely; Emad, Chitral, Refat, Ahmed, Saleh, Mahdi, Michael that made it a pleasant environment to work. In particular, I would like to give a special thanks to Dr. Chitral Angammana who spent a lot of time to help me at the beginning this project.

I also wish to express my appreciation to my PhD Committee (Dr. John Wen, Dr. Dayan Ban, Dr. Karim Karim, and Dr. Eric David) for their valuable suggestions and constructive comments.

Finally, my deepest gratitude goes to all the members of my family and to my friends, for their life-long love, care, and support.

The financial support provided by NSERC of Canada is also greatly appreciated.

Last but not least, I would like to thank Mrs. Gloria Rose for proofreading this thesis.

Dedication

To my beloved husband Reza,

To my dear parents

Table of Contents

List of Figures ..... **ix**
List of Tables ..... **xiii**

Chapter 1 Introduction……..**1**
1.1 Polymeric Materials in Insulation Applications……..…1
1.2 Introduction to Nanofillers…….……2
1.3 Literature Review……...5
1.3.1 Performance of Various Nanofillers…….....…5
1.3.2 Filler Dispersion……...…….....11
1.4 Electrospinning……....16
1.4.1 Electrospinning Setup……...…….…..18
1.4.2 Electrospinning of Nanofibres with Nanofillers…….....18
1.5 Objective and Organization of the Thesis ..... ……22
Chapter 2 Materials and Experiments……..……..……...**25**
2.1 Selection of Nanofillers and Polymers……25
2.2 Sample Preparation …….....27
2.3 Effect of Ethanol …….... .30
2.4 Performance Evaluation and Procedures …….....33
2.4.1 Scanning Electron Microscopy (SEM)……34
2.4.2 Energy Dispersive X-ray Spectroscopy (EDX)……..…34
2.4.3 Contact Angle Measurement…….…….....34
2.4.4 Evaluation of the Mechanical Characteristics……...…….....35
2.4.5 Dielectric Parameter Measurements……..……...36
2.4.6 Evaluation of the Thermal Characteristics……37
2.4.7 Erosion and Aging Tests……..…..…..39
Chapter 3 Results……..…**43**
3.1 Performance of Silicone Rubber Nanocomposites ……..44
3.1.1 Morphology Observation…….…….....44
3.1.2 Contact Angle Comparison……..…….....45
3.1.3 Mechanical Properties…….....…..47
3.1.4 Dielectric Constant…….…….....48
3.1.5 Thermal Properties…….……..49
3.2 Performances of Nano-Micron-filled SiR Composites…….……..…….... 58
3.2.1 Heat and Erosion Resistance of Nano-Micron-filled SiR…….…….…...59
3.2.2 Inclined Plane Test (IPT) Comparison…….…….63

3.2.3 Filler Dispersion and Interaction……..…….....68
3.2.4 Thermal Stability and Thermal Degradation…….…….....69
3.3 EpoxyResin Nanocomposites……...…….……71
3.3.1 Morphology and Elemental Analysis…….…...…….....71
3.3.2 Heat and Erosion Resistance of Epoxy Composites…….....80
Chapter 4 Discussion.....83
4.1 Advantages of Electrospinning for Filler Dispersion.....83
4.2 Thermal Stability and Thermal Degradation.....89
4.3 Heat Erosion Performance of SiR Composites 92
4.4 Mechanisms of Improved Thermal Performance of Electrospun SiR Composites.....94
4.5 Possible Mechanisms of Electrospinning for Nanofiller Dispersion 100
Chapter 5 Conclusions and Suggestions for Future Work……..……..……103
5.1 Conclusions 103
5.2 Suggestions for Future Work.....106
References 108
Appendix A.....117
Appendix B.....119

List of Figures

Figure 1.1: Illustration of (a) the electrospinning stages with the increase of applied voltage, and (b) bending instability [93]. ....…17
Figure 1.2: Schematic of typical electrospinning. 18
Figure 1.3: SEM images of tin nanofillers embedded in PLLA fibres by electrospinning [101]. 19
Figure 1.4: SEM micrographs showing the effect of electrospraying on CNT dispersion [104], (a) Sonicated solution drop without electrospraying, and (b) CNT dispersion after electrospraying. 20
Figure 1.5: Observation of the electrosprayed CNTs under the optical microscope: (a) Clean glass slide (b) drop of sonicated CNT solution (without electrospraying), (c) electrosprayed cnts (flow rate: 7 ml/min, voltage 25 kv, CNT concentration: 600 mg/L MWNT in water, needle-target distance: 30 cm) for sample 1, and (d) electrosprayed CNTs (flow rate: 0.5 ml/min, voltage 25 kv, CNT concentration: 600 mg/L MWNT in water, needle-target distance: 30 cm) [104] for sample 2. 21
Figure 2.1: Single needle electrospinning setup…….. ..... …….29
Figure 2.2: The electrospun jet behaviour of SiR under different conditions: (a) pure RTV 615 under external electric field (b) pure RTV 615 without ethanol under an external electric field, and (c) RTV 615 with ethanol under an external electrical field..... 31
Figure 2.3: The SEM images of the quickly cured RTV 615 silicone rubber during the electrospinning process: (a) under low magnification; and (b) under high magnification. 32
Figure 2.4: The viscosity of RTV 615-A with and without electrospinning versus crosshead speed. The blue line represents original pure RTV 615-A, and the red line represents electrospun RTV 615-A. 33
Figure 2. 5: Definition of contact angle. 35
Figure 2.6: (a) Schematic diagram of the laser setup, (b) the experimental laser setup, and (c) the temperature on the sample surface in the LHTA test measured by an infrared camera. 39
Figure 2.7: Schematic diagram of the IPT test. 41
Figure 2.8: (a) The electrode configuration for the corona resistance test based on IEC 60343 standard [130] , and (b) the assembly of six pairs of electrodes. 42
Figure 3.1: The morphology of silicone rubber nanocomposites with different nanosilica loadings, prepared by using two methods, (a) 3 wt% nanosilica-filled SiR, (b) 6 wt% nanosilica-filled SiR, and (c) 10 wt% nanosilica-filled SiR. Left columns are ES samples, and right columns are CS samples. ..... …45
Figure 3.2: The variation of a droplet of 10 μL deionized water on the nanocomposite's surfaces. The left columns in each figure show samples mixed by the mixer, and the right columns, by the electrospinning: (a) silicone rubber composites with 3 wt% nanosilica, and (b) silicone rubber composites with 6 wt% nanosilica. 46
Figure 3.3: Static contact angle as a function of time on flat surfaces of various nanocomposites (ES=electrospun samples; CS=conventional samples)..... 47

Figure 3.4: The relative permittivity of the composites as a function of the frequency. (ES = electrospun sample; CS = conventional sample). 49
Figure 3.5: The thermal degradation of the unfilled silicone rubber and nanosilica-filled silicone rubber composites, prepared by two methods (ES = electrospun sample; CS = conventional sample) (a) with 3 wt % nanosilica, and (b) with 6 wt % nanosilica. 50
Figure 3.6: The thermal profiles of the maximum temperature along a line that passes through the center of the laser-heated area on the surfaces of the samples, (ES = electrospun sample; CS = conventional sample), (a) The thermal profile for the conventional samples and pure silicone rubber, and (b) the thermal profile for the electrospun samples and pure silicone rubber. 53
Figure 3.7: The temperature profiles of the different areas along a line passing through the center of the laser-heated area on the surface of the 10 wt% electrospun SiR nanocomposite (ES = electrospun sample; CS = conventional sample)..... 54
Figure 3.8: The temperature distribution in the 2D models (a) unfilled SiR (b) microsilica-filled SiR, and (c) nanosilica-filled SiR. 55
Figure 3.9: The temperature distribution trends along a line passing through the center of the heat source on the surface of simulated samples, (a) unfilled pure SiR, (b) micron silica filled SiR ,and (c) nanosilica filled SiR..... 55
Figure 3.10: The average eroded mass after three repetitions of the laser erosion tests for pure silicone rubber and nanosilica-filled conventional samples and electrospun samples (ES = electrospun sample; CS = conventional sample)..... 57
Figure 3.11: The eroded mass for the formulas with 5 wt% nanosilica and 10 wt% to 40 wt% microsilica (ES = electrospun sample; CS = conventional sample). 59
Figure 3.12: The surface patterns of the samples in the laser erosion test..... 61
Figure 3.13: The eroded mass for the electrospun samples with 40 wt % microsilica and 5 to 10 wt% nanosilica (ES = electrospun sample; CS = conventional sample)..... 62
Figure 3.14: The eroded mass for the formulas with 20 wt% nanosilica and 2.5 to 6 wt% microsilica; 20 and 3 wt% microsilica-filled samples are used as references (ES = electrospun sample; CS = conventional sample). 63
Figure 3.15: The IPT test durations for the different formulas with 20 wt% nanosilica and 2.5 wt% to 6 wt% microsilica. 20 wt% and 30 wt% microsilica-filled samples are used as a references (ES = electrospun sample; CS = conventional sample)..... 64
Figure 3.16: The surface erosion patterns of conventional and electrospun samples (with 20 wt% microsilica plus 5 wt% nanosilica loading) after the IPT test..... 65
Figure 3.17: The hardness of conventional and electrospun samples with 20 wt% microsilica plus 5 wt% nanosilica loading for the IPT test. 66
Figure 3.18: Records the maximum current for IPT sample 1 and sample 2 of the electrospun and conventional SiR composites (with 20 wt% microsilica plus 5 wt% nanosilica loading) during the last hour prior to the sample failure

(ES = electrospun sample; CS = conventional sample) (a) IPT sample 1 means CS_1 and ES_1in Figure 3.14, and (b) IPT sample 2 means CS_2 and ES_2 in Figure 3.14. 67
Figure 3.19: The morphology of the filler distribution in the SiR samples, under a 1000 x magnification, (a) The distribution of the 20 wt% microsilica in the SiR composite, (b) the distribution of 20 wt% microsilica plus 5 wt% nanosilica in the conventional SiR composite, and (c) the distribution of 20 wt% microsilica plus 5wt% nanosilica in the electrospun SiR composite. 69
Figure 3.20: The TGA curves for the 20wt% microsilica-filled sample (designated 20M), the conventional sample filled with 20 wt% microsilica plus 5 wt% nanosilica (designated 20M_5N_CS), and the electrospun sample filled with 20wt% microsilica plus 5 wt% nanosilica (designated 20M_5N_ES). 70
Figure 3.21: The SEM images of the 20 wt% micron TiO2 plus 5 wt% nano SiO2 epoxy resin samples, (a) the SEM image, for the cross-section of the conventional epoxy resin sample at 300 and 3000 magnifications, and (b) the SEM image for the cross-section of the electrospun epoxy sample at 300 and 3000 magnifications. 72
Figure 3.22: EDX-mapping and elemental analysis for the CS sample in location 1, (a) the CS sample EDX-mapping in location 1; top left is the SEM image, bottom left is the Si element mapping, bottom right is the Ti element mapping, top right is the overlap mapping for both the Si and Ti element, and (b) the CS sample EDX elemental analysis in location 1. 73
Figure 3.23: EDX-mapping and elemental analysis for the CS sample in location 2, (a) the CS sample EDX-mapping in location 2; top left is the SEM image, bottom left is the Si element mapping, bottom right is the Ti element mapping, top right is the overlap mapping for both the Si and Ti element, and (b) the CS sample EDX elemental analysis in location 2. 74
Figure 3.24: EDX-mapping and elemental analysis for the CS sample in location 3, (a) the CS sample EDX-mapping in location 3; top left is the SEM image, bottom left is the Si element mapping, bottom right is the Ti element mapping, top right is the overlap mapping for both the Si and Ti element, and (b) the CS sample EDX elemental analysis in location 3. 75
Figure 3.25: EDX-mapping and elemental analysis for the ES sample in location 1, (a) the ES sample EDX-mapping in location 1; top left is the SEM image, bottom left is the Si element mapping, bottom right is the Ti element mapping, top right is the overlap mapping for both the Si and Ti element, and (b) the ES sample EDX elemental analysis in location 1. 76
Figure 3.26: EDX-mapping and elemental analysis for the ES sample in location 2, (a) the ES sample EDX-mapping in location 2; top left is the SEM image, bottom left is the Si element mapping, bottom right is the Ti element mapping, top right is the overlap mapping for both the Si and Ti element, and (b) the ES sample EDX elemental analysis in location 2. 77
Figure 3.27: EDX-mapping and elemental analysis for the ES sample in location 3, (a) the ES sample EDX-mapping in location 3; top left is the SEM image, bottom left is the Si element mapping, bottom right is the Ti element mapping, top right is the overlap mapping for both the Si and Ti element, and (b) the ES sample EDX elemental analysis in location 3. 78

Figure 3.28: The element weight percentage comparison between the CS and the ES samples (the reference represents the calculated element weight ratio of Ti to Si in the formulated epoxy composite). 80
Figure 3.29: The eroded mass for the epoxy formulas with the 40wt% microsilica plus 2 wt% to 4 wt% nanosilica, pure epoxy resin, 40 wt% microsilica filled epoxy resin and 44 wt% microsilica filled epoxy resin (ES = electrospun sample; CS = conventional sample). 81
Figure 4.1: The effect of electrospinning on the agglomeration reduction in silicon rubber composites, (a) nanosilica-filled conventional silicone rubber, and (b) nanosilica-filled electrospun silicone rubber 85
Figure 4.2: The load force vs. different filler loading (blue line represents the electrospun SiR samples; red line represents the conventional SiR samples). 86
Figure 4.3: The SEM images of the composite surface after the 12 hours corona aging test at a 12 kV AC voltage: (a) the surface morphology of the 3 wt% aged SiR nanocomposites, and (b) the surface morphology of the 6 wt% aged SiR nanocomposites. The left image shows the conventional samples and the right image shows the electrospun samples. 88
Figure 4.4: The TGA curves for the pure epoxy, epoxy composites with 4 wt% nano Al fillers, and epoxy composites with 20 wt% micro and 4 wt% nano aluminum fillers (CS= conventional sample, ES=electrospun sample). 91
Figure 4.5: The SEM and EDX analysis for the TGA test residues, and each sample was analyzed from a randomly selected small area and a big area (a) pure silicone rubber residues, (b) conventional nanosilica-filled SiR residues, and (c) electrospun nanosilica-filled SiR residues 98
Figure 4.6: The SEM images of nano silica and nano titanium dioxide filled epoxy composites. (a) nanosilica-filled epoxy, and (b) nano titanium dioxide-filled epoxy 101
Figure 4.7: EDX-mapping of of nano silica and nano titanium dioxide filled epoxy composites. (a) nanosilica-filled epoxy, and (b) nano titanium dioxide-filled epoxy 102
Figure B.1: The 3D cell model of the dispersed composites [131] 119
Figure B.2: The simple 2D model of the dispersed composites: (a) the middle cross-section one cubic cell of the microsilica filler, and (b) the middle cross-section of 6 × 6 × 6 cubic cells of the nanosilica filler in the same volume size as in (a). 120
Figure B.3: The temperature distribution in the 2D square cell (a) unfilled SiR cell, (b) 30 wt% microsilica-filled SiR cell , and (c) 5 wt% nanosilica-filled SiR cell. 120

List of Tables

Table 2.1: Characteristics of the Silica Fillers.…….……..…27

Table 2.2: Characteristics of the Base Polymers.…….……..27

Table 3.1: The Mechanical Properties of the SiR Nanocomposites…….....48

Table 3.2: Thermal Conductivity of the Nanocomposites Based on Modified ASTM D5470 [88]…51

Table A 1: Characteristics of Some Commonly Used Nanofillers in the Literature…..…….……..117

Table A 2: Characteristics of Some Commonly Used Dielectric Materials……...…….....118

Chapter 1

Introduction

1.1 Polymeric Materials in Insulation Applications

For many years, solid electrical insulating materials were mainly composed of glass and ceramic materials. These materials, exhibited stable properties resisting UV light, surface electrical activity, and exhibited sufficient mechanical strength for supporting transmission lines, and cable termination bushings. However, the materials' heavy weight, brittle nature, and easy wettable surface are the main weaknesses of porcelain or glass materials for insulation applications. For the last several decades, polymeric materials with their lighter weight, excellent mechanical flexibility and better surface characteristics have gradually replaced previous conventional materials in electrical applications. Commonly used polymeric materials in insulation applications include epoxy resins, silicone rubber, ethylene propylene monomer (EPDM), polyimide, polyethylene (XLPE), ethylene-vinyl acetate (EVA) copolymer, polypropylene, and polystyrene [1-9].

Epoxy resins are typically used in indoor and sealed applications, but they also perform well in contaminated outdoor environments [10-11]. Epoxy resins are castable and impregnable, in addition, they are suitable, because of their versatility, low shrinkage, chemical resistance, high thermal stability and outstanding adhesion [12-13]. Therefore, these epoxy resins can be used as coatings for metal components, bushings, cable terminations, various post and support insulators, or encapsulation of electrical components.

Silicone rubbers are used extensively in a variety of electrical insulation applications such as insulators and bushing coatings owing to their excellent dielectric properties [14-15]. They are characterized by high thermal stability, stable performance under a wide temperature range, and excellent resistance to corona, ozone and

weathering. The most important features of silicone rubbers are their hydrophobicity characteristic and their ability of recovering from a temporary loss of hydrophobicity. The synergism of electrical activities, pollution, temperature, weathering and moisture results in the loss of hydrophobicity of most polymeric insulating materials, thereby leading to the final failure of the insulation. However, silicone rubber materials can keep their hydrophobicity even after long-term outdoor use, and they are able to recover the hydrophobicity after few hours under a normal environment through the diffusion of low molecular weight from the bulk material to the surface [16].

There are three types of silicone rubber compounds: high temperature vulcanization (HTV) silicone rubber, room temperature vulcanization (RTV) silicone rubber, liquid silicone rubber (LSR). RTV rubbers can be one-part or two part addition cure silicone rubbers. Two-part RTV silicone rubber not only has almost the same outstanding properties as regular HTV silicone rubber but also has longer shelf-life and controllable curing speed. Therefore, two-part RTV silicone rubber is chosen as the main polymer in this study.

1.2 Introduction to Nanofillers

(a) Advantages of Nanofillers

Although polymeric materials have many excellent properties, most polymers are thermally poor conductors and mechanically weak materials. The miniaturization of electronic devices and the increasing power level and continuing compaction of electrical power equipment have created new challenges in insulating materials. The current need is to develop advanced materials with excellent properties including high thermal conductivity, low coefficient of thermal expansion, variable dielectric constant , high electrical resistivity, high breakdown strength, high tensile strength and, most importantly low cost. Increasing demands for special materials have led to the development of polymeric composites, since polymeric materials are easy to process, allowing the valuable properties of different types of materials to be combined.

Inorganic fillers such as silica, alumina, barium titanate, and titania (titanium dioxide) have been largely used to impart resistance to the effects of various stresses from environmental, electrical, thermal, and mechanical aspects such as UV light, moisture, dry band arcing, partial discharge, and cyclic loads [17]. The physical properties of a composite consisting of fillers of one material embedded in a polymer matrix is a function of the physical properties of the constituents, the loading level, the shape and size, and the dispersion, as well as the interfacial properties between the fillers and matrices. Different composites for a wide range of applications have been developed by using microfillers, and extensive research into the effects of microfillers on composites has been reported [18-28]. However, due to the processing limitation, it has appeared that further improvements to the physical properties of composites may not be feasible.

On the other hand, nanocomposites, consisting of nanofillers embedded in a polymer matrix, have attracted a great deal of attention due to their unique properties. Nanofillers are defined as structures that are less than 0.1 μm in any one dimension. These fillers can be in the form of spheres, platelets, fibres and mixtures of various materials. Compared to microfillers, nanofillers provide similar properties to those of microfillers at a considerably lower volume fraction, but also enhance properties in a complex and often non-intuitive way [18]. Large interfacial phases between nanofillers and base polymers significantly impact the properties of bulk materials [29-30], and they are critical in determining the properties of composites. Nanofillers have a large surface area-to-volume ratio, compared to microfillers, at the same filler loading; and this ratio increases with decreasing nanofiller size. The large surface area provides many regions for the base polymers to strongly bond to the nanofiller [31] augmenting mechanical strength of the base polymers, and possibly the thermal and electrical properties as well. With the significant advantages and unique impact on the electrical insulation, nanocomposites have attracted more and more attention than the extensively studied conventional microfiller-filled materials.

There are many possible applications of nanocomposites in electrical engineering field such as insulators, bushings, cable terminations, and bus bar insulation. Any improvements in erosion resistance, thermal stability and thermal conductivity, tensile strength, elongation at break, hardness, surface hydrophobicity, dielectric strength are crucial for insulation applications. Most high voltage apparatus and electrical components must exhibit excellent insulating properties. The development of composite materials that filled with nanofillers holds the promise of further improving the electrical insulation grade and the development of nanocomposites also can lead to a longer lifetime of the electrical components and a significant savings for the manufacturing and maintenance.

(b) Problems of Using Nanofillers

The properties of nanocomposites have demonstrated much better results than composites filled with microfillers in terms of their thermal, electrical, and mechanical properties [32-35]. The principal barrier in achieving uniform nanocomposites is filler agglomeration. Agglomeration occurs as a result of nanofiller small size and the strong forces between the filler particles. Moreover, agglomeration is also one of the primary reasons for contradictory results regarding the physical properties prevalent in the literature. This inconsistency has also hindered the potential improvement of the physical properties of nanocomposites. The object of this thesis is to study the properties of nanocomposites used for insulation application prepared by a new filler dispersion method and investigate the effects of the filler dispersion on the performances of the developed nanocomposites.

Since the year 2000, many polymer nanocomposites have been prepared and numerous papers have been published on the performances of different nanofillers. It is necessary to obtain a general idea on properties of different nanofillers before using them. This is the subject of the next section.

1.3 Literature Review

1.3.1 Performance of Various Nanofillers

Recent developments in nanofillers' synthesis and their availability have promoted nanocomposite research. Numerous nanofillers have been embedded into various base polymers to achieve nanocomposites with improved thermal, mechanical, and electrical properties. A review of the literature, related to the various performances of nanofillers in polymeric materials, is given in this section.

(a) Thermal Properties

Lan et al. [36] studied nano-silica-x and nano-layered silicate added to room temperature vulcanizing (RTV) silicone rubber. It is reported that both nanocomposites exhibited better corona resistance than the neat RTV material. In other work, EI-Hag et al. [37] compared the erosion resistances of RTV silicone rubber filled with nanosilica or microsilica. It is confirmed that the eroded mass decreases with increasing the filler concentration in the composites. A nano composite of 10 wt% nanosilica performs in a similar way to a composite of 50 wt% microsilica in terms of eroded mass after the inclined plate tracking and erosion test. However, the transmission electron microscope (TEM) image of the composite with 10 wt% nanosilica indicates that the fillers are not well dispersed in the silicone rubber matrix, and that the size of nanosilica agglomerations even approaches micron size range. Nevertheless, there is no significant difference in the thermal conductivity between the unfilled silicone rubber and the silicone rubber composites filled with 10 wt% nanosilica. The authors concluded that thermal conductivity has little effect on the improvement of the nanocomposite erosion resistance for the chosen range of filler concentrations. On the contrary, Meyer et al. [38] and Rätzke et al. [39] reported that the thermal conductivity of composites increases with the increasing filler concentration. The erosion resistances of the silicone composites indicate a positive correlation with the thermal conductivity. However, the concentrations of the fillers in their research are very high. For instance, Rätzke et al.

mentioned that their samples can contain 40 wt% nanosilica and that only at this high concentration, is the resistance to the arcing distinct. Usually nanofillers are more difficult to mix into base polymers at high concentrations to get uniform dispersions. As mentioned in [39] that even adding four weight percent of nanofiller, primary particles cannot be split up (sheared) at the dispersion process and aggregates are formed. But micron particles are obviously larger and do not form aggregates or agglomerates. Hence, it is expected nanosize filler behaves generally as microfiller. Unfortunately the contrast of the TEM pictures at higher filler concentrations is insufficient, so we cannot infer as to the quality of the dispersion of the nanofillers at such high concentrations.

Boron nitride is a ceramic dielectric material with a high thermal conductivity. Kochetov et al. [40] used both nano and micro boron nitride to improve the thermal conductivity of epoxy. The boron nitride filler loading of 10 wt% enhanced the thermal conductivity of the composites by 39-57% compared to that of neat epoxy. Among four different boron nitride composites filled with different diameters of fillers (70 nm, 500 nm, 1.5 μm and 5 μm), the 500 nm boron nitride-filled samples had a highest thermal conductivity and after modification by a silane coupling agent, the thermal conductivity of 500 nm boron nitride- filled composites increased by 7 %.

In [36], thermogravimetric (TGA) tests confirm that the thermal stabilities of both nanocomposites are higher than those of neat RTV silicone rubber. Frormann et al. [41] employed a high shear force mixer to disperse and distribute platelet carbon nanofibres in polypropylene. TGA analysis indicates thermal stability enhancement due to the presence of CNTs in the polypropylene. By using TGA, Zhang et al. [42] and Zhou et al. [43] also confirmed the improvement of the thermal stability of polyimide by the addition of nanosilica and nanoalumina. But in [37] TGA reflects that there is no significant reinforcement in the stability of the chemical bonding for the 10 wt% nanosilica samples, as compared to the 10 wt% microsilica samples when nanofillers are not well dispersed.

(b) Mechanical Properties

Typically, pure silicone rubber, without any filler, is very soft. To improve the mechanical properties of the silicone rubber, Koo et al. [31] added micron and nano silica, thereby increasing the mechanical strength and toughness. The thermal and mechanical properties of the polyimide nanocomposites were also tested by Irwin et al. [44]. The nanocomposites exhibit a significant increase in the ratio of elongation to failure, scratch hardness, and thermal conductivity compared to the unfilled or micro-filled samples.

Guo et al. [45] incorporated nano copper oxide into the virgin vinyl-ester. A considerable enhancement in the thermal stability and reinforcement in mechanical properties occurs after nano copper oxide is modified by a bi-functional coupling agent, methacryloxy-propyltrimethoxysilane. These improvements are attributed to the good filler dispersion in the polymer matrix, introducing a strong chemical bonding between the nanofillers and the base polymer. Compared with pure resin the tensile moduli increase by about 6 % and 15 % with the functionalized nanofiller loading of 3 wt% and 10 wt%, respectively. Similar results are reported for the as-received nanofiller filled composites. Compared with pure resin, there is a decrease in the tensile strength for the composites filled with as-received nanofillers. However, increases of about 8% and 50% in the tensile strength are evident, respectively, for the composites filled with 3 wt% and 10 wt% functionalized nanofillers.

Zhang et al. in [46] demonstrated that nano magnesium hydroxide ($Mg(OH)_2$), an inorganic flame retardant, can reinforce the mechanical properties and improve the fire resistance of rubber composites. Ethylene-propylene-diene monomer rubber (EPDM), filled with nano $Mg(OH_2)$ have far stronger mechanical properties than those using micron size fillers. The fire resistance of nano $Mg(OH_2)$ filled rubber also exceeds that of micro $Mg(OH_2)$ filled rubbers. The improved dispersion of the nanofillers reinforces fire resistance and the mechanical properties of composites. The material behaviour is influenced significantly by the filler content as well.

Beatty et al.[47] found that, compared with 50 nm unagglomerated silica fillers, 20 nm agglomerated fillers produce resin composites with a higher surface hardness, further improved three-body abrasion resistance, increased water-uptake, and greater resistance to toothbrush wear.

Weymans et al. [48] investigated the influence of nano clay and carbon blacks on the mechanical properties of styrene-butadiene rubber (SBR), a prominent tire rubber. The authors also reported that the elongation at break and tensile strength depend on the type and concentration of the fillers. Only when the rubbers are reinforced by suitable fillers, the demands of exacting mechanical properties are satisfied. When the addition of fillers is increased, the crosslink density is increased; thus, mechanical properties such as elongation and stress-strain are reinforced by bonding the filler to the polymer. However, when the filler concentration is elevated, it is difficult for the nanofillers to disperse homogeneously in the polymer matrix. Consequently, the tensile strength and elongation at break are impaired, worse than that of unfilled SBR. Also, Alfred et al. [49] noted that the nanofillers with a length of 0.1-100 nm approached the length scale of a polymer chain. The crosslinking of polymer chains forms polymer networks. Hence, the addition of nanofillers influences the structure of the local network and crosslinking reactions. The presence of the nanofillers leads to a secondary network due to the adhesion of the polymer to the filler surface. The secondary network dominates the mechanical properties, at forming severe deformations. The particular synergy of polymer chains and nanofillers give rise to optimal control of the mechanical properties. As a result, the transfer of stress between the composite components is enhanced.

Mechanical tests of nano calcium carbonate ($CaCO_3$) filled poly (methylmethacrylate) (PMMA) showed that both unmodified and modified nano $CaCO_3$ are responsible for the increased Young's Modulus, reinforced abrasion resistance, and wear mechanism [50]. However, the PMMA with well-dispersed nano $CaCO_3$ does not change the impact strength. In contrast, the performances of the unmodified nano $CaCO_3$ are strongly deteriorated, compared with that of the unfilled PMMA.

Carbon nanotubes (CNTs) are considered as the ultimate carbon fibre, since they have large aspects ratios, high thermal conductivity, and high break strength. The significant toughening of polymer composites with CNTs has been reported [51-52]. In randomly distributed 1 % by weight multiwall carbon nanotubes (MCNTs) of polyethylene film, the strain energy density increased by 150 % and ductility by 140 % [53]. Nanofillers can provide resistance to degradation [54] and improvement in the thermal and mechanical properties without causing a reduction in the dielectric strength [55].

(c) Electrical Properties

Polymer nanocomposites also exhibit enhanced dielectric strength and voltage endurance compared to pure base polymer and microfilled composites [56]. Kozako et al. [57] demonstrated that composites, mixed with smaller size fillers presents a superior partial discharge resistance than that of composites with larger size fillers. Nelson et al. [58] pointed out that nano titanium dioxide (TiO_2) in epoxy resin can mitigate the interfacial polarization characteristics of a base polymer with a reduction in the internal field accumulations. The enhanced electric strength and reduced space charges are recorded for by nano TiO_2 filled epoxy resin instead of micro TiO_2 filled epoxy composites [59]. The optimum loading of nano TiO_2 is about 10 % by weight. Nelson et al. [60] indicated that the voltage endurance of the epoxy composite enhanced by nano TiO_2 is orders of magnitude greater than that of the pure epoxy and micro-filled epoxy composite. Alapati et al. [61] showed that the addition of nano alumina to the epoxy mitigates the electrical tree initiation and propagation even with a small amount of nanofillers.

Capacitors with a higher energy and power density are required for many applications, such as compensation systems or electric cars. The energy density is proportional to the relative permittivity of the capacitor dielectrics. Hence, some high permittivity nanofillers such as barium titanate with a permittivity of more than 1200 are often added to polymers to attain higher energy density capacitors, or electric stress

grading materials [62-65]. However, the increase of the effective permittivity of the nanocomposites is significantly affected by the permittivity of the base polymers [66].

Singha et al. [67] also demonstrated when a low percentage of nanofillers (titanium oxide TiO_2, zinc oxide ZnO, and alumina Al_2O_3) were added to pure epoxy respectively. The permittivity of the TiO_2 filled sample is reported as less than that of unfilled epoxy, when the filler concentration is lower than 0.5 wt%. Subsequently, the permittivity of epoxy composites increases with the increasing filler percentage. Similar tendencies are also observed for nano ZnO-filled composites. However, the distinct change concentration of nano ZnO is 1 wt%, indicating different distinct change concentrations for different nanofillers. Below the threshold, the permittivity of nanocomposites can be less than that of the unfilled polymer matrix. The dielectric loss of nanocomposites is less than that of the unfilled epoxy at lower filler concentrations. However, at higher filler concentrations, the dielectric loss increases compared to that of pure epoxy. The micro TiO_2-filled samples display a higher permittivity than that of the TiO_2 nanocomposites at the same filler concentration. However, the composites, filled with microfillers, consistently exhibit a higher dielectric loss than the unfilled epoxy. It is suggested that the size and concentration of the nanofillers have significant effects on the properties of nanocomposites.

Based on the extensive research, the use of nanofillers for polymers is well reported. Nanofillers are usually employed to improve one of the material properties for a particular application, and the addition of nanofillers can reduce the total cost of the composites as well, because the price per unit polymer is typically higher than that of fillers [68]. According to the literature the positive effects of these fillers can be summarized as follows.

From the thermal perspective, once the thermal conductivity of the compositions increases, heat is dissipated quickly and average local heating is reduced. Furthermore, the interaction between the fillers and polymer matrix greatly improves the thermal stability and thermal degradation of compositions. The addition of inorganic nanofillers

reduces the portion of the organic polymer materials, exposing themselves to the heat of electrical activity and interrupting the carbonization of the surfaces.

Secondly, from the mechanical perspective, most of the polymers are not mechanically strong. It has been reported that the addition of inorganic fillers can increase such properties as the hardness, tensile strength, and elongation at break of base polymers.

Lastly, from the electrical viewpoint, the addition of the appropriate nanofillers can reduce the accumulation of space charges and increase the dielectric strength, voltage endurance, and partial discharge resistance of composites. Composites with an adjusted permittivity (low or high permittivity), by adding either a different filler or different loadings of fillers, can be obtained for various applications. Furthermore, the increased interfacial regions between the nanofillers and dielectric materials increase the discharge resistances as well. However, the achievement of these positive effects for a given formula depends on various factors such as filler type, filler size, filler loading, and filler dispersion.

1.3.2 Filler Dispersion

Ideal nanocomposites must be free of any agglomerates, contain the optimum filler content, and maintain physicochemical characteristics of their individual components. Although many other parameters influence the properties of nanocomposites, the improper dispersion of nanofillers is often cited as a process limitation, and a key diminishing factor in the improvement of composite properties [69-74].

Achieving a uniform dispersion of fillers is difficult, since nanofillers are highly prone to agglomerate. Nano-scale materials have very large specific surfaces which are inversely proportional to the diameters of the nanofillers. If the specific surfaces increase with the decreased filler diameter, the atom content at the surface of the material becomes significant. When the filler diameter decreases to less than 1nm, the ratio of the surface atoms over the total bulk atoms can exceed 90 %. These surface atoms are in a highly activated state which leads to the lack of a coordination number

and a high surface energy of the nanofillers. Consequently, under the strong influence of this surface effect, nanofillers tend to agglomerate to reach a steady state [75]. Van der Waals force is also inversely proportional to the diameters of nanofillers, and hence there is a stronger Van der Waals force between the nanofillers than microfillers [76]. There are numerous hydroxyl groups (-OH) on the surface of nanofillers [77-78]; these groups have a very strong tendency to form hydrogen bonds with each other. Therefore, all of these factors, including the surface effect of the nanofillers, Van der Waals force, the electrostatic interactions between the molecules and fillers, and hydroxyl groups on the surface of the nanofillers cause nanofillers to easily coagulate. If the nanofillers cannot be separated and dispersed homogeneously in the polymer matrices, not only can the desired properties of the nanocomposites be unattainable, but also the properties of the composite may be worse than the original properties of the polymers sometimes.

There are several mixing techniques to improve filler dispersion. They can be classified as physical and chemical methods. They are discussed in the next section.

(a) Physical Dispersion Methods

The physical methods for dispersing fillers include conventional mechanical mixing and ultrasonic agitation. Mechanical mixing is achieved by using shear force to activate the filler surface, changing the external crystal structure and physicochemical properties. In the ultrasonic agitation, the vibrations release trapped gases, preventing the formation of voids in the composites. The advantage of physical methods is that no extra additives are required.

Typically, simple mechanical mixing is not normally enough in homogeneously dispersing nanofillers. Such a method breaks up some large filler coagulations (larger than 1μm) in a short time by mixing, but after that, the filler dispersion cannot be further improved even with prolonged mixing. Another drawback of physical mixing is its inherent limitation, that is, the possible degradation of the base polymers due to shear heating, especially when the mixing time is long. For ultrasonic agitation, a lengthy period of vibration may result in filler agglomerations again due to the formation of high active sites on the fillers' surfaces that result from the highly

energetic ultrasonic waves. Highly active fillers easily impact each other and form new agglomerations.

Singha et al. [79] adopted mechanical mixing and ultrasonic agitation to disperse micron and nano TiO_2 in an epoxy resin. Ultrasonic agitation can effectively disperse large microfillers in the matrix, although the micron particles are to some extent clustered with groups of particles without touching each other. And by using mechanical mixing although the particles are dispersed, the clustering still exists. For nanofiller, agglomerates cannot be effectively broken by using any single mixing method, but the clusters of nanofillers can be reduced by using a combination of mechanical mixing followed by ultrasonic agitation. Also, processing methods significantly contributed to the variations in the dielectric properties of nanocomposites due to the variations in the distributions of the particles in the polymer matrix. A reduced interfacial polarization in nanocomposites contributed by a reduced size of filler results in a lower value of tan delta in nanocomposites compared to microcomposites. The lowest tan delta and the highest breakdown strength in nanocomposites are observed when the dispersion is the best.

Physical mixing breaks microfiller agglomerations easily but when the filler size is in the nano-scale, the interfiller forces dramatically increase. In fact, the interfiller interaction is so intense that the shear force, provided by conventional mechanical facilities often fails to break apart the nano-aggregations in either a polymer or a solution [80-81]. Some researchers also established with physical mixing, nanofillers cannot exhibit uniform filler distribution, especially in relatively high concentrations [82]. The incorporation of fillers changes the flow properties of the polymers; as a result, simply using physical mixing cannot satisfy the requirement of uniform nanofiller dispersion.

In [83], both single and twin screw extruders were selected to disperse nanosilica with an average size of 792 nm into base polymer poly (ethylene terephthalate) PET and poly (butylenes terephthalate) PBT. It was shown that single screw extrusion is only preferred for processing the modified nanosilica, while twin screw extruder can

provide homogenous nanosilica in the polymers even without silane treatment in low filler loading (3 wt%). However, at high filler concentration (7 wt%), filler agglomeration occurs again. Single or twin screw extruders are normally used to process of melt compounding. Particularly, these kinds of extruders require a lot of space to operate, and use large amount of compound.

(b) Chemical Dispersion Methods

Chemical dispersion methods depend on other additives to modify the surface of fillers. Surface modifications include physical and chemical modifications. For physical surface modifications, some macromolecule chemical additives operate in aqueous media to absorb or cover the nanofillers. The effect of steric hindrance prevents the agglomeration of the nanofillers. First, dispersants and surfactants are common chemical additives for physical surface modification. Dispersants are electrified due to the dissociation process, and when they are absorbed in the fillers' surface, the surface properties of the fillers change, and the surface potential improves so that electrostatic repulsive forces between the fillers become stronger [84]. If the repulsive forces are higher than the attractive forces between the fillers, the filler agglomeration can be broken. Secondly, surfactants are characterized by hydrophilic and hydrophobic chain segments within the same molecule, whereas inorganic fillers are primarily hydrophilic in nature [22]. These characteristics cause the adsorption of the polar end of the surfactant molecules on the surface of the fillers, and the hydrophobic tail remains in contact with the hydrophobic polymer matrix. As a result, the surfactant lowers the surface energy of the nanofillers and the interfacial tension between the fillers and the matrix, facilitating the separation of the fillers and enhancing their dispersion during mixing. In one report CNTs were treated by concentrated aqueous acids [85]. This process introduces acidic groups to the surface of the carbonaceous materials, especially to carbon tubes. The oxidation of the nanotubes induces a negatively charged surface, particularly by the ionization of the acidic surface group. The resulting electrostatic repulsion leads to a dramatic increase in the stability of the carbon tube dispersion. Ramirez et al. [86] used surfactant Triton^{TM} X-100 (Triton) for the physical surface

modification of nanosilica, enhancing the filler dispersion in the RTV silicone rubber matrix. The improvements in filler dispersion are confirmed by the SEM images and smaller eroded mass after aging. However, it is mentioned that the addition of surfactant can impart adverse effects to the chemical bonding and mechanical properties of nanocomposites. TGA tests do not indicate much improvement, unlike the samples without the surfactant. The authors also emphasized that Triton can separate nanosilica much better than other nanofillers. So, there is no universally effective surfactant for most nanofillers; the choice depends on the applications. It is possible the addition of a surfactant can lead to the flocculation of intrinsically stable suspensions of nanofillers [87] or to other side effects to on the properties of nanocomposites [86]. Therefore, the quantity of surfactant must be controlled very carefully to diminish the side effects of the surfactant to the utmost degree.

Chemical modifications by means of chemical reactions between additives (various coupling agents and surface-reactive compounds) and fillers reinforce the filler surface and permanently alter the filler structures, reducing the surface energy of nanofillers. Chemical modifications are effective but involve a complicated process.

Numerous coupling agents have been used to provide a stable bond between the fillers and matrices, and act as a chemical bridge between the two interfaces, significantly improving the reinforcement performance. The most commonly used coupling agents include trialkoxysilanes, titanates, zirconates, and organic acid-chromium chloride coordination complexes. The addition of silane coupling agent can significantly enhance the homogenous distribution of nano silver (Ag) particles in an epoxy matrix. Therefore, the electrical and flexural properties of composites are also enhanced [88]. The compatibility between the nanosilica and the epoxy matrix is substantially by silane modification of nanosilica surface. The etherification between nanosilica and oleic acid leads to the formation of a hydrophobic modified layer existing on the surface of the SiO_2, improving the dispersiveness of nanofillers in non-polar organic solvents [89]. Non-modified fillers are severely aggregated, and the diameter of the aggregation measures in thousands of nanometers. The surface modified

nanofillers are distinct and the individual fillers distinguishable because the nanofillers' cores are kept apart by the surface-modification layer and the repulsion between the fillers are increased. Tee et al. [90] applied the conductive nano silver which was treated by silane coupling agent in an epoxy to produce nanocomposites. The morphological studies have shown noticeable improvement in the filler's ability to disperse in the treated composite system, compared to those untreated. Nano silver (Ag) treated with a silane-based coupling agent exhibited remarkable improvement in the electrical and flexural properties of the composite system. However, the incorporation of treated Ag into the epoxy matrix has resulted in a dramatic reduction in the strain at break which might be due to the interfacial bonding existing between the constituent phases.

All the composites with nanofillers that undergo surface modification have obvious improvements in comparison with composites with untreated nanofillers. However, in most cases, a special additive works for only one type of filler. The selection of chemical additives and the determination of the optimum concentrations must be carefully controlled to attain the desired results. In addition, the removal of the additives is quite challenging.

1.4 Electrospinning

Electrospinning was discovered by Formhals in 1934, wherein an experimental setup was used for the production of polymer filaments by using electrostatic force [91]. Thereafter, Taylor, Saville, Denn, and others significantly contributed to the understanding of the electrically driven jets, and laid the groundwork for electrospinning research in the late 1960s and early 1970s [21-25]. After the 1990s, with the recent trends in the nanomaterials use this simple and versatile technique attracted much attention for both academic research and industrial applications, since electrospinning can produce low cost and high-yield nanofibres. Electrospinning is a straightforward and inexpensive process that produces continuous nanofibres from a submicron diameter down to a nanometer diameter [92]. The method involves the

application of a strong electrostatic field to the metallic needle of a syringe which contains the polymer solution. Under the influence of the electrostatic field, the surface of the polymer solution is charged. At first, the pendent droplet is held by its own surface tension at the needle tip. However, when the applied voltage increases, the interactions of the electrical charges in the polymer fluid with the external electric field result in the droplet deforming into a Taylor cone. The processes are depicted in Figure 1.1 (a). When the applied voltage reaches the critical value, electrostatic forces overcome the surface tension force, and an electrically charged jet erupts. When the jet flies away from the tip of the high voltage needle towards the grounded collector, the travelling liquid jet is subjected to a variety of forces such as the Coulomb force, the electric force imposed by the external electric field, the strong shear force produced during the jet stretching, viscoelastic force, surface tension force, and gravitational force [93]. As a result, the jet bends into a complex path. Furthermore, the jet stretches and thins in large ratios, as evident in Figure 1.1 (b). During the process, the solvent evaporates and solid fibres are eventually left on the collector. As long as a sufficient feeding of solution is insured, the nanofibres are continuously generated.

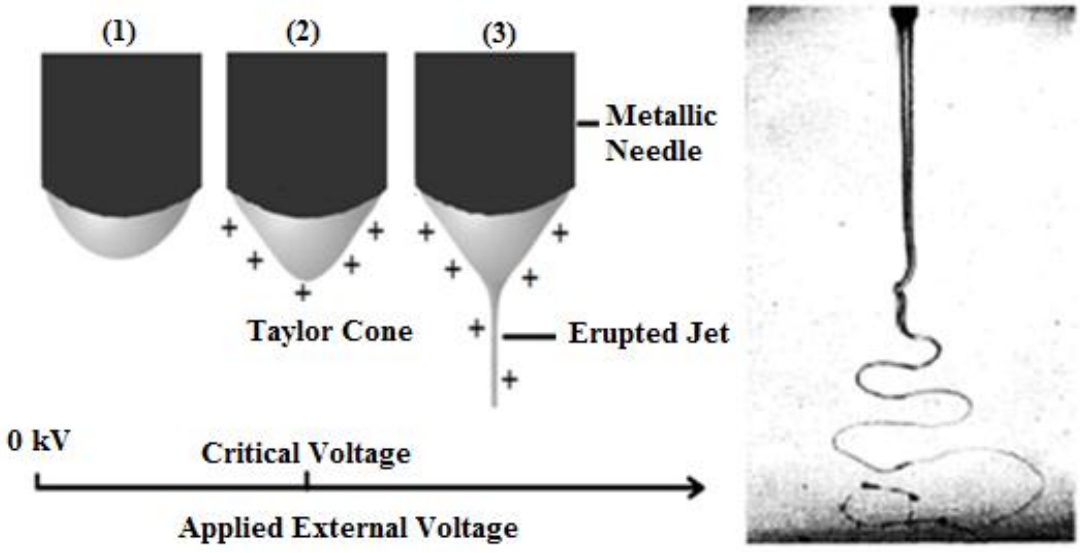

(a) (b)

Figure 1.1: Illustration of (a) the electrospinning stages with the increase of applied voltage, and (b) bending instability [94].

1.4.1 Electrospinning Setup

A schematic of typical electrospinning is shown in Figure 1.2. The following four components are essential: a syringe pump, a syringe with a small diameter metallic needle, a high voltage dc supply, and a grounded collector plate.

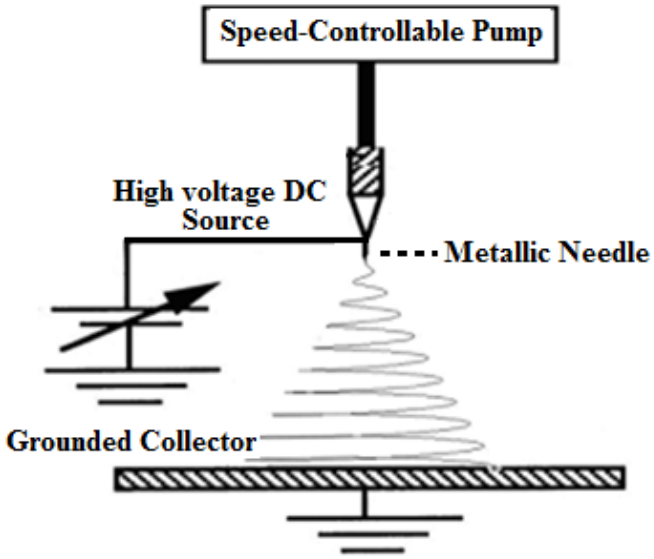

Figure 1.2: Schematic of typical electrospinning.

The similar configuration has been used by several researchers for their electrospinning experiments [92, 95-98]. During the electrospinning process, the polymer solution in the syringe is pushed through the needle at a constant speed with the control of a syringe pump. A high voltage DC source is used to supply the voltage so that the polymer solution can be electrified; typically, 10 kV or higher voltage is applied between the needle and the grounded collector.

The electrospinning setup and process can be modified for different polymers in order to overcome the various limitations of the typical electrospinning configuration and to yield nanofibres with the desired morphologies and properties.

1.4.2 Electrospinning of Nanofibres with Nanofillers

The ultrathin nanofibres produced by electrospinning look promising for many applications such as drug delivery, high-performance filters, wound dressing, artificial tissue, and protective clothing. The high surface area-to-volume ratio, high specific

surface area, superior mechanical properties, and flexibility of the surface functionalities make nanofibres desirable for such varied uses.

Many different types of materials have been used to form nanofibres, including synthetic and natural polymers, copolymer and polymer blends, ceramic, and composites. The individual material properties must be considered for each area of application. Recently, there has been an explosive growth in the use of electrospinning for fibre synthesis, and more recently, in the production of fibres incorporating nanofillers.

Small insoluble fillers can be added to the polymer solution, and are encapsulated in the dry nanofibres. Similarly, soluble drugs or bacterial agents can be added and electrospun into non-woven mats [99]. Yu-Hsun Nien et al. [100] introduced TiO_2 nanofillers into a poly vinyl alcohol (PVA) polymer solution to change the morphology of nanofibres. The authors hypothesized that the nano TiO_2 tends to aggregate together as the amount of fillers are increased. However, the researchers found that nano TiO_2 fillers demonstrated the appropriate distribution in the PVA matrix. Tin nanofillers mixed with poly L-lactic acid (PLLA), were electrospun as well [101]. It has been claimed that the oxidation of the tin nanofillers is prevented, and the tin nanofillers are well dispersed and stable as a metal state in the PLLA fibre (Figure 1.3).

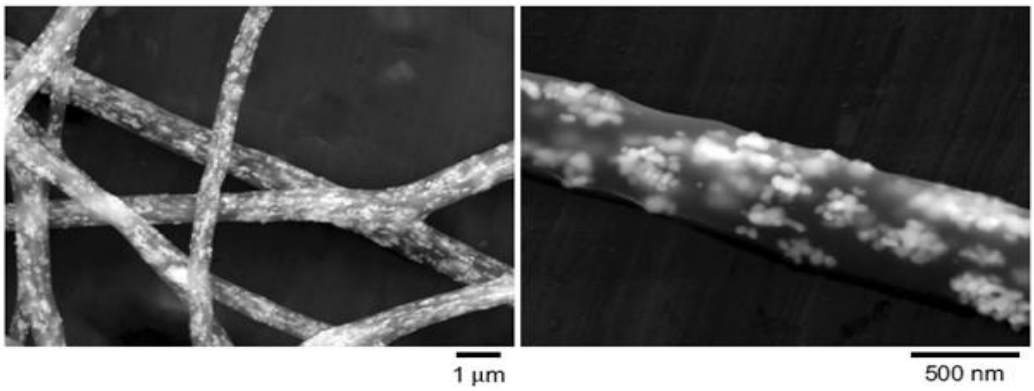

Figure 1.3: SEM images of tin nanofillers embedded in PLLA fibres by electrospinning [101].

By electrospinning, Zhang et al. [102] successfully produced the fibres of magnetic polyacrylonitrile (PAN) with nano ferroferric oxide (Fe_3O_4) fillers. The infusion of Fe_3O_3 nanofillers has a considerable effect on the crystallinity of the PAN,

and a strong interaction between the PAN and Fe_2O_3 nanofillers is produced. However, when the filler concentration is elevated to 5 or 9 wt%, the polymeric mixture gains a high viscosity which ultimately prevents the electrospinning process; but, Zhang et al. did not comment on the quality of the filler dispersion, achieved at a low concentration

CNTs have an exceptionally high axial strength, elastic modulus, tensile strength, and compressive strength to weight ratios [103]. However, because of the Van der Waals interaction between CNTs, they are easily held together as bundles. Chen [104] used electrospraying to separate the CNTs (CNTs mixed with water) and a coated nylon filtering membrane. In the SEM images of Figure 1.4 and optical microscope images of Figure 1.5, electrosprayed CNTs illustrates a much better dispersion than the sonicated solution drop.

Chen concluded that electrospraying is an efficient method of dispersing CNTs. The flow rate of the CNT solution, CNT concentration, and the distance between the needle and collector are three important factors which can affect the dispersion degree of CNTs even more than the applied voltage.

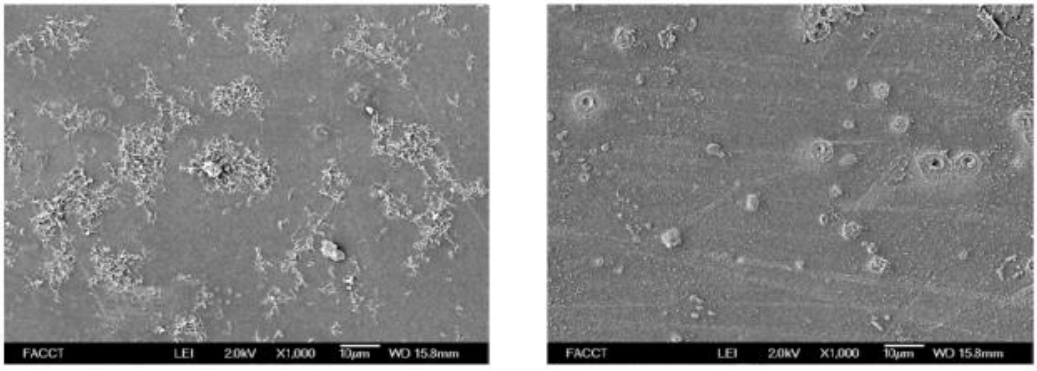

(a) (b)

Figure 1.4: SEM micrographs showing the effect of electrospraying on CNT dispersion [104], (a) Sonicated solution drop without electrospraying, and (b) CNT dispersion after electrospraying.

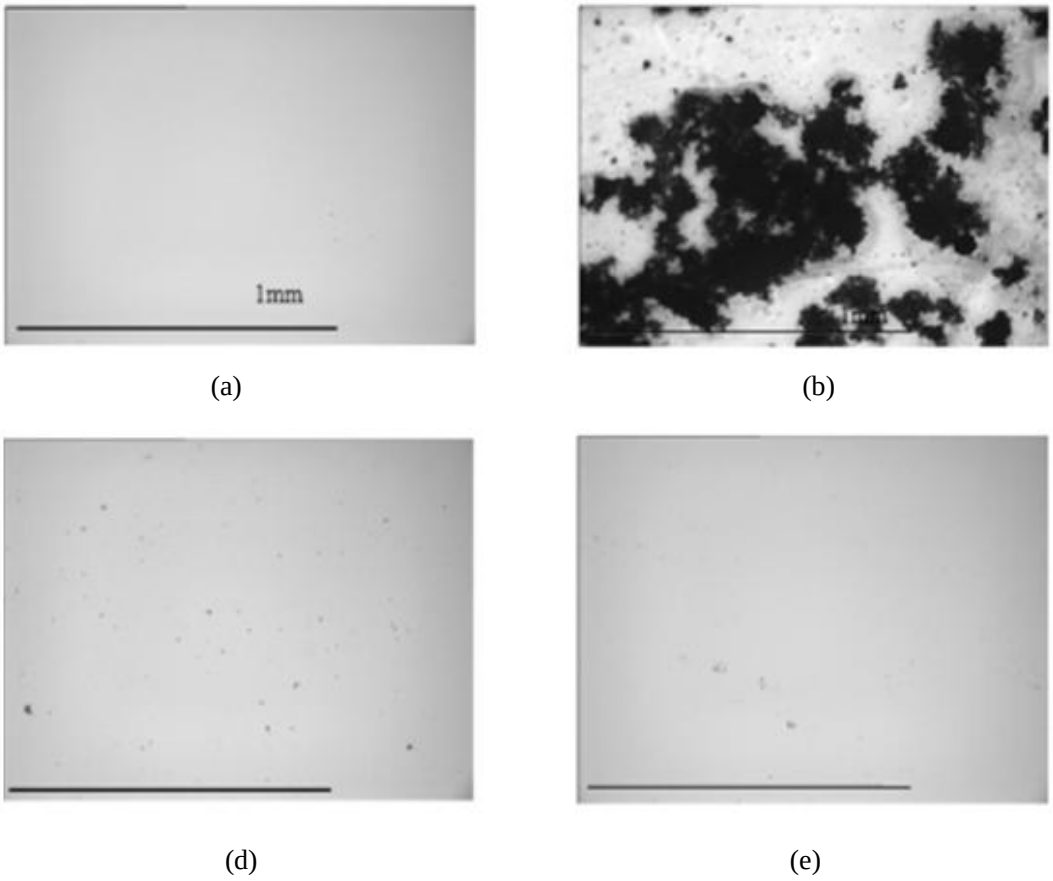

Figure 1.5: Observation of the electrosprayed CNTs under the optical microscope: (a) Clean glass slide (b) drop of sonicated CNT solution (without electrospraying), (c) electrosprayed CNTs (flow rate: 7 mL/min, voltage 25 kV, CNT concentration: 600 mg/L MWNT in water, needle-target distance: 30cm) for sample 1, and (d) electrosprayed CNTs (flow rate: 0.5 mL/min, voltage 25 kV, CNT concentration: 600 mg/L MWNT in water, needle-target distance: 30 cm) [104] for sample 2.

In addition, some recent work has demonstrated the feasibility of the incorporation of CNTs into nanofibres [105-108]. Nanofibres, containing CNTs, exhibit improvement in electrical conductivity [109] and mechanical properties [110]. The orientation of the CNTs within the polymer matrix is particularly important for the reinforcement of polymers and for the improvement of the mechanical properties of nanocomposites. In electrospinning, due to the large shear forces in a fast fibre-drawing process, embedded CNTs are oriented parallel to the nanofibre's axis [111]. Gao et al. [112] prepared poly vinylpyrrolidone composite nanofibres containing single walled nanotubes (SWNTs). After removing the polymer by pyrolysis, they found that the aligned SWNTs existed primarily as individual nanotubes. This indicates that the electrospinning process

facilitates both the debundling and aligning of the SWNTs. However, most reports focus only on the alignment of CNTs. There are a few papers that mention the effect of electrospinning on debundling CNTs, although as mentioned some reports already presented the debundling function of electrospinning on CNTs.

1.5 Objective and Organization of the Thesis

A large number of studies have demonstrated that nanofillers can effectively improve the properties of various base polymers. Most research has confirmed that the homogeneous distribution and de-agglomeration of nanofillers help to achieve and develop high performance nanocomposites. There is no doubt that aggregations substantially undermine the effort of introducing the exceptional properties of nanofillers.

Existing filler dispersion methods, such as mechanical mixing, ultrasonic agitation, and chemical modification or functionalization, have certain drawbacks. Existing physical methods are environmentally friendly, but they cannot effectively break up fillers less than 1 μm. In addition, for mechanical blending, a long period of mixing does not further improve the filler dispersion. Moreover, such ultrasonic agitation can also adversely deteriorate the dispersion of some fillers. Chemical methods can improve the filler dispersion significantly, but selecting chemical additives which work optimally for a given filler and polymer is complicated. Moreover, the existence of chemical additives may degrade the properties of the resulting nanocomposites, and the complete removal of these additives is quite challenging.

Some research has been conducted on electrospinning composite fibres and revealed the feasibility of incorporating nanofillers into nanofibres by electrospinning. However, only a few researchers have paid attention to the function of electrospinning in the filler dispersion or simply mentioned that, after electrospinning, the fillers showed the proper dispersion in the polymers. Little research has been done to examine the effects of electrospinning on filler dispersion. Furthermore, no research has been

done to establish the relationship between the reduction of filler agglomeration and improvements in the properties of various composites.

The existing dispersion methods of fillers have been discussed. However, a simple and effective mixing method is desired due to the drawbacks of those mixing methods. The dispersing function of electrospinning has been shown in some literature. Hence, there is the potential to use electrospinning as a tool to improve the dispersion of nanofillers in base polymers and to enhance the various properties of the so developed nanocomposites.

Consequently, the focus of this thesis is primarily on using electrospinning to improve the nanofiller dispersion in the base polymers. The neat polymers (pure polymer) are selected due to their most general use in outdoor insulation application, primarily silicone rubber and to a certain extent, epoxy resin. Based on the literature, the most commonly used nanofillers are selected to reinforce and enhance the desired composite properties. Not only are the nanofiller composites prepared, but also microfiller composites and composites with both nanofillers and microfillers are also prepared for study. The nanocomposites are examined from the thermal, electrical, and mechanical aspects to study the improvements in properties arising from uniform dispersion of nanofillers. In addition, the mechanism of electrospinning in nanofiller dispersion is investigated.

The main objectives of this thesis are as follows:

[1] To develop a mixing method for homogenous dispersion of nano sized fillers in polymeric materials by electrospinning technique.

[2] To investigate the performance of silicone rubber nanocomposites developed by electrospinning, and analyze the role of filler dispersion, filler interaction, and loading in the composites.

[3] To understand the interaction between nano and micron fillers with base polymer; and the protective mechanisms of the above nanocomposites exposed to heat ablation.

[4] To understand the possible underlying mechanisms of nanofiller dispersion by electrospinning.

In view of the above objectives, this thesis is organized as follows:

✧ Chapter 2 presents the selection of materials, procedures of composite preparation, methodology of the performance evaluation on composites and the thermal modelling of composites. Two mixing methods are adopted in this investigation, commonly used conventional mechanical mixing and the proposed electrospinning. For all the evaluations, comparisons are made between conventional and electrospun samples. Various formulas of nanocomposites are evaluated by using the infrared laser ablation test and ASTM standard incline plane test. Scanning Electron Microscopy (SEM), Energy Dispersive X-ray Analysis (EDX), Thermal Gravimetric Analysis (TGA) methods are to examine the samples.

✧ Chapter 3 lists all the experimental results of the different composites from the thermal, mechanical, and electrical aspects. Parameters, such as eroded mass, surface temperature distribution, maximum temperature, tensile strength, elongation at break, contact angle, and permittivity, are indicated, including several tables and graphs.

✧ Chapter 4 presents a series of comparison and discussion about the results. The advantage of using electrospinning as a new nanofiller dispersion method and the possible effect of electrospinning on nanofiller dispersion and the enhancement mechanism of the thermal performances of electrospun nanocomposites such as heat erosion resistance and thermal degradation are addressed.

✧ Chapter 5 provides a conclusion of this thesis and suggestions for the future work.

Chapter 2

Materials and Experiments

The benefits of using nanocomposites are self-evident. Obtaining the optimum final nanocomposites depends on many factors, but one of the crucial factors is the dispersion and distribution of the nanofillers in the base polymers [113]. Although many mixing methods have been researched, an alternative new mixing technique, a novel electrospinning method, is developed and investigated in this thesis to obtain uniform nanofiller dispersion and distribution.

The composite preparation, sample assessment, and thermal modelling are described in the following sections. The performance assessments of the composites include the standard inclined plane test, laser ablation test, corona aging test, dielectric parameter measurements, viscosity measurement and various analytical tests such as SEM, EDX, and TGA.

In industry, microfillers are usually loaded into the polymers at more than 30 wt% to reduce the cost and obtain better performances of composites. The addition of nanofillers can further improve the interaction between the microfillers and the polymer matrices. Therefore, to meet the cost reduction requirements of manufacturers and based on research [33-35], optimum levels of composite performance can be attained by using a combination of nanofillers and microfillers to gain the benefits of both fillers [114]. Consequently, in the thesis, the microfiller and nanofiller-filled composites are also investigated.

2.1 Selection of Nanofillers and Polymers

Based on the literature review of nanofiller performances, Table A1 in the Appendix lists the commonly used inorganic fillers with base polymers to achieve engineered materials for various purposes. As described in the table, some of these fillers exhibit a high permittivity; some a high thermal conductivity; and others, valuable good mechanical

properties. Therefore, these fillers are expected to improve many desired properties of composites for different applications. Table A2 in the Appendix summarizes the common base polymers for possible study as well.

The polymers, silicone rubber is the base materials used in this thesis and epoxy resin is also selected for some further study. Pure silicone rubber and epoxy resin are chosen as the polymeric matrix which have no other fillers or diluents are included in the as-received polymers. This diminishes the effects of the other impurities in the final properties of the investigated composites.

Titanium dioxide was used in the first commercial silicone rubber compounds, those rubbers exhibited good physical and electrical properties but the electrical properties were adversely affected by moisture. Therefore, silica fillers which also have excellent dielectric properties but fewer effects by water received the attention [115]. In this thesis, the chosen fillers are nano fumed silica and microsilica due to their commercial availability, price, and good physical properties present in the insulation composites, well supported by research and industry. Fumed silica, also known as phylogenic silica, it is an amorphous material that derived from the flame pyrolysis of silicon tetrachloride. Fumed silica has an extremely low bulk density and large surface area which easily agglomerate, but performance well [116-117], it is used as reinforcement in silicones and hydrocarbon vulcanized rubbers [118-119]. Nano fumed silica is obtained from Sigma Aldrich and microsilica (Min-U-Sil5), from US Silica. Some of the physical properties of fillers are summarized in Table 2.1.

In this research, General Electric RTV 615 silicone rubber (SiR) is selected as one of the base polymers. RTV 615 is a transparent, low viscosity vinylpolydimethylsiloxane silicone rubber. However, it has the similar, excellent properties as the regular heat curing silicone rubber that is often used for insulator housings. This type of SiR is a two-part cured silicone rubber compound consisting of part-A, a liquid silicone rubber, and part-B, a curing agent with a 10:1 mixing ratio of part A to part B. The curing process of RTV 615 is quite simple and does not need a highly controlled curing temperature for the reproducibility of vulcanization of the SiR. However, an elevated temperature cure is

necessary for achieving the optimum properties of the silicone rubber. Another base polymer is chosen to investigate: XR7 2184/CLH 5185 epoxy resin, obtained from Crosslink Technology INC. Also, the resin is a two-part compound consisting of part-A XR7 2184, a liquid epoxy resin, and part-B CLH 5185, a multiring alicyclic anhydride curing agent. The mixing ratio of part-A to part-B is 1:1. Some of the physical properties of the base polymers are summarized in Table 2.2.

Table 2.1: Characteristics of the Silica Fillers.

Filler	Average Particle Size	Density (g/m^3) @25°C	Surface Area (BET)* (m^2 / gram)
Nano Fumed Silica	7 nm	2.20	350-430
Micron Silica	1.5 μm	2.65	5

BET* stands for Brunauer, Emmett, and Teller, the three scientists who optimized the theory for measuring surface area.

Table 2.2: Characteristics of the Base Polymers.

Base polymer	Viscosity (cps)	Mixing Ratio (by weight)	Curing Temperature (°C)
Silicone Rubber RTV 615	4000	1:10	Room Temperature
Epoxy XR2184	700-1000	1:1	125

2.2 Sample Preparation

The composite samples were prepared according to the weight percent (wt%) of the nanofillers and base polymers in the composites. For example, the 3 wt% nanosilica composites refer to samples that are made by mixing 3 g of nanosilica with 97 g of RTV 615 silicone rubber in a 100 g sample. Also, a 10:1 ratio, based on the weight of the base rubber (Part A of RTV 615, hereafter called RTV 615-A) to a crosslinker (Part B of RTV 615, hereafter called RTV 615-B) is chosen for preparing the silicone rubber composites.

Thus, in the example, 3% nanosilica composites refer to 3 g nanosilica, 88.1 g RTV 615-A and 8.82 g RTV 615-B. For epoxy resin with a mixing ratio 1:1, then a 3 % by weight nanosilica composite is 3g nanosilica. The rest both part-A XR7 2184 and CLH 5185 are 48.5 g. In this research, the maximum nano fumed silica loading was limited to 6 wt% for the samples, produced by conventional mixing. For the samples produced by electrospinning, the maximum nano fumed silica loading is 10 wt% by weight but it is still possible to incorporate more nanosilica in the SiR by electrospinning.

A Ross Type HSM-100LSK laboratory mixer with a high shear mixing blade is selected for the preparation of the samples. Degussa, the manufacturer of the fumed silica, recommends a peripheral mixing blade velocity (tip speed) in excess of 10m/sec (peripheral velocity) to obtain sufficient shear for good dispersion [120]. The speed of the mixing blade is calculated from:

$$rpm = \frac{\text{peripheral velocity (m/sec)*60*1000}}{\text{d (mm)*}\pi} \tag{2.1}$$

Since the Ross high shear mixer used in this work has a 16 mm blade diameter, the necessary speed recommended for mixing fumed silica is 12,000 rpm. As the viscosity of the mixture increases with the increasing wt% of the nanofillers, the mixing time is specific to the amount of the nanofillers to that is incorporated into the base rubber. Also, because high shear mixing heats the mixture, the mixing vessel is placed in a container with cold water.

The conventionally produced samples, hereafter referred to as the conventional samples, are prepared in two steps. In the first step, the dry nanofillers are gradually added to RTV 615-A (or part-A epoxy), while mixing at a low speed to wet-out the filler. When the nanofillers are visibly wetted-out, the mixing speed is gradually increased to 12,000 rpm which continues until the mixture exhibits no visible signs of lumps. After 2-3 minutes of cooling, RTV 615-B (or part-B epoxy) is added and mixed at low speed for two minutes by a standard mixer, and then degassed in a vacuum at 27 inHg until the bubbles are completely removed (for epoxy the vacuum time is limited to less 3 mins; otherwise the additives in the epoxy resin are pulled out). The silicone rubber mixture is then poured

into moulds and allowed to cure for 24 hours at room temperature. Following curing, the samples are stabilized according to the manufacturer's recommendation by post-curing in an oven (Lab Line Model 3620 Duo Vac Vacuum Oven) for 4 hours at 87 ^{o}C. For epoxy, the compound is cured at 125 ^{o}C for 8 hours after vacuum.

An experimental apparatus is built to perform the electrospinning dispersion without any complexity in the vertical and horizontal directions, as shown in Figure 2.1.

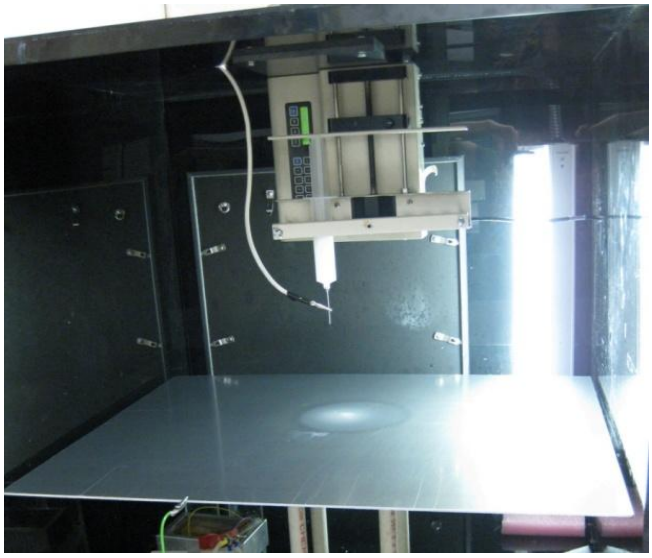

Figure 2.1: Single needle electrospinning setup.

The samples produced by electrospinning, hereafter referred to as the electrospun samples, require the appropriate amount of ethanol; otherwise, RTV 615-A (or epoxy) cannot be properly electrospun due to their low electrical conductivity. The amount of ethanol, determined through trial and error for the experimental conditions at hand, is roughly 1 mL per 2 g of RTV 615-A. For the epoxy used in this thesis, only a few drops of ethanol is sufficient to enable epoxy mixture to electrospin. Ethanol increases the conductivity of the mixture to satisfy the requirements of electrospinning, and also can reduce the viscosity of the compound a little bit, a benefit, when more nanofillers are loaded.

The ethanol is first mixed with nanosilica by using a magnetic stirrer (Fisher Scientific Isotemp Magnetic Stirrer 11-100-49S), gradually adding nanosilica during stirring until the fillers are totally wetted by the ethanol. Then, RTV 615-A (or epoxy part-A) is added and mixed by the Ross high shear mixer at a high speed for approximately

5 minutes. The mixture is then injected with a pump at the rate of 0.3 mL/min into a 60 mL syringe with a stainless steel needle (2.16 mm diameter flat-end), which is energized at a nominal voltage of 12-16 kV DC. The separation between the needle tip and the ground plate is nominally 20 cm but also varies with the formulas. The applied voltage and distance between the energized needle and ground plate are system specific. To speed up the evaporation of the ethanol, a fan is installed in the electrospinning chamber. In the practical experiment, the curing agent, RTV 615-B (or epoxy part-B) is not added to the compounds of fillers and SiR (or epoxy) polymers during the electrospinning process. Therefore, after electrospinning the collected compounds are still in liquid form. The collected electrospun compounds are mixed with RTV 615-B (or epoxy part-B) for two minutes at a low speed by using a standard mixer. After pouring the mixture into the molds, curing occurs, following the same procedure as that for the conventionally produced samples previously described.

2.3 Effect of Ethanol

The viscosity and conductivity of a polymer solution influences the formation of nanofibres [92,121-123]. During the electrospinning process, the surface charge of the solution causes a polymeric jet to elongate under the electrical forces. If the conductivity of the solution is too high, it is very difficult or impossible to spin the jets even at very high voltages. Similarly, it is not possible to form nanofibres if the solution has a low electrical conductivity. The standard polymers used for the electrospinning are dried powders before they are mixed with solvents. When the solvent evaporates, solid fibres remain. The solution's properties are adjusted by controlling the quantity of the solvent or by adding a small amount of salt or polyelectrolyte to the polymer solution to adjust the electrical conductivity of the solution.

To electrospin the insulating polymeric materials, the conductivity of the compound must be high enough to ensure there are sufficient repulsive charges on the surface of the electrospinning jets. Since other additives are not expected to be added to the final polymers, a solvent is the best selection to increase the conductivity of the SiR and epoxy

solution. Due to the hydrophobic characteristics of the SiR and epoxy resin, typical solvents, such as water cannot be used. After several tests, ethanol is determined as the solvent to increase the conductivity. Figure 2.2 denotes the effect of ethanol on the electrospinning of pure RTV 615 SiR.

(a) (b) (c)

Figure 2.2: The electrospun jet behaviour of SiR under different conditions: (a) pure RTV 615 under external electric field (b) pure RTV 615 without ethanol under an external electric field, and (c) RTV 615 with ethanol under an external electrical field.

As illustrated in Figure 2.2 (a), without an external electric field, no induced charges exist on the surface of the rubber to form the Taylor cone and fluid jet. Figure 2.2 (b) signifies the behaviour of pure RTV 615 silicone rubber during electrospinning. It is difficult to observe the ejection of any thin jets. There are not enough surface charges at the fluid's surface due to the very low conductivity of RTV 615 SiR. However, as shown in Figure 2.2 (c), with the correct amount of ethanol, RTV 615 has the ability to transfer the induced ions in the fluid to the surface. Due to the existence of adequate surface charges, a thin jet can be pulled out from the Taylor cone; therefore, RTV 615 SiR can be electrospun. With the help of ethanol, the electrospinning of low conductivity SiR is possible, so is epoxy resin.

In order to check the morphology of pure SiR during electrospinning, only two-part RTV 615 (A and B) and the correct amount of ethanol mixture are prepared and electrospun. To accelerate the curing time, the collector plate is heated up to 200 ^{o}C during the electrospinning process. The collected pure SiR polymers are analyzed under a scanning electron microscope (SEM), Figure 2.3.

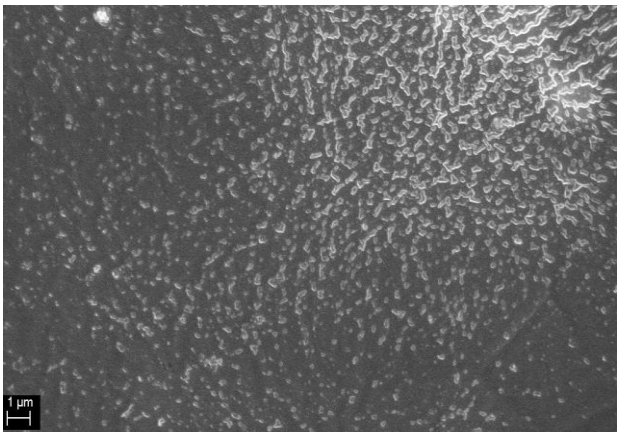

(a)

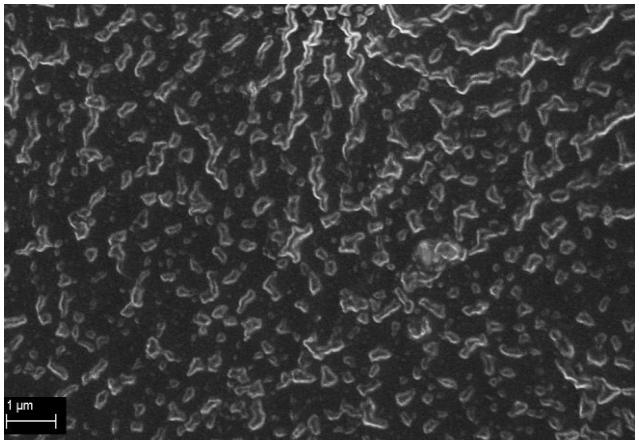

(b)

Figure 2.3: The SEM images of the quickly cured RTV 615 silicone rubber during the electrospinning process: (a) under low magnification; and (b) under high magnification.

Some of the collected streams are droplets, and most of them appear to be filaments in the SEM images. Both of them are acceptable due to their nanometer diameter. The most important thing is they are uniformly distributed; thus, the feasibility of electrospinning of SiR to disperse fillers is confirmed. Consequently, it is possible to electrospin insulating polymers which have a low conductivity in a similar manner.

The comparison of the viscosity is made between the pure RTV 615-A and electrospun RTV 615-A. Figure 2.4 depicts the viscosity of RTV 615-A as a function of the crosshead speed.

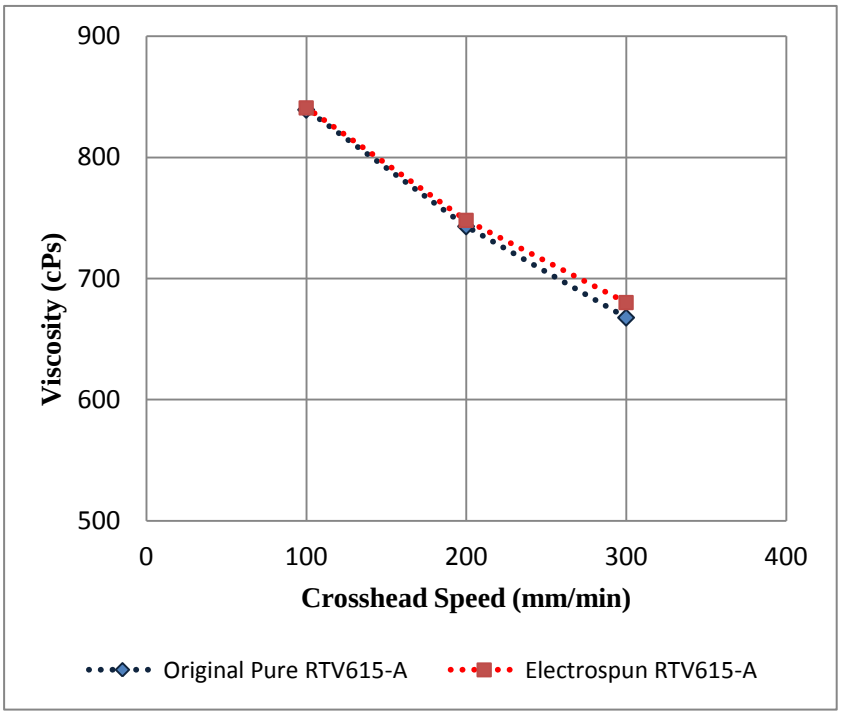

Figure 2.4: The viscosity of RTV 615-A with and without electrospinning versus crosshead speed. The blue line represents original pure RTV 615-A, and the red line represents electrospun RTV 615-A.

The measurement is conducted by a shear capillary rheometer, mounted on an Instron Universal Testing Machine (Model 1122; Instron, Norwood, Mass., U.S.A.). A 50 mL polymer solution is loaded in the machine barrel at three crosshead speeds (100, 200, and 300mm/min), respectively. All the tests are carried out at room temperature. The viscosity of the electrospun RTV 615-A undergoes conductivity modification by ethanol, compared with that of the pure RTV 615-A. It conveys that the ethanol, the only additive, evaporates entirely during the electrospinning process.

2.4 Performance Evaluation and Procedures

The optimum loading of the nanofillers is determined by trial and error and is system specific. Therefore, performance tests must be conducted to ensure that the loading level and dispersion process are adequate to meet the requirements of the applications.

2.4.1 Scanning Electron Microscopy (SEM)

SEM is used to image the sample surface by scanning the surface with a high-energy beam of electrons. The electrons interact with the atoms of the sample, producing signals that contain information, including the sample's surface topography, composition, and other properties such as electrical conductivity. In this study, a LEO 1530 FE-SEM system is chosen to analyze the cross-section of the composites to ascertain the dispersion of the nanofillers within the polymer matrices. All of the samples that are prepared for the SEM observation are the cross-sections of the nanocomposites. The samples are cut into thin pieces with a sharp blade, and were then sputter-coated with a thin layer of gold to overcome the charging effect.

2.4.2 Energy Dispersive X-ray Spectroscopy (EDX)

EDX is an analytical technique used for the elemental analysis or chemical characterization of a sample. EDX is carried out by using the LEO 1530 FE-SEM microscope, equipped with an EDX Pegasus 1200 integrated EDX system. The EDX analysis collects the X-rays information when the sample is hit with the electron beam during the SEM. Each element has unique atomic structure, allowing the X-rays to provide the particular information about the elemental composition of the samples. All of the X-ray number counts are composed of EDX-mapping to assess the homogeneity of the fillers and interactions of the different fillers in the polymers.

2.4.3 Contact Angle Measurement

The hydrophobicity of the composite surface changes with time due to the effects of the environment and partial discharge. It is noteworthy that the hydrophobicity of the material surface necessitates that the contact angle (θ) must be taken into account. It is the angle that liquid and vapour interface meet a solid surface. The definition of contact angle is shown in Figure 2.5. The shape of the droplet is determined by three surface tensions, acting on the droplet according to Young’s relation:

$$\gamma_{sv} + \gamma_{sl} = \gamma_{lv} \cos\theta \tag{2.2}$$

where θ is the contact angle, and γ_{sv} , γ_{sl} and γ_{lv} are the surface tensions between the solid-vapour, solid-liquid, and liquid-vapour phases.

If the surface is rough and homogeneous after adding the nanofillers, the addition of the liquid droplet grows without moving the periphery. Therefore, the contact angle enlarges, indicating improvement of material's hydrophobicity.

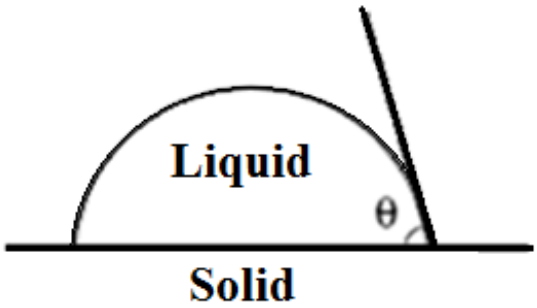

Figure 2. 5: Definition of contact angle.

The contact angle not only reflects the hydrophobicity characteristics of the surface but also indicates whether the nanofillers on the surface are uniformly distributed. In this study, the contact angle measurement is conducted on the nanocomposite's flat surface. First, the surfaces of the composite samples are cleaned by deionized water, and then the samples are placed on a flat plate after the surface is dried in desiccators for 24 hours. A precision pipette is used to drop one 10 μL droplet of deionized water on the composite's surface. The static contact angle is obtained from the photographs, taken by a digital camera every 10 mins and stored on a computer. The contact angle is measured by a custom developed software using Adobe Photoshop.

2.4.4 Evaluation of the Mechanical Characteristics

One of the reasons that fillers are added to polymers is to reinforce the mechanical properties of the base polymer. It is well known that the microfillers can improve hardness of composites at a high filler concentration. It is also well known that nanofillers can

improve tensile strength at a very low level. Therefore, depending on the application, the optimum filler loading will vary.

There are standards for the measurements of the hardness, tensile strength, and elongation at break. According to ASTM D2240 [124], a durometer Model 408 (type A) is used to measure the hardness of each sample. The sample surface must be smooth and clean, and the thickness is 6mm. Each sample is measured five times to determine the mean value of the hardness. The samples should be large enough so that the five tests can be performed at least 6mm apart from each other.

The tensile strength and elongation at break measurements are conducted according to the ASTMS D1708 standard [125]. An instron machine 4465 is used to do the test. For each formula, 5 to 10 samples with the dumb bell shape are tested at room temperature. The test speed is 100 mm/min (speed D). The stress, σ, is calculated by

$$\sigma = {}^{f}/_{A_0} \tag{2.3}$$

where f and A_0 are the force and the initial cross sectional area, respectively.

2.4.5 Dielectric Parameter Measurements

Permittivity is an important parameter of dielectric materials, and reflects the insulating properties of the materials. Permittivity is a measure of how an electric field affects a dielectric material. An Agilent E4980A LCP meter is chosen to measure the capacitance and dissipation factor of the composites under the same voltage but with a variable frequency. The permittivity is calculated by the following:

$$C = \varepsilon_0 * \varepsilon_r * A/d \tag{2.4}$$

where ε_0 is the vacuum permittivity, ε_r is the relative permittivity, A is the area of overlap of the electrodes, and d is the separation between the electrodes or the thickness of samples.

All the samples consist of a thin film, whose thickness d is 1-2 mm. In order to obtain a good contact between the silicone rubber composites and electrodes, a thin aluminum

foil with a diameter of 4 cm and a thickness of 70-80 μm is pasted onto both sides of the samples with a minimal quantity of silicone oil. Samples are placed between the stainless steel electrodes afterwards to perform the measurements. The applied voltage is the maximum voltage of the setup, 20 V, and the frequency is varied from 2 to 100 kHz.

2.4.6 Evaluation of the Thermal Characteristics

(a) TGA

TGA is a simple analytical technique to measure the weight loss of the material as a function of the increasing temperature. It reflects the stability of the materials under high temperatures and determines the characteristics of materials that exhibit weight loss due to loss of volatiles. This test is performed with a thermogravimetric analyzer TGA-Q500 from TA Instruments. The measurements are taken in the ambient air and the temperature is increased at a rate of 20 ^{o}C/min from 250 to 800 ^{o}C.

(b) Thermal Conductivity of Composites

Improvement in the thermal conductivity of dielectrics is desirable for many applications. The thermal conductivity of composites are calculated by [126]：

$$K = \frac{K_1 K_2}{K_1 X_2 + K_2 X_1} \tag{2.5}$$

where K_1 and K_2 are the thermal conductivities of the base polymers and fillers, respectively. $X_1 + X_2 = 1$, X_1 and X_2 are the volume fractions of the base polymers and fillers in the composites.

Usually, the thermal conductivity of fillers is higher than that of base polymers. Therefore, based on the calculation, the high filler concentration or the high thermal conductivity fillers improves the thermal conductivity of composites [39]. However, some of the published work does not show such a proportional relation between the amount of fillers and the thermal conductivity [37]. These conflicting results may relate to the filler concentration and/or filler distribution in the composites.

In this research, the thermal conductivity of the prepared nanocomposites is measured on a modified version of ASTM D5470-95 [127], by using the thermal interface material (TIM) test apparatus in the Microelectronics Heat Transfer Laboratory (MHTL) in University of Waterloo. The measurements determine the thermal joint resistance of each of the materials as a function of bond-line thickness; and the data is used to calculate the thermal conductivity. By using a laser scan micrometer, LSM 503H, bond-line thickness measurements are performed during the test. Tests are performed under atmospheric conditions for a mean joint temperature of 353 K. The temperature readings from the resistance temperature detectors in the heat flux meters are used to calculate two quantities, namely, the total heat flow rate through the joint, Q, and the temperature drop across the joint, ΔT. From these two quantities, the joint resistance is attained by calculating:

$$R_j = \frac{\Delta T}{Q} \tag{2.6}$$

Then, the thermal conductivity is calculated through:

$$k = \frac{t_{BLT}}{R_j A} \tag{2.7}$$

where the bond-line thickness (sample thickness), $t_{BLT,}$ is obtained from the laser scan micrometer. A is the cross-section of an area that is 25 mm × 25 mm.

For each formula, three different thicknesses of the thin composite samples are measured to obtain more precise thermal conductivity results.

(c) Laser Heating and Thermal Analysis (LHTA)

To examine the local effects of the particle dispersion, a near infrared laser, operating in the continuous mode at a wavelength of 802 nm is selected to irradiate the composite samples at a low and constant power for a certain number of minutes so as not to burn the samples. The samples are located at a constant distance from the laser source for all the tests. Each sample is a thin piece with the same shape, and the laser beam is incident normal to the samples' surface. The silicone rubber composite samples have different shades of white after adding fillers, in order to make them to absorb a constant and sufficient heat from the radiation of the laser. All the samples are coated with a thin layer

of graphite. It is assumed that the emissivity is the same for both the conventional and electrospun samples, because, for a relative comparison, an absolute value of emissivity is not necessary. Therefore, the scattering of energy from the incident beam is assumed to be the same for all the samples. Then, the energy can be equally transferred to each sample's surface that abuts the conductive tape. A FLIR-SC500 infrared camera records the temperature distribution on the front side and/or back side of the samples. The setup is illustrated in Figure 2.6.

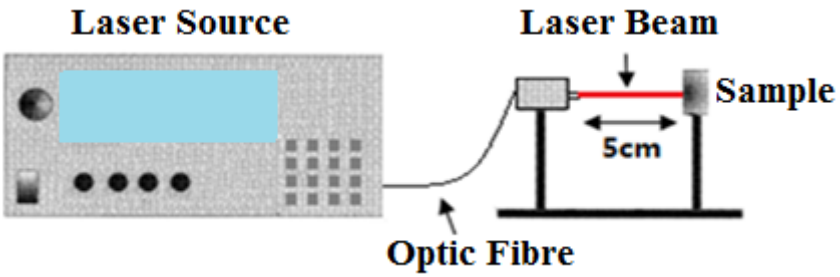

(a)

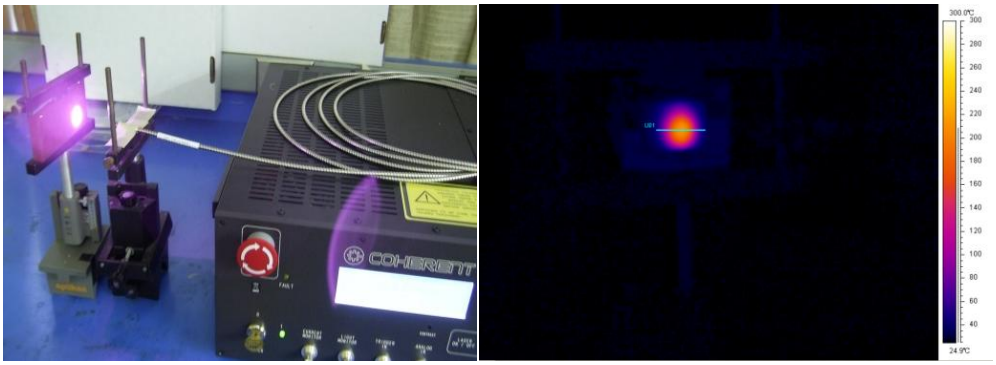

(b) (c)

Figure 2.6: (a) Schematic diagram of the laser setup, (b) the experimental laser setup, and (c) the temperature on the sample surface in the LHTA test measured by an infrared camera.

2.4.7 Erosion and Aging Tests

(a) Laser Ablation Test

The infrared laser-based technique, developed by Meyer et al. [128], is adopted in this research as well. Following the same procedures of LHTA measurement, the same infrared laser is used to produce a constant and stable energy to heat the sample. However, this

time, the heat must be high enough to damage the composites' surfaces. By comparing the eroded masses of the composites, this test analyzes whether the heat resistance of the dielectrics is enhanced. High temperature spots are observed, when a higher energy is available, which can be easily adjusted from the panel of the laser setup by changing the voltage, current, or other variables. The same infrared laser is used in the heat resistance test. The distance between the samples and the laser source is constant. All the arrangements are the same with the LHTA tests, except the power and irradiation time. In the continuous mode, a high and constant power is irradiated on the samples for a constant time. This is the amount of energy that sufficiently damages the sample surface, but does not severely burn the sample. The weight of the samples is measured by a Sartorius balance AC 211S-00MS, with a readability of 100 μg, before and after each test. For each sample, the test is repeated at least three times to attain the average of the eroded mass.

(b) ASTM D 2303 Standard Inclined Plane Test (IPT)

The IPT test procedures in the ASTM D2303 standard [129] are followed to conduct the test in this research. The experimental setup for the IPT test is shown in Figure 2.7. For each formula, six samples of size: 50 mm wide × 130 mm long × 5 mm thick, are tested.

Based on the previous experiments, initial applied voltage of 3 kV is selected for the SiR sample (2 kV for the epoxy resin sample), and the voltage is then increased at a rate of 0.25 kV/h. According to the standard, the test duration is 4 h in order to qualify the acceptability of the samples. In this case, to investigate the voltage-to-tracking for the different samples, the voltage is continuously increased until the tracking length of most of the samples' surface is more than half of the distance (2.5 cm) between the top and bottom electrodes, as observed in Figure 2.7. The flow rate of the NH_4Cl contaminant is 0.3 mL/min, and is increased to 0.4 mL/min, when the applied voltage is more than 3.75 kV. The concentration of the contaminant is 0.1 wt% NH_4Cl and 0.02 wt% nonionic wetting agent, Triton^{TM} X-100, in the deionized water.

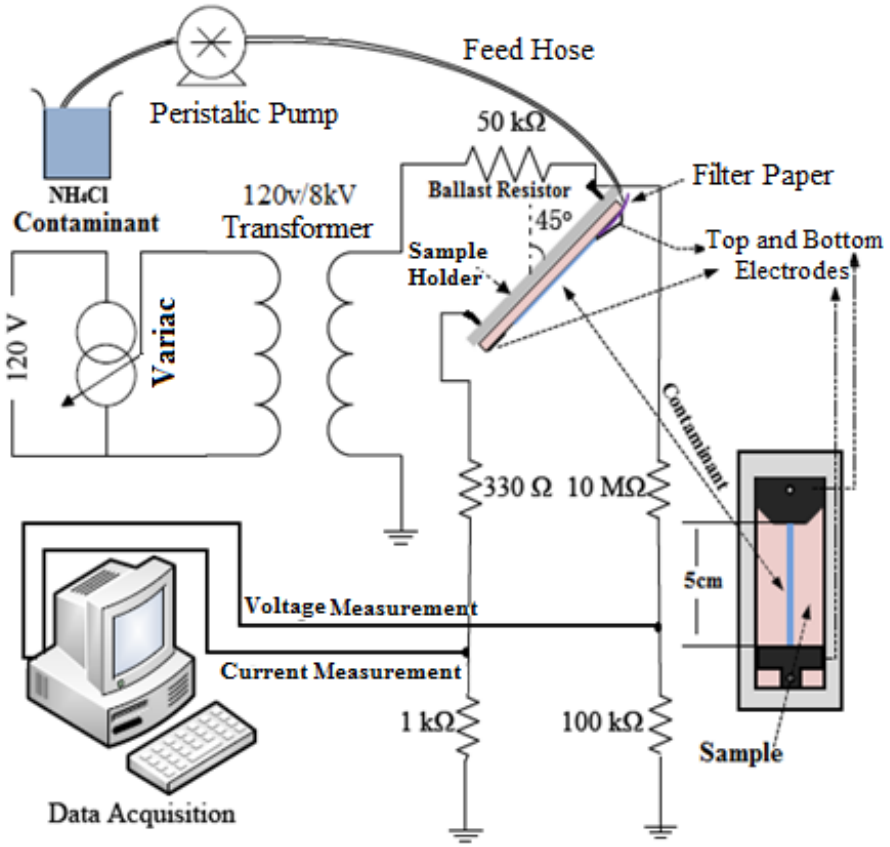

Figure 2.7: Schematic diagram of the IPT test.

During the IPT test, the current and voltage for each sample are recorded on a PC-based data acquisition system. The frequency of the data acquisition card is 100 kHz, and the acquisition card has 16 channels. Each second, four 60 Hz cycles of data are acquired at a sampling rate of 7680/s. According to the acquired voltage and current data, the level of the maximum power consumption is calculated for each sample.

After the test, the samples are inspected and cleaned for further evaluation. The tracking length of each sample or the depth of the erosion area is recorded.

(c) Corona Resistance Test

The objective of the corona test is to determine whether the addition of nanofillers to the SiR base polymer can improve the resistance to discharges, and whether the filler dispersion can influence the corona resistance.

Eight stainless steel electrodes were fabricated according to IEC 60343 standard [130]. Figure 2.8 illustrates the structure and dimensions. Each high-voltage electrode is 6 ± 0.3

mm in diameter, and the silicone rubber composite samples are approximately 5 cm x 5 cm with a thickness of 2 mm. To establish a good contact between the samples and bottom electrodes, the bottom of the sample is fixed to thin aluminum foil with a diameter of 3 cm by silicone oil before being placed on the bottom stainless steel electrode. A voltage of 12 kV is applied in the corona resistance test by using an AC high voltage test system. Each time, 6 samples are tested for 12 hours simultaneously, before any of the samples fail.

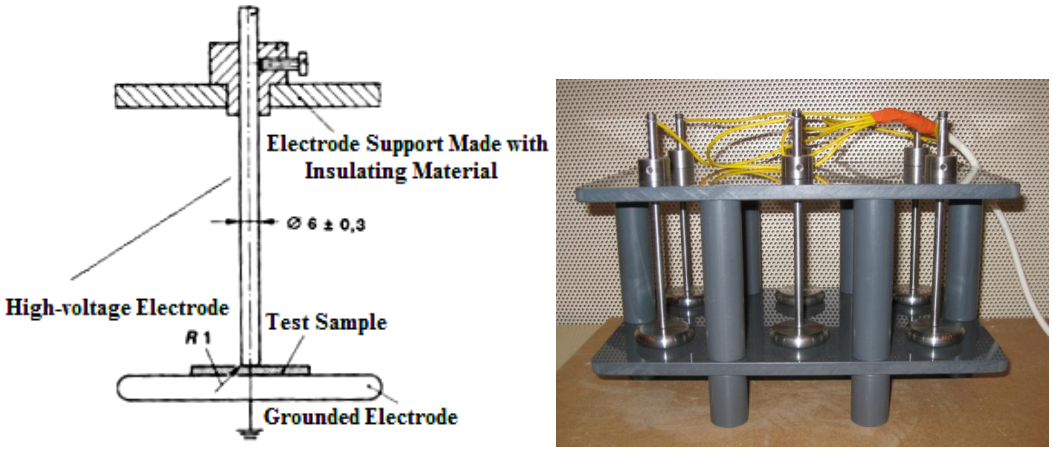

(a) (b)

Figure 2.8: (a) The electrode configuration for the corona resistance test based on IEC 60343 standard [130] , and (b) the assembly of six pairs of electrodes.

After 12 hours of aging, the central parts of samples under the high voltage electrodes are cut and cleaned with ethanol, lastly the morphology of the aged parts is imaged by SEM.

Chapter 3

Results

Uniform filler dispersion is pivotal for obtaining consistent composite properties. Both nanosilica and microsilica were used to study the properties of SiR composites, and epoxy resin was also used to confirm some aspects of the dispersion. According to the sample preparation in section 2.2, the performance evaluation procedures in section 2.4, and the thermal modelling in section 2.5, conventional and electrospun nanocomposites are prepared separately to investigate the effect of the nanofiller dispersion on the final composite properties.

In the first stage, nanosilica is dispersed in the SiR matrix. Several analysis methods are used to compare the electrospun composites and conventional composites to assess their electrical, mechanical, and thermal properties. The best improvement observed is the thermal performances for the SiR nanocomposites such as thermal degradation and heat erosion resistance. Therefore, in the second stage to further enhance the improved thermal properties, the nanocomposites are reinforced by microsilica. The effects of the nanofiller dispersion on the thermal stability, thermal degradation, and thermal resistance of microcomposites and nanocomposites; and the interactions between fillers and between filler and matrix are carefully investigated. In the last stage, to examine the application scope of electrospinning for dispersion, and also to conduct some further analysis epoxy resin composites are prepared and compared in the similar way as the SiR composites. The dispersion morphology, EDX elemental analysis, and heat erosion resistance of the epoxy resin composites are presented in this chapter. In addition, a simplified 2D thermal model is developed to analyze and understand the effect of the filler dispersion on the local temperature distribution of the composites.

3.1 Performance of Silicone Rubber Nanocomposites

3.1.1 Morphology Observation

The filler dispersion in the SiR matrix is analyzed by SEM analysis. The SEM images, in Figure 3.1, exhibit the morphology of the cross-sections of the samples with different formulas. In Figure 3.1 (a) and (b), the SEM images on the right side are for conventional samples, and the left sides are the SEM images of electrospun samples.

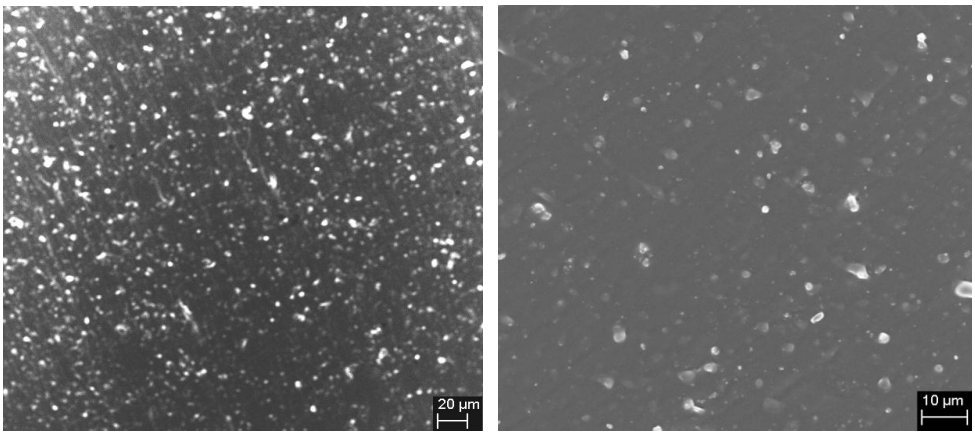

(a)

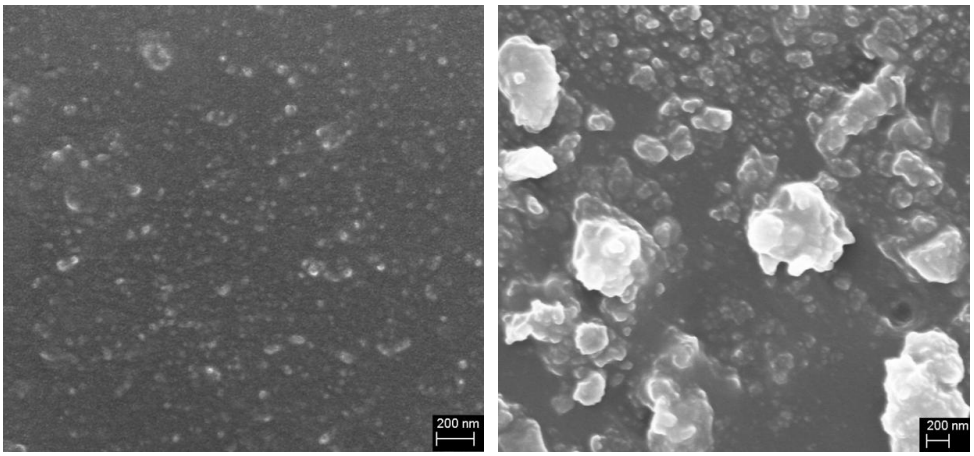

(b)

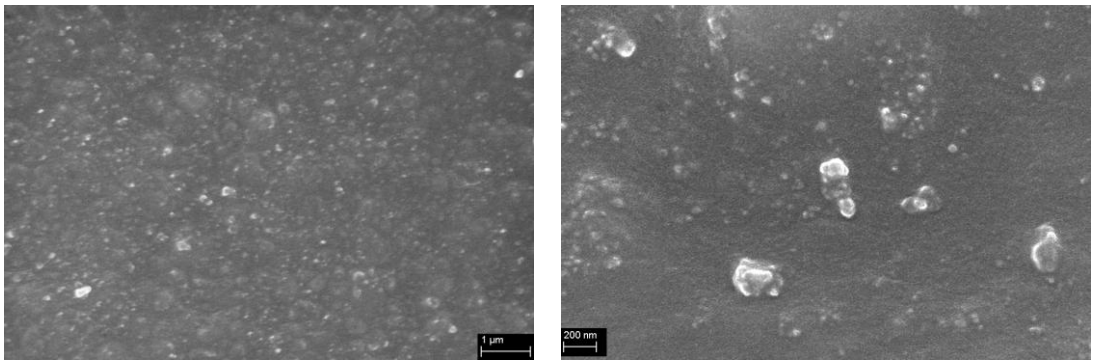

(c)

Figure 3.1: The morphology of silicone rubber nanocomposites with different nanosilica loadings, prepared by using two methods, (a) 3 wt% nanosilica-filled SiR, (b) 6 wt% nanosilica-filled SiR, and (c) 10 wt% nanosilica-filled SiR. Left columns are ES samples, and right columns are CS samples.

It is evident that the electrospun samples exhibit reduced filler agglomerations and a more homogenous filler dispersion than the conventional samples. Although the filler agglomerations in electrospun samples still cannot be fully avoided, the filler clusters are still in the acceptable nano-scale, confirming the improved dispersion of the nanofiller.

Due to the limitations of the mechanical mixing process, the silicone rubber composites with 10 wt% nano-fumed silica are prepared only by electrospinning, because the viscosity of this mixture is too high to be handled by a mixer. In the presence of the solvent and with the better dispersion of the nanofillers, a 10 wt% electrospun silicone rubber nanocomposite is easily prepared. The dispersion of the nanosilica for such a high filler loading level is still homogenous, as shown in Figure 3.1 (c).

3.1.2 Contact Angle Comparison

The contact angles on the flat surface of the silicone rubber nanocomposites are measured to examine whether the surface condition of the composites are changed by the filler dispersion. After following the procedures in section 4.3.2, the contact angles on the composite surfaces are photographed over times as shown in Figure 3.2.

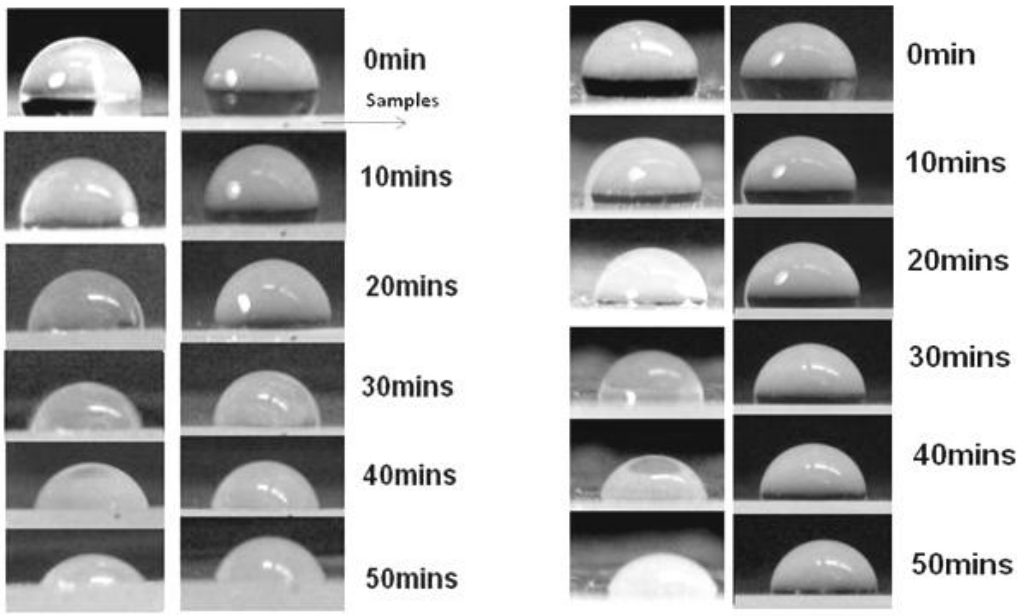

(a) (b)

Figure 3.2: The variation of a droplet of 10 μL deionized water on the nanocomposite's surfaces. The left columns in each figure show samples mixed by the mixer, and the right columns, by the electrospinning: (a) silicone rubber composites with 3 wt% nanosilica, and (b) silicone rubber composites with 6 wt% nanosilica.

Figure 3.3 depicts the curves of the contact angles on the surfaces of the nanomaterials as a function of time. The contact angles on the electrospun samples are greater than those on the unfilled silicone rubber. For different formulas, all the contact angles on the electrospun samples change slowly over time. However, the contact angles on the conventional samples, at first, exhibit almost no change, compared to those of the unfilled rubber, and even worsened over time.

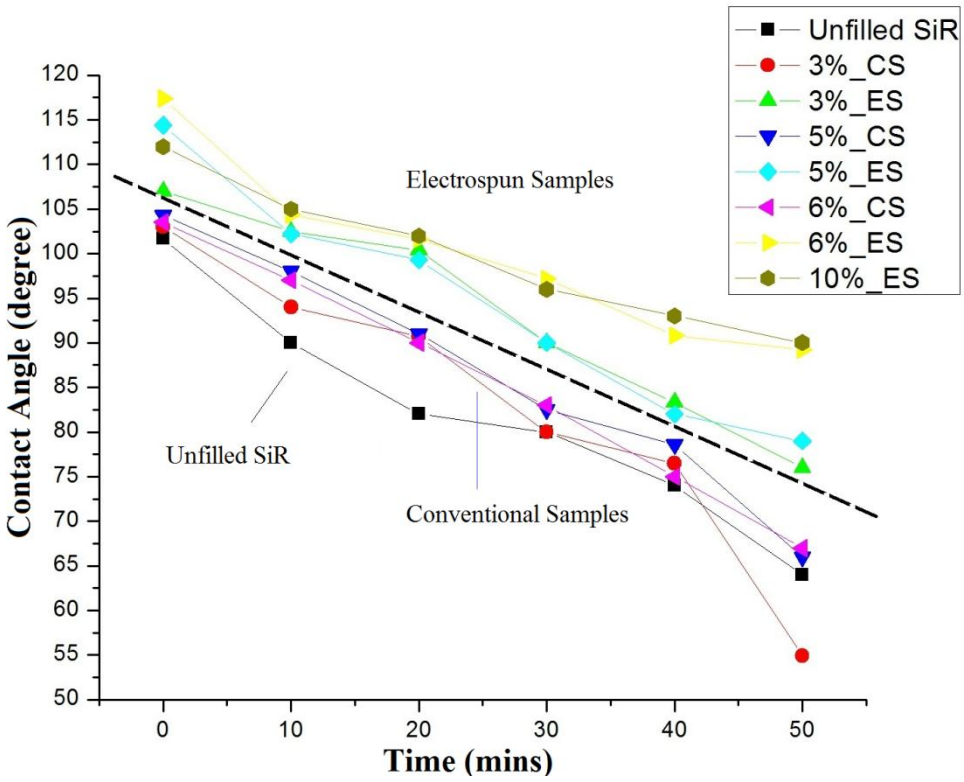

Figure 3.3: Static contact angle as a function of time on flat surfaces of various nanocomposites (ES=electrospun samples; CS=conventional samples).

After the possibility of using the electrospinning technique to disperse nanofillers in dielectrics is confirmed, the SiR nanocomposites are evaluated from the electrical, thermal, and mechanical perspectives. The results are presented below.

3.1.3 Mechanical Properties

The mechanical properties such as tensile strength, elongation at break, and hardness are crucial bulk material parameters for composite materials. These parameters are sensitive to the type of filler, the loading, and the interaction between the filler and the matrix. Typically, the optimum filler loading should achieve a balance among the mechanical properties. To study the effect of the filler dispersion on these characteristics, the conventional samples and the electrospun samples are compared for filler concentrations ranging from 3 to 10 wt%. The results are shown in Table 3.1.

Table 3. 1: The Mechanical Properties of the SiR Nanocomposites.

Samples	Tensile Strength (Mpa)	Elongation at Break (%)	Hardness
Pure SiR	5.53	142	47.2
3%_CS	5.96	150	48.5
3%_ES	6.20	142	49.6
6%_CS	6.53	140	55.8
6%_ES	6.75	168	56.2
10%_ES	6.99	169	58.5

CS: conventional SiR Sample; ES: Electrospun Sample.

After the addition of the nanofillers to the silicone rubber, the mechanical properties do improve with the increased filler loading. The noticeable improvement is the elongation at break indicates a better tension tolerance for the electrospun samples compared to the conventional samples. Other than that, there is no significant difference is observed between the mechanical properties of the conventional samples and those of the electrospun samples. The increased mechanical properties of the composites are believed to be the stronger interactions between the polymer and fillers. If the fillers disperse uniformly and fewer agglomerations are present in the base polymer, stronger interaction occurs between the fillers and the polymer matrix, filler and matrix can be better bonded.

3.1.4 Dielectric Constant

The dielectric constant (permittivity) is measured at three different frequencies (2 kHz, 10 kHz, and 100 kHz) for samples with filler loadings from 3 to 15 wt%, and a fitted curve is then obtained based on the test points, as reflected in Figure 3.4.

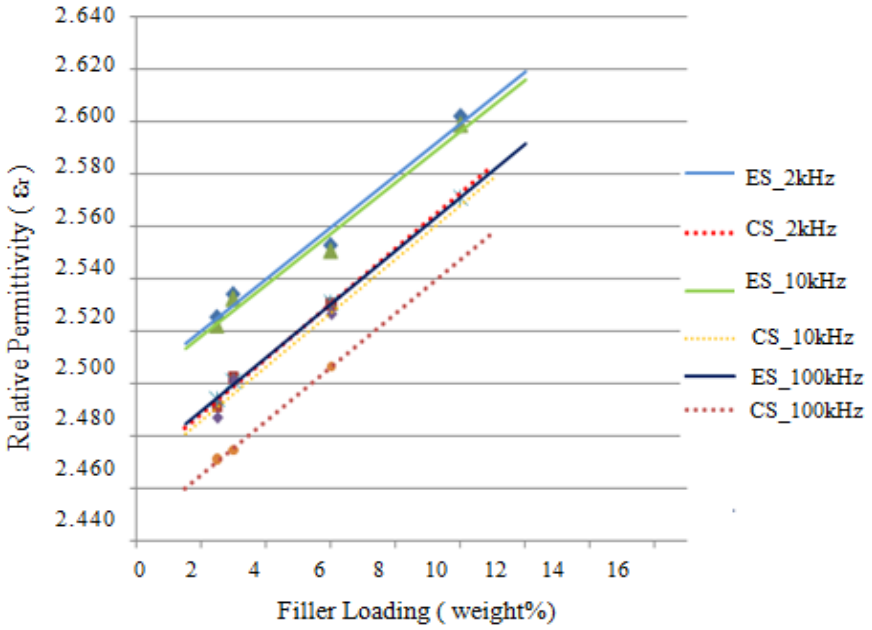

Figure 3.4: The relative permittivity of the composites as a function of the frequency. (ES = electrospun sample; CS = conventional sample).

The relative permittivity of the composites is increased as the filler concentrations are increased, but no significant difference is exhibited between the two methods. The similarity of the results is likely due to the averaging effect of using bulk materials. Another possible explanation is that both nanosilica and silicone rubber have low relative permittivity values: approximately 2.7-3.8. Therefore, significant difference between the two methods for the same filler-loading level is not expected. The results reconfirm the evidence that the ethanol solvent entirely disappears from the electrospun samples.

3.1.5 Thermal Properties

(a) TGA Results

To investigate a possible improvement in the thermal stability and thermal degradation due to the improved dispersion of the nanofiller, a TGA analysis is conducted. The results of the unfilled pure silicone rubber are compared with those of the nanocomposites with 3 and 6 wt% nanosilica fillers. Each is prepared by using the two methods discussed in the Section 2.2. The TGA curves are shown in Figure 3.5.

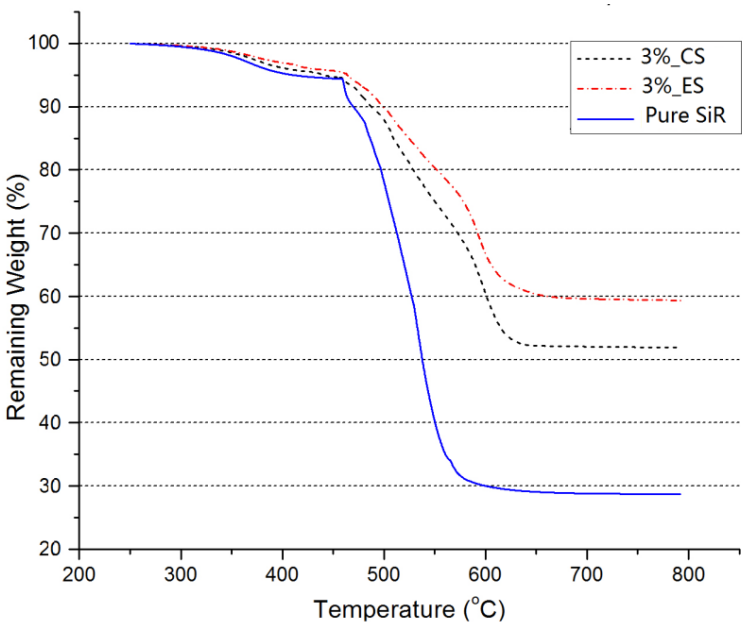

(a)

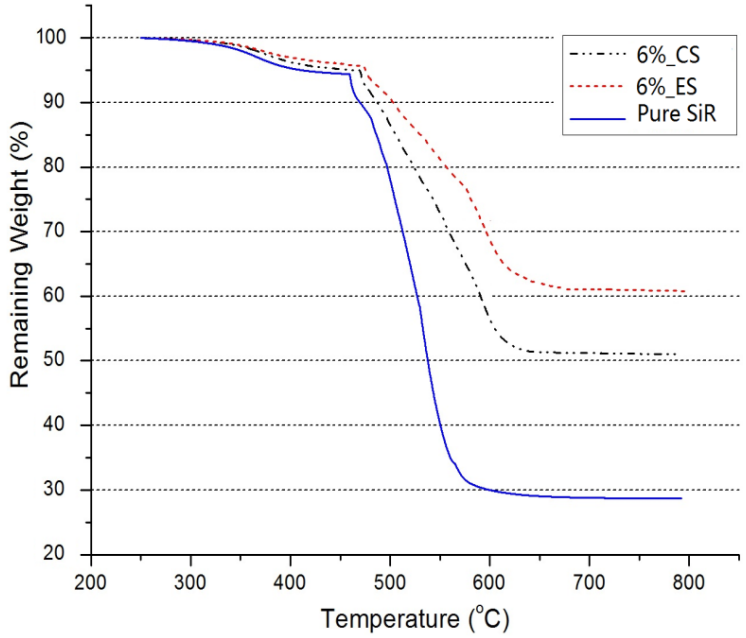

(b)

Figure 3.5: The thermal degradation of the unfilled silicone rubber and nanosilica-filled silicone rubber composites, prepared by two methods (ES = electrospun sample; CS = conventional sample) (a) with 3 wt % nanosilica, and (b) with 6 wt % nanosilica.

For both formulas, the rate of change in weight is about 0.18 (% /^{o}C) for the electrospun samples with a remaining weight of about 60 %, and 0.26 (%/^{o}C) for the conventional samples with a remaining weight of about 50 %, respectively. However,

the weight change is more rapid for pure silicone rubber: about 0.56 (%/^{o}C) with a remaining weight of about 28 % as expected.

(b) Thermal Conductivity of the Composites

The measured thermal conductivity of the nanosilica composites with different filler concentrations and mixing methods are listed in Table 3.2.

Table 3.2: Thermal Conductivity of the Nanocomposites Based on Modified. ASTM D5470 [88].

Formula	Thermal Conductivity (W/mK)
3 wt%_CS	0.23
3 wt% _ES	0.22
6 wt%_CS	0.25
6 wt% _ES	0.28
10 wt% _ES	0.27

Note: The thermal conductivity of pure SiR is around 0.19 and the thermal conductivity of silica is around 1.5.

There is no significant difference in the thermal conductivity between the composites with different filler concentrations in terms of the two mixing methods. It is evident that microsilica can enhance the thermal conductivity of the SiR composites at a large volume fraction. Thus, the reason for the inconspicuous difference in the thermal conductivity of the nanofilled silicone rubber composites may be due to the low nanofiller concentration that the percolation threshold of fillers for a significant thermal conductivity change has not been reached. There are many factors affecting the thermal conductivity of composites, including the filler size, filler loading, and distribution of the fillers. Therefore, improving only the dispersion of the nanofillers may not be enough to obtain a high thermal conductivity of the composites. In future

studies, high conductivity nanofillers such as nano boron nitride and CNTs should be chosen to enhance the thermal conductivity of the composites.

(c) Thermal Profile Analysis

The laser-based thermal profile analysis is conducted in order to study the local thermal characteristics of the nanocomposites. A laser power of 0.9 watts is applied to the sample surface, for three minutes without burning the samples. The samples are located 5 cm from the laser source for all the tests. Each sample is 6 mm thick, and the laser beam is incident normal to the samples' surfaces. The thermal profiles are shown in Figure 3.6.

The temperature decreases with the increased concentrations of the filler, but only at 6 wt% filler loading is the temperature notably reduced. It can be readily understood that the fraction representing the volume of filler is a factor that strongly affects the transfer of heat. The profile for the electrospun samples on the surface of the laser-incident side results in the temperatures of approximately 7 to 11 ^{o}C lower than those for the conventional samples. Apparently, an optimum heat transfer depends on the filler loading and the filler interaction and distribution. Although the global thermal conductivity is not improved but thermal profiles suggest that the "localized" thermal conductivity of the electrospun samples is higher than that of the conventional samples for the same filler loading, a condition which can be attributed to the reduced nanofiller agglomeration and the enhanced interaction between the filler and the base polymers.

Figure 3.7 confirms the repeatability of this analysis by obtaining the thermal profiles from different areas on the surface of 10 wt% electrospun SiR nanocomposites.

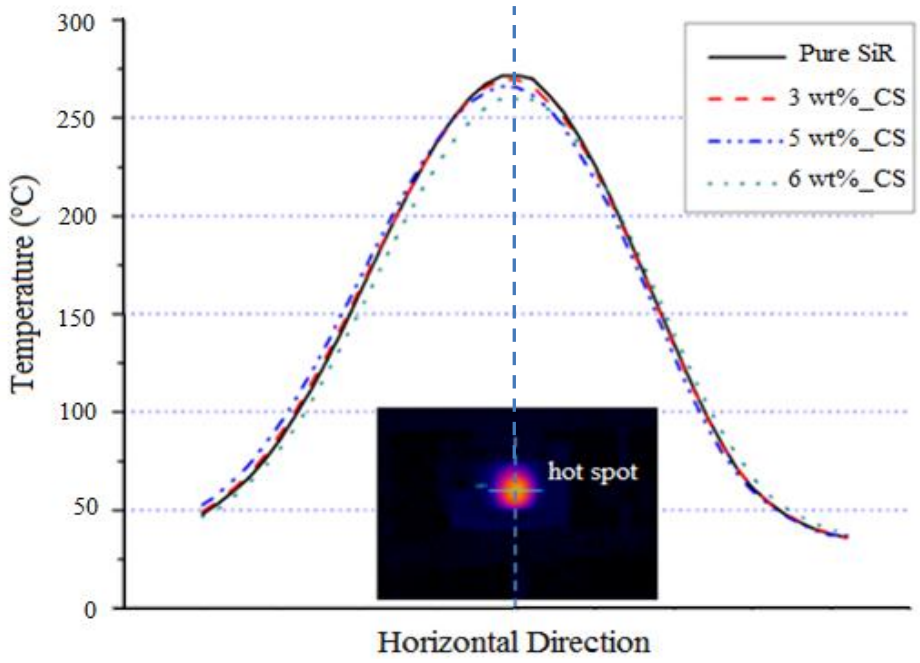

(a)

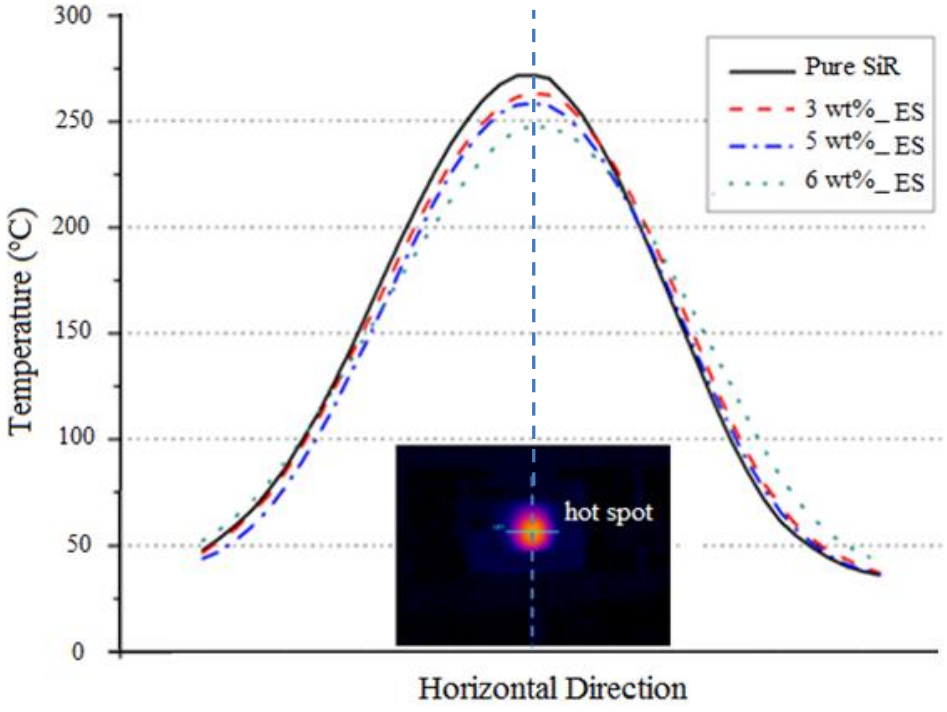

(b)

Figure 3.6: The thermal profiles of the maximum temperature along a line that passes through the center of the laser-heated area on the surfaces of the samples, (ES = electrospun sample; CS = conventional sample), (a) The thermal profile for the conventional samples and pure silicone rubber, and (b) the thermal profile for the electrospun samples and pure silicone rubber.

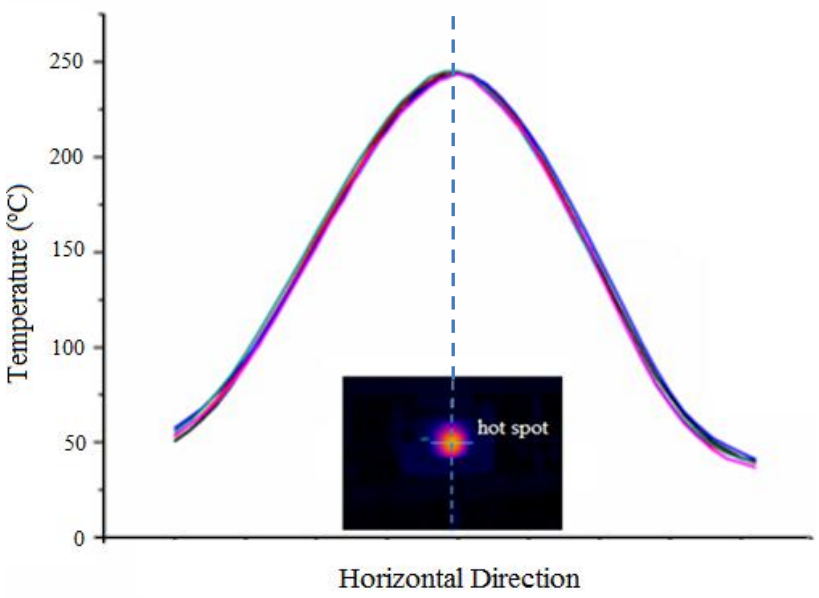

(c)

Figure 3.7: The temperature profiles of the different areas along a line passing through the center of the laser-heated area on the surface of the 10wt% electrospun SiR nanocomposite (ES = electrospun sample; CS = conventional sample).

To analyze the effect of filler size and dispersion on the local temperature distribution of the composites, a simple 2D model is employed. The simulated microsilica and nanosilica filler size are 5μm and 500 nm, respectively. The details of the simulation settings are provided in the Appendix B. The results of the temperature distribution for pure silicone rubber, microsilica and nanosilica filled silicone rubber composites from the simulation are shown in Figure 3.8 and Figure 3.9.

From the simulation results, the advantages of using the nanofillers are well demonstrated. Figure 3.8(c) shows that the nanofillers compel a more uniform temperature distribution than that of the microfillers, shown in Figure 3.9 (b). The temperature distribution along the vertical direction for the unfilled silicone rubber sample is 486-463 K; for the microsilica filled sample, it is around 462-458 K; and for the nanosilica-filled sample, it is 462-443K. The simulation results confirm that the addition of fillers reduces the maximum temperature on the sample's surface and the nanofillers dissipate the heat better; thus keeping the maximum temperature in

nanosilica-filled composites less than the microsilica filled samples, even though the loading of the microfillers is more than that of the nanofillers.

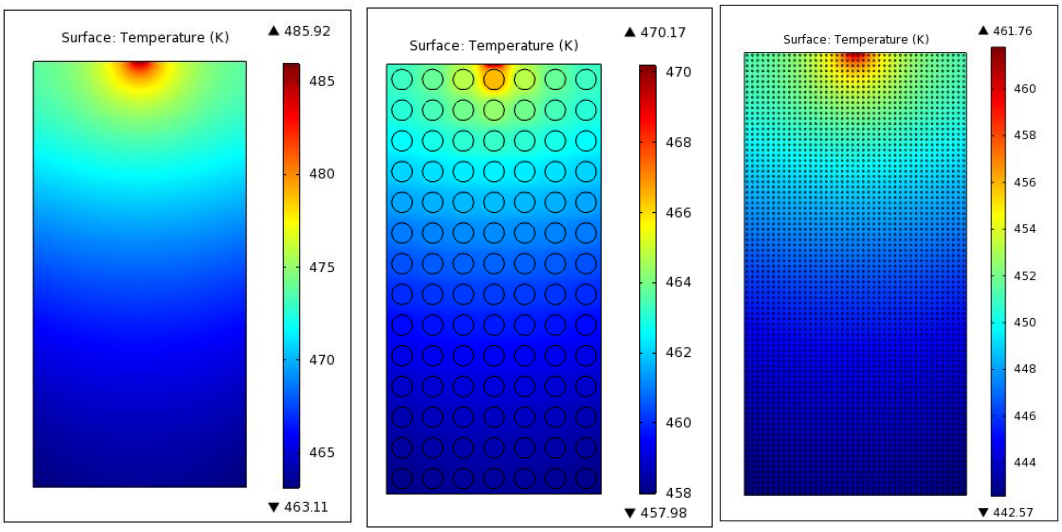

(a) (b) (c)

Figure 3.8: The temperature distribution in the 2D models (a) unfilled SiR (b) microsilica-filled SiR, and (c) nanosilica-filled SiR.

Figure 3.9 displays the temperature trends in the horizontal direction of the samples, where the temperature along the sample surface passing through the center of the heat source.

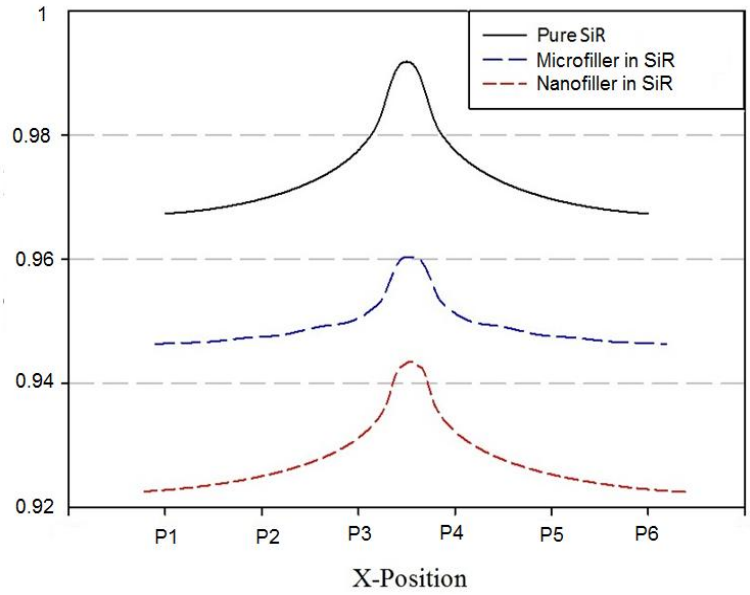

Figure 3.9: The temperature distribution trends along a line passing through the center of the heat source on the surface of simulated samples, (a) unfilled pure SiR, (b) micron silica filled SiR ,and (c) nanosilica filled SiR

The temperatures in the horizontal direction decrease for the inorganic filler-filled samples. The nanosilica filled sample demonstrates the most substantial temperature reduction. These temperature trends are similar to those experimental thermal profiles shown in Figure 3.6.

Well dispersed nanofiller prepared by electrospinning leads to a lower and even temperature distribution than those of unfilled silicone rubber or silicone rubber which is filled with microfiller or agglomerated nanofiller. Therefore, it is inferred that homogeneous distribution of nano fillers assists in dispersing the heat well; hence, resulting in reduced thermal stresses in the composites.

(d) Heat and Erosion Resistance of Nanofilled SiR Composites

For the erosion resistance test, for the samples to absorb the same energy, a thin slice of a black semi-conductive layer of non-woven polyester fleece is fastened onto the surface of the sample. The fabric, on the nanocomposites is impregnated with conductive resin and is carbon loaded. As with the previous test LHTA measurement, the samples are located 5 cm from the laser source, but for this test, the laser beam irradiates the samples for 1 min with a sufficient power of 3.6 W to erode the sample but not to damage the black slice. For each sample, this test is conducted at least three times to attain the average.

For the nanofumed silicone rubber composites, the eroded masses of samples with different filler concentrations in terms of the two mixing methods: conventional mixing and electrospinning are given in Figure 3.10.

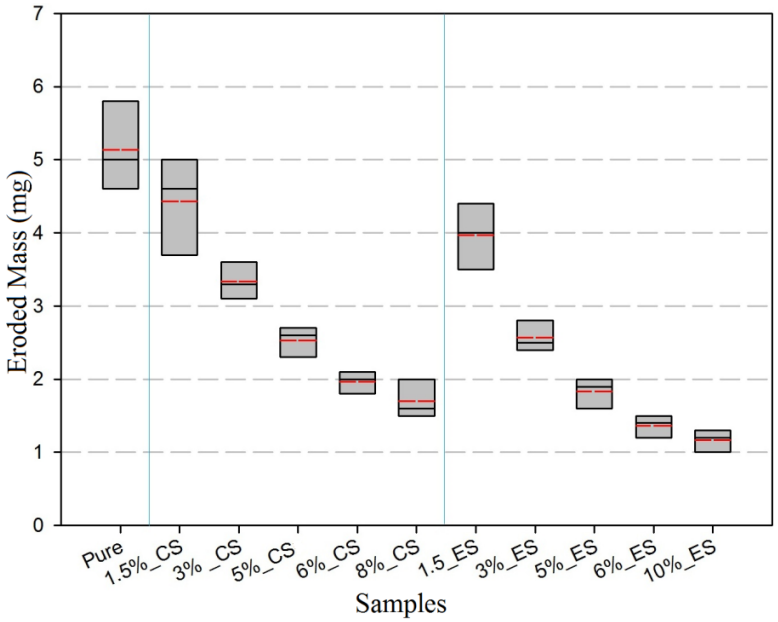

Figure 3.10: The average eroded mass after three repetitions of the laser erosion tests for pure silicone rubber and nanosilica-filled conventional samples and electrospun samples (ES = electrospun sample; CS = conventional sample).

The average eroded mass is represented by a red dash line in each box. The boundary of the box that is closer to zero indicates the 25th percentile, and the other boundary that is farther from zero indicates the 75th percentile. The solid black line in the box represents the median value. All of the eroded mass plots included in this thesis follow the same designations. The plots of the values for the eroded mass indicate that the weight loss decreases almost linearly with the increased nanosilica concentrations. Compared to the unfilled silicone rubber, the electrospun sample with 10 wt% nano-fumed silica exhibits an improved amount of eroded mass of about 80%, with a small variation. Also, the 8 % conventional samples demonstrated a reduced amount of eroded mass, but the variation is larger than that for the electrospun sample, which may imply a nonuniform distribution of filler. As expected, the overall extent of the reduction in the eroded mass for the electrospun samples is higher than that for the conventional samples, which matches the results of the TGA test as well. However, it should be noted that the slopes of the eroded mass curves for all the methods are not as steep, possibly because the nanofiller loading neared saturation and the dispersion of the filler becomes more difficult and not as effective.

Although the nanofillers improve the properties, it is difficult to add lots of nanofillers into polymers. Also, from a cost-savings perspective, microfillers are usually loaded into polymers at more than a 30 wt% in the industry. Therefore, the optimum performance of the composites may result from a combination of nanofillers and microfillers. The addition of a large amount of microfillers can lower the cost of composites and the combination of nanofillers can further improve the properties of composites. Based on the performance results of the silicone rubber nanocomposites, the significant improvements of the nanosilica-filled silicone rubber composite come from the thermal properties, especially the heat erosion resistance. Therefore, for both nano and micro silica enhanced silicone rubber composites, the focus is on the further improvement of heat erosion resistance.

3.2 Performances of Nano-Micron-filled SiR Composites

Based on the results presented in the previous section, a uniform dispersion of the nanosilica in the silicone rubber by using the electrospinning technique is confirmed. Nevertheless, 7 nm nanosilica cannot be loaded at more than 10 wt% due to the large volume fraction of nanofillers and the increased viscosity of composites because of the addition of nanofillers and the processing limitation.

The samples are again prepared by two methods: electrospinning and conventional high shear force mixing. After the RTV 615-A silicone rubber and nanosilica are mixed by high shear force or by electrospinning, as mentioned in section 2.2, the collected compound are then mixed with microsilica using high shear force mixer before adding the RTV 615-B curing agent. For the laser ablation test, a small amount of iron oxide (Fe_2O_3), 2.5 wt% of the microsilica weight, is added to all the samples to obtain the same absorption. The vacuum and cure procedures are the same as those for the silicone rubber nanocomposites.

3.2.1 Heat and Erosion Resistance of Nano-Micron-filled SiR

It is difficult for the high shear force mixer to handle more than 6 wt% nanosilica, for both the conventional and electrospun samples, the nanosilica is kept constant at 5 wt% (a high nanofiller loading). This nanofiller loading is considered for all the formulas, and the weight percentage of the microsilica keeps increasing on the basis of 5wt% nanosilica until the maximum.

For each formula, three laser erosion tests are conducted. The distance between the sample and the laser tip is 5 cm so that the laser beam is incident normal to the surface of the sample. Each sample is irradiated by the laser beam for three mins, with a constant power of 5.5 watts. The values for the eroded mass of the different SiR composites with 5 wt% nanosilica and 10 to 40 wt% microsilica are shown in Figure 3.11.

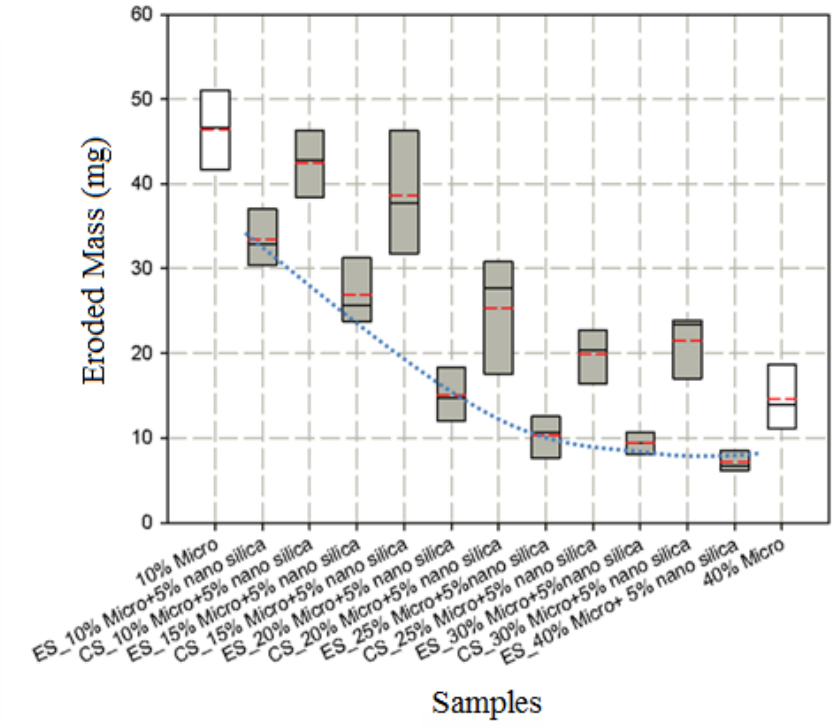

Figure 3.11: The eroded mass for the formulas with 5 wt% nanosilica and 10 wt% to 40 wt% microsilica (ES = electrospun sample; CS = conventional sample).

For the conventional samples, the maximum microsilica loading is 30 wt% microsilica plus 5 wt% nanosilica, which is difficult to process with the high force

shear mixer. However, for the electrospun samples, the maximum loading of microsilica is 40 wt%. The compounds with the same weight percentage of microsilica loading are much easier to mix for the electrospun samples than for the conventional samples, which probably contributes to the uniform dispersion of the nanosilica. In addition, only the 10 and 40 wt% microsilica-filled composites are prepared as references. All micro-filled samples are represented by the white boxes in the eroded mass plots in Figures 3.11, 3.13, and 3.14.

In Figure 3.9, the plot of the eroded mass shows that, as expected, the eroded mass of almost each formula is mitigated when the microsilica loading is augmented. Compared with the conventional samples, the electrospun samples exhibit a significantly greater reduction of the eroded mass, and the variation in the eroded mass for each electrospun sample is also much smaller. For the samples filled with 5 wt% nanosilica and 10 wt% microsilica, the eroded mass is lower by only about 8% for the conventional sample, but by about 28% for the electrospun sample, compared to the eroded mass of the 10 wt% micro-filled sample. For the electrospun sample with 5 wt% nanosilica and 40 wt% microsilica, the eroded mass is improved by almost 85% compared to that of the 10 wt% micro-filled sample. The result is an approximate a 54% improvement compared to the eroded mass of the 40 wt% micro-filled sample. All of these results confirm the advantage of using a combination of microfillers and a small amount of nanofillers to improve the erosion behaviour of the SiR composites. Some of the surface patterns for the laser erosion tests are apparent in Figure 3.12 (a) and (b).

To study the erosion resistance of the electrospun samples with a high filler loading and to determine what percentage by weight of the nanosilica can be combined by using the electrospinning technique, the 40 wt% microsilica amount is kept constant, and 5 wt% to 10 wt% nanosilica is combined as long as the samples are still easy to process. Due to the small eroded mass of the electrospun sample filled with a 40 wt% microsilica and a 5 wt% nanosilica, as shown in Figure 3.10, the laser power is set to 6.5 W to verify the results of the eroded test but at a slightly higher

filler loading. The plot of the eroded mass is shown in Figure 3.13. It displays that the amount of the eroded mass that can be further improved if more nanosilica is loaded, but the rate of reduction is slow. No significant changes are observed, when the nanosilica is loaded at such high levels, like 5 to 10 wt%.

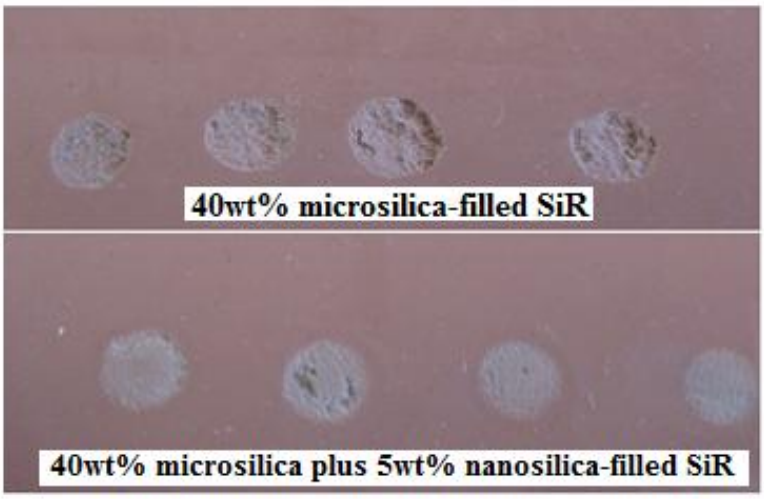

(a)

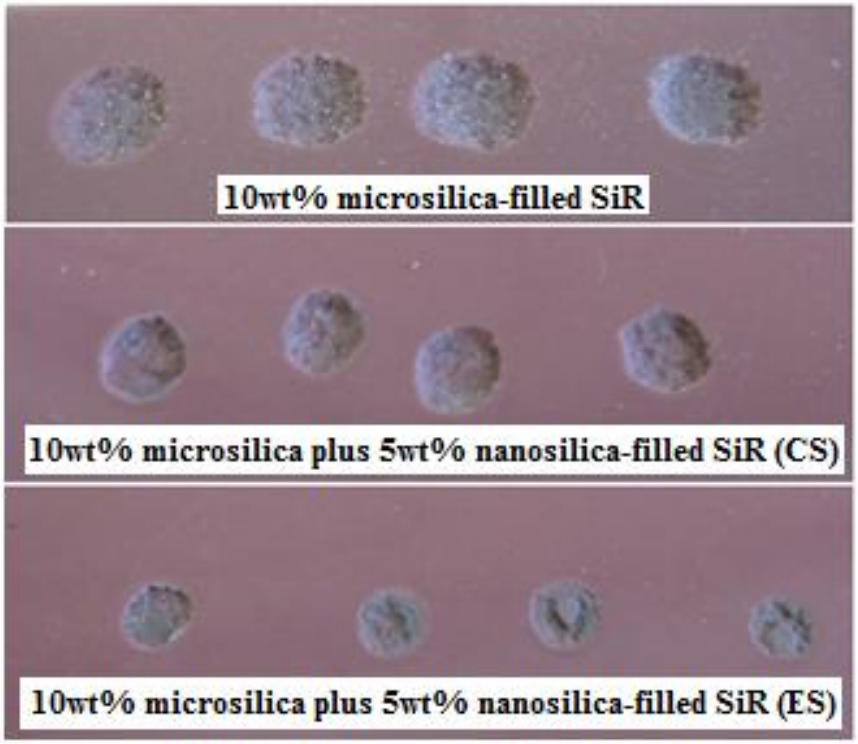

(b)

Figure 3.12: The surface patterns of the samples in the laser erosion test.

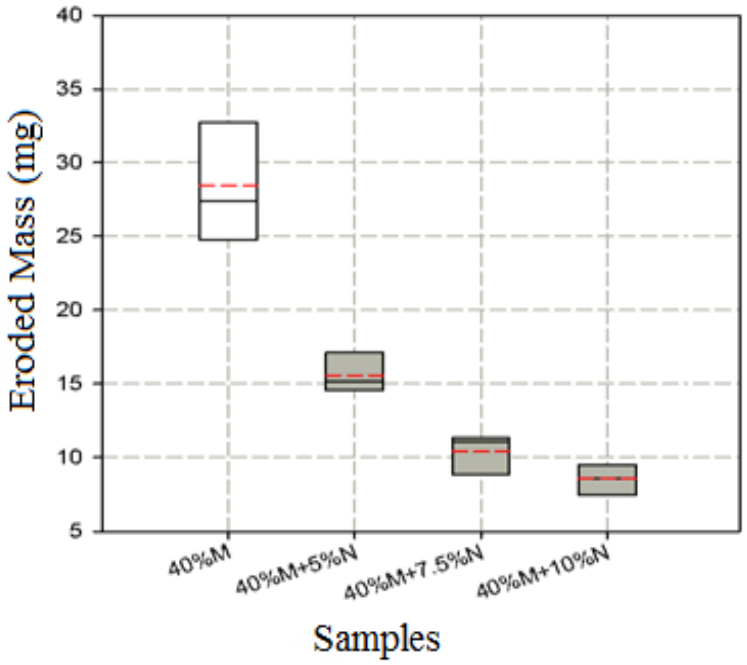

Figure 3.13: The eroded mass for the electrospun samples with 40 wt % microsilica and 5 to 10 wt% nanosilica (ES = electrospun sample; CS = conventional sample).

Based on the previous tests and the difficulty of the sample preparation, the samples with 20 wt% microsilica and 2.5 wt% to 6 wt% nanosilica are selected to be evaluated by the laser-based erosion test and the IPT test. At these filler loadings, the high shear force mixer can still handle the conventional samples, and the filler loading is also not too low for industrial requirements. The applied laser power is 5.5 W. The plot of the eroded mass is presented in Figure 3.14. It is obvious that the results of the electrospun samples are better than those of conventional samples. The eroded mass of the SiR composite is reduced with the increased nanosilica loading, but the reduction is not linear.

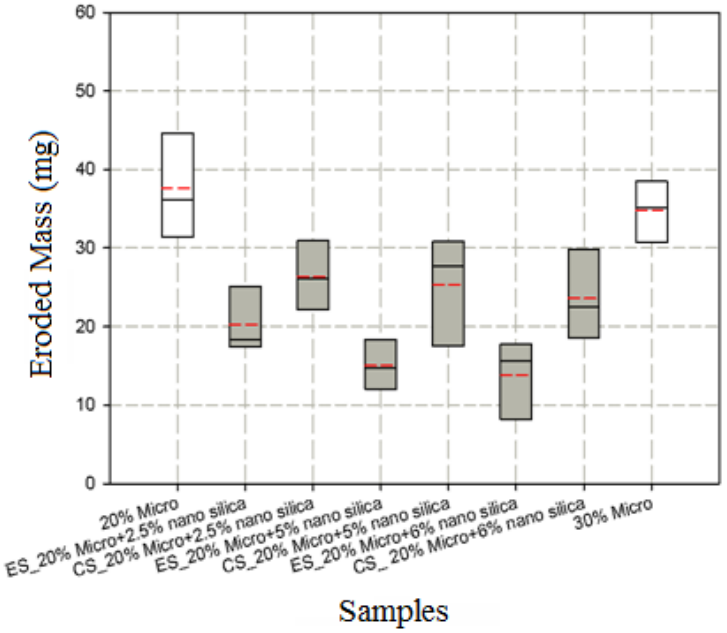

Figure 3.14: The eroded mass for the formulas with 20 wt% nanosilica and 2.5 to 6 wt% microsilica; 20 and 3 wt% microsilica-filled samples are used as references (ES = electrospun sample; CS = conventional sample).

3.2.2 Inclined Plane Test (IPT) Comparison

The laser erosion test reflects the heat resistance that characteristic of the SiR composites mainly in terms of the thickness, and the voltage-to-tracking IPT test reflects the heat resistance that characteristic of the SiR composites mainly along the surface of the sample.

For the IPT test, the applied voltage is continually increased, until the tracking length on all or most of the six samples reach 2.5 cm, which is the midpoint of the distance between the top and bottom electrodes. During the IPT test, when the tracking length of any of the six samples exceeds the 2.5 cm position or when any of the samples begins to burn (i.e., the erosion is deep but does not propagate along the surface), the voltage applied to that sample is removed, and the test is continued for the other samples. Consequently, the duration of the test for the different formulas is proportional to the applied voltage, which is increased by 0.25 kV every hour during the voltage-to-tracking IPT test. This relationship means that if the sample can

withstand a higher voltage, it takes longer to attain the tracking length. Figure 3.15 shows the duration of the IPT test plotted in relation to the formulas.

As with the plot of the eroded mass, the average time is represented by a dash line in each box. Based on the results of the IPT test, the best formula is the electrospun sample with a loading of 20 wt% microsilica plus 5 wt% nanosilica (in the dotted circle) in the filler loading range considered. The average test time indicates that this formula can withstand 290 min (4 h and 50 min) of the IPT test with an applied voltage of 3 kV to 4 kV.

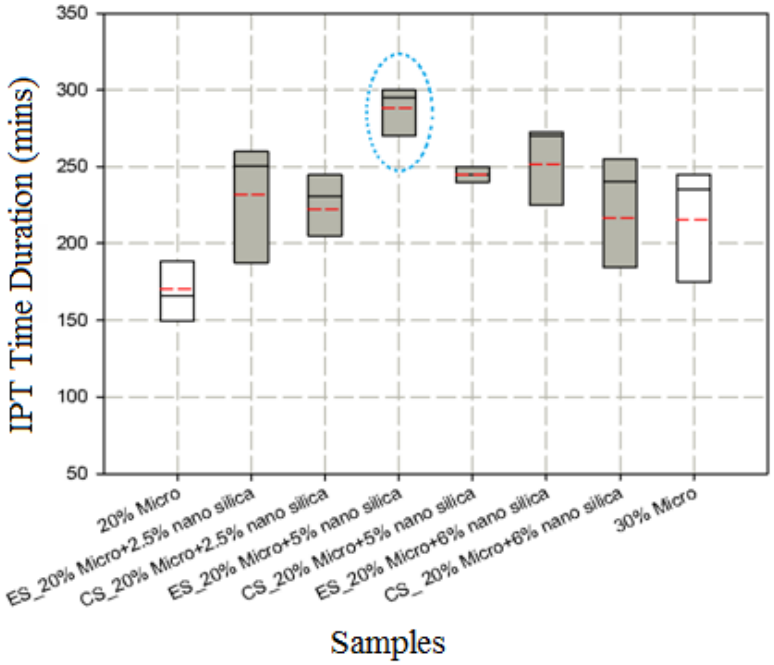

Figure 3.15: The IPT test durations for the different formulas with 20 wt% nanosilica and 2.5 wt% to 6 wt% microsilica. 20 wt% and 30 wt% microsilica-filled samples are used as a references (ES = electrospun sample; CS = conventional sample).

Figure 3.15 indicates that the best formula is the 20 wt% micro plus 6wt% nano-filled electrospun sample, but that there is no significant improvement with this formula compared to the 20 wt% micro plus 5 wt% nano-filled electrospun sample with respect to the average eroded mass. Therefore, based on the laser erosion test and the voltage-to-tracking IPT test, of all the test formulas considered, the optimum combination of fillers for the SiR composites is 20 wt% microsilica plus 5 wt% nanosilica. It is interesting to note that when the nanofiller loading of the samples is more than 5 wt%, the

tracking behaviour deteriorates somehow. This effect may also relate to the dispersion of the nanofiller, or it may indicate that in the case of the nanofillers, a higher concentration is not necessarily very beneficial.

The surface patterns of the SiR composites with 20 wt% microsilica plus 5 wt% nanosilica for the conventional and electrospun samples are shown in Figure 3.16. The six conventional samples are displayed in the top row, and the electrospun samples appear in the bottom row.

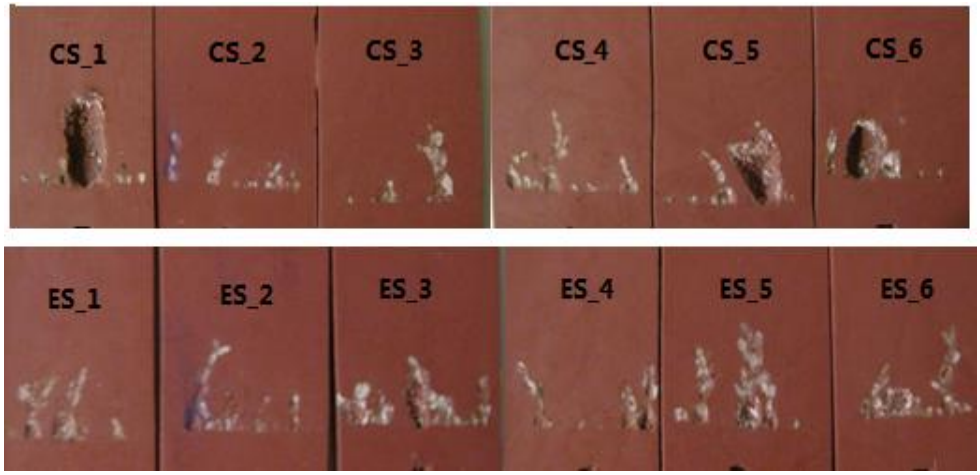

Figure 3.16: The surface erosion patterns of conventional and electrospun samples (with 20 wt% microsilica plus 5 wt% nanosilica loading) after the IPT test.

The duration of the IPT test for the electrospun sample is almost 50 mins longer than for the conventional sample, as shown in Figure 3.15. During this time, the applied voltage was 4 kV and 3.75 kV for the electrospun and conventional samples, respectively. The surface patterns of the electrospun samples are almost identical with no deep erosion. However, for the conventional samples, the surface patterns vary with three of them exhibiting severe tracking erosion (CS_1, CS_5, and CS_6). The measured global thermal conductivity of above electrospun sample and conventional sample are 0.5 W/ m Ŧ and 0.31 W/ m Ŧ, respectively. Also, the hardness of above samples is measured according to the procedures in section 2.4.4 and the results are provided in Figure 3.17. The variations in the hardness may somehow imply non-uniformity filler distribution in the conventional samples.

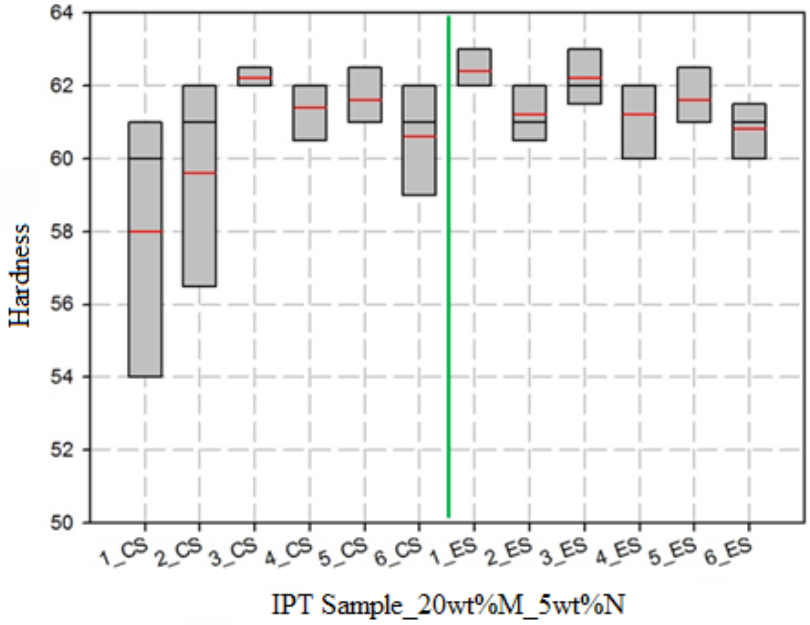

Figure 3.17: The hardness of conventional and electrospun samples with 20 wt% microsilica plus 5wt% nanosilica loading for the IPT test.

In addition, based on the acquired voltage and current data, recorded by the PC-based data acquisition system, the maximum power needed for each sample to reach the 2.5 cm tracking length is calculated. The formula with 20 wt% microfillers plus 5 wt% nanofillers is used as an example. The data for the maximum current in the last hour prior to the sample failure are taken from the recorded data file for both the conventional and the electrospun composites. The plots of the maximum current for IPT sample 1 and IPT sample 2 are shown in Figure 3.18 (a) and (b), respectively. Electrospun sample 1 fails at 4 kV, with test duration of 270 mins, and electrospun sample 2 failed at 4 kV, with test duration of 300 mins. For the conventional sample, sample 1 failed at 3.75 kV, with test duration of 244 mins, and sample 2 failed at 3.75 kV, with test duration of 250 mins.

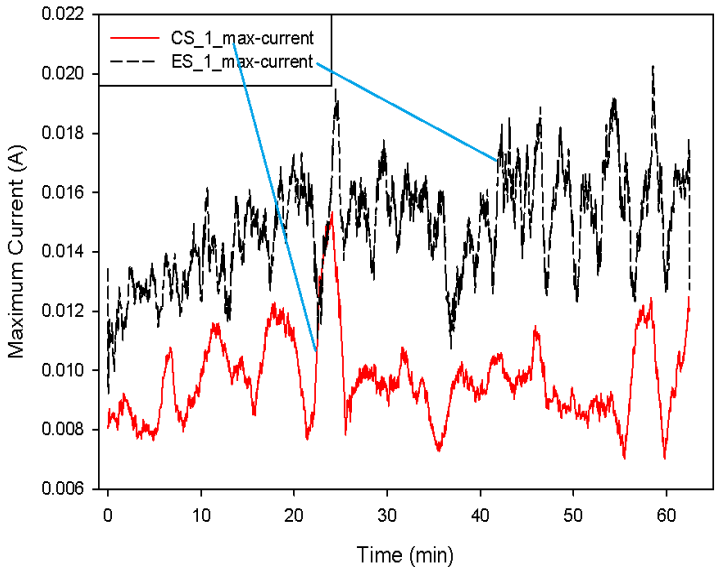

(a)

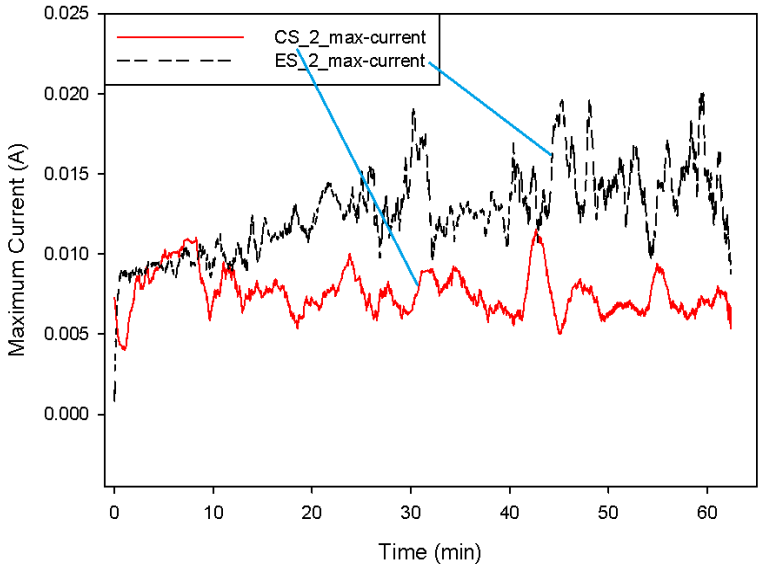

(b)

Figure 3.18: Records the maximum current for IPT sample 1 and sample 2 of the electrospun and conventional SiR composites (with 20 wt% microsilica plus 5 wt% nanosilica loading) during the last hour prior to the sample failure (ES = electrospun sample; CS = conventional sample) (a) IPT sample 1 means CS_1 and ES_1in Figure 3.14, and (b) IPT sample 2 means CS_2 and ES_2 in Figure 3.14.

From Figure 3.18 (a) and (b), it is evident that the maximum current levels, prior to the failure for electrospun sample 1 and conventional sample 1, are about 20 mA and 10mA, respectively. For electrospun sample 2 and conventional sample 2, the maximum current levels are about 18 mA and 10 mA, respectively. Thus, the electrospun samples

require twice the power the conventional samples required to reach the failure point. These results indicate an enhanced interaction between the fillers and the SiR matrix which means more energy is needed for electrospun sample to erode.

3.2.3 Filler Dispersion and Interaction

With the help of electrospinning, the nanofiller can be dispersed reasonably well, permitting additional filler (nanofiller or microfiller) to be added. As a demonstration for this study, three formulas are chosen: an SiR composite filled with only 20 wt% microsilica, a conventional SiR composite and an electrospun SiR composite, filled with 20 wt% microsilica plus 5 wt% nanosilica. The SEM images of the cross-sections of the SiR samples are presented in Figure 3.19.

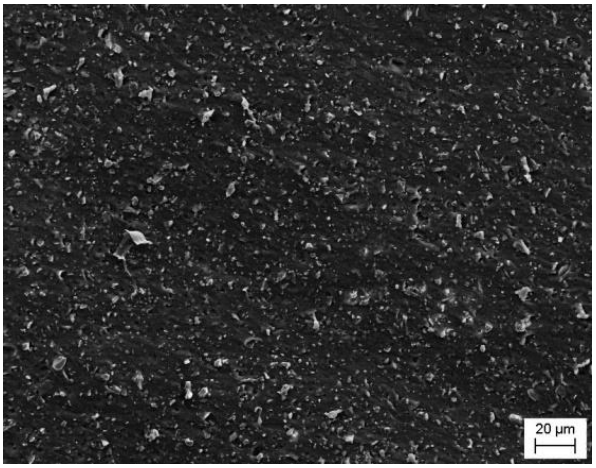

(a)

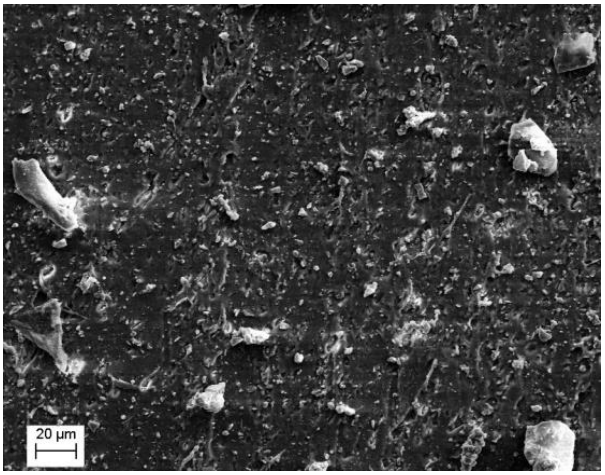

(b)

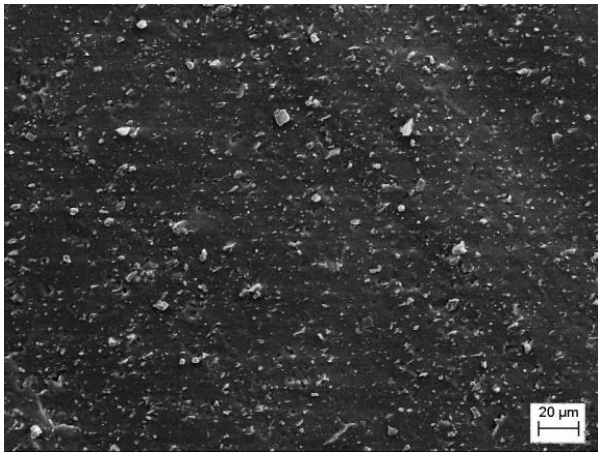

(c)

Figure 3.19: The morphology of the filler distribution in the SiR samples, under a 1000 x magnification, (a) The distribution of the 20 wt% microsilica in the SiR composite, (b) the distribution of 20 wt% microsilica plus 5 wt% nanosilica in the conventional SiR composite, and (c) the distribution of 20 wt% microsilica plus 5 wt% nanosilica in the electrospun SiR composite.

For all the formulas, the microsilica is mixed by using the high shear force mixer with identical mixing conditions. The SEM images clearly show that the SiR sample with 20 wt% microsilica has a filler distribution, similar to that of the electrospun sample with 20 wt% microsilica plus 5 wt% nanosilica. However, the conventional sample exhibits larger filler agglomerations, which may be the result of the poor dispersion of the nanosilica on its own, which may or may not have been exacerbated by the addition of the microsilica. In either case, the cause of the agglomeration in the conventional sample is the poor dispersion of the nanofillers, which leads to a greatly increased viscosity in the polymer mixture, and in turn, further reduces the dispersion of the microfillers. Therefore, the effectiveness of the electrospinning technique, with respect to the dispersion of the nanofillers is further verified.

3.2.4 Thermal Stability and Thermal Degradation

A thermal-gravimetric analysis is also conducted for the previous SEM samples: the 20 wt% microsilica-filled SiR composite, the conventional SiR composite filled with 20 wt% microsilica plus 5 wt% nanosilica, and the electrospun SiR composite

filled with the 20 wt% microsilica plus 5wt% nanosilica. The TGA curves are shown in Figure 3.20.

$T_{95\%}$ is the temperature at which the sample loses only 5 % of its weight. Typically, this value represents the temperature at which the onset of thermal degradation occurs [133]. From the curves, it is evident that for the 20 wt% micro-filled SiR composite, the $T_{95\%}$ is approximate 455 ^{o}C, but for the conventional sample and the electrospun sample filled with 20 wt% microsilica plus 5 wt% nanosilica, the $T_{95\%}$ for both is about 472 ^{o}C. Therefore, the addition of 5 wt% nanosilica modifies the thermal stability of the SiR composite during the onset stage, although not showing a significantly higher temperature transfer. The TGA curve for the electrospun sample after $T_{95\%}$ exhibits a short period in which the slope of the TGA curve is flat, indicating that the onset of the degradation of the electrospun sample is not as severe as that of conventional sample.

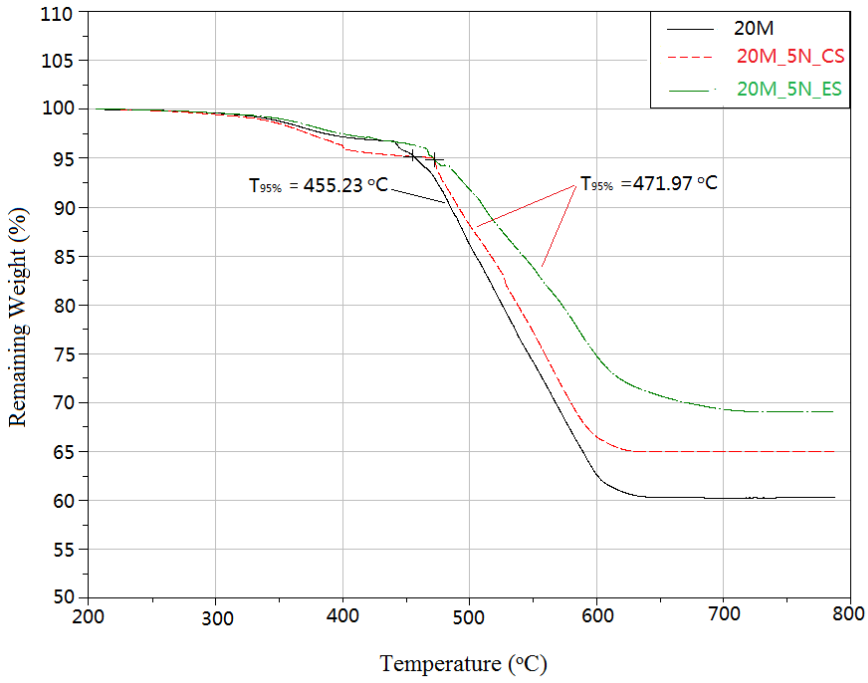

Figure 3.20: The TGA curves for the 20 wt% microsilica-filled sample (designated 20M), the conventional sample filled with 20 wt% microsilica plus 5 wt% nanosilica (designated 20M_5N_CS), and the electrospun sample filled with 20 wt% microsilica plus 5 wt% nanosilica (designated 20M_5N_ES).

Moreover, the rate of the weight loss from $T_{95\%}$ until 600 ^{o}C (the point at which the remaining weight of the sample is almost stable) for the 20 wt% microsilica-filled sample is about 23 %/^{o}C, for the conventional sample, filled with 20 wt% microsilica plus 5wt% nanosilica is about 21 %/^{o}C, and for the electrospun sample, about 15 %/^{o}C. The remaining weight of the 20 wt% microsilica-filled sample is approximate 60 %, and for the conventional and the electrospun samples, the remaining weights are about 65 % and 68 %, respectively. Slower weight loss and higher remaining weight of the electrospun sample suggests that the interaction between the filler and the SiR matrix is improved, strengthening the thermal degradation.

3.3 Epoxy Resin Nanocomposites

Epoxy resin as the second chosen polymer is investigated in this thesis to examine the possibility of using the proposed electrospinning technique to disperse the nanofillers within the other polymers other than silicone rubber and also to do some further tests that cannot be accomplished in SiR composites. All the samples, preparation procedures are the similar as for the silicone rubber samples. The component percentage is still based on the weight percentage, and ethanol is still selected as the conductivity modification solvent for the epoxy resin. The volume of ethanol is decided based on the epoxy resin viscosity and epoxy resin electrospinning behaviour.

3.3.1 Morphology and Elemental Analysis

In the silicone rubber composites, both the filler and polymer matrix have a Si chemical element. Therefore, it is difficult to use the EDX analysis to distinguish between them. In epoxy resin composites, there is no common element in the polymer and fillers except oxygen. To verify the interaction between the nano and micro fillers, 5 μm TiO_2 microfiller is used in this section, instead of microsilica, just for the EDX and SEM analysis purposes. 20 wt% micron TiO_2 plus 5 wt% nanosilica epoxy resin

composites are prepared by the two methods as mentioned in section 2.2. The SEM images, EDX elemental analysis, and mapping are shown in Figure 3.21 and Figure 3.22 - Figure 3.27. SEM analysis was done at both low and high magnifications to exam the how the morphology looks like in a big and a small area in the composites.

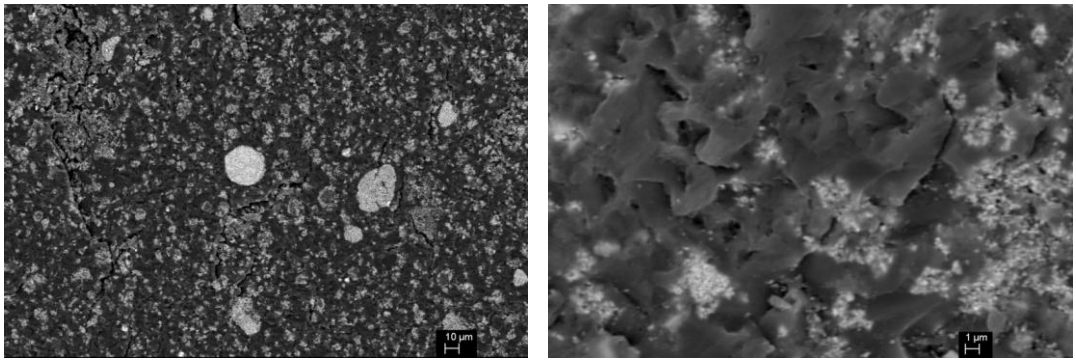

300X 3000X

(a)

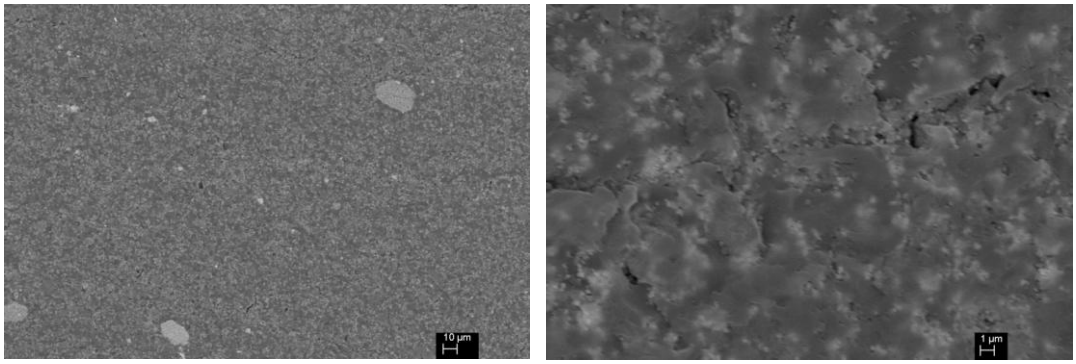

300X 3000X

(b)

Figure 3.21: The SEM images of the 20 wt% micron TiO_2 plus 5 wt% nano SiO_2 epoxy resin samples, (a) the SEM image, for the cross-section of the conventional epoxy resin sample at 300 and 3000 magnifications, and (b) the SEM image for the cross-section of the electrospun epoxy sample at 300 and 3000 magnifications.

The EDX-mapping is carried out for each sample in three different locations: the evaluated area is 40 μm × 40 μm, the purple color represents the element Si, and the green color represents the element Ti.

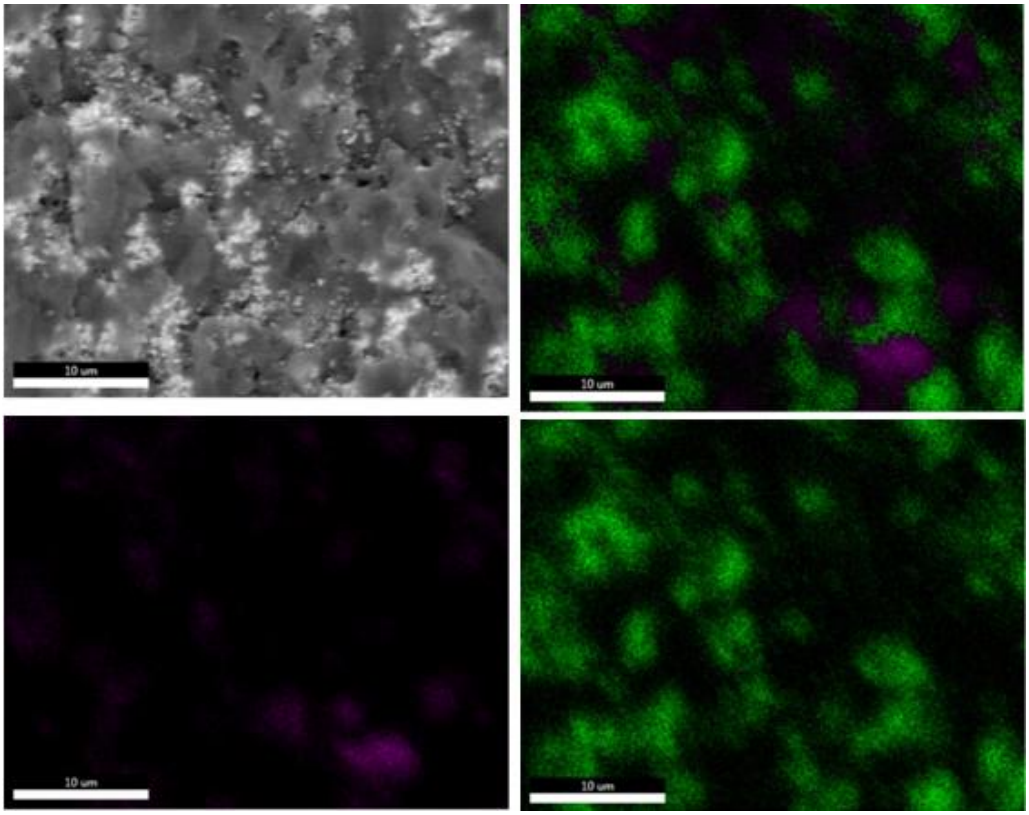

(a)

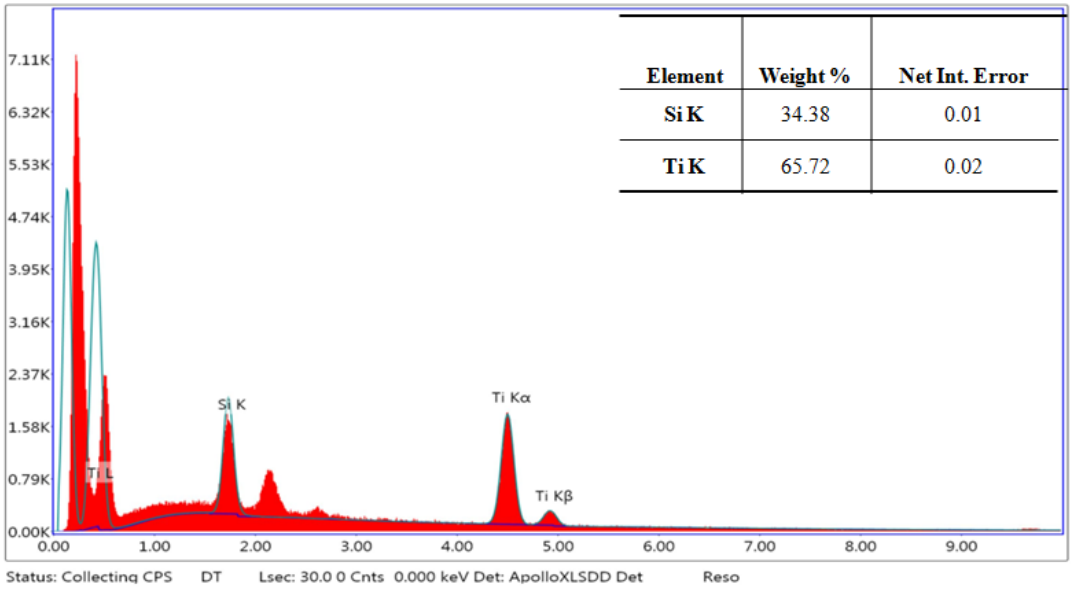

Element	Weight %	Net Int. Error
Si K	34.38	0.01
Ti K	65.72	0.02

(b)

Figure 3.22: EDX-mapping and elemental analysis for the CS sample in location 1, (a) the CS sample EDX-mapping in location 1; top left is the SEM image, bottom left is the Si element mapping, bottom right is the Ti element mapping, top right is the overlap mapping for both the Si and Ti element, and (b) the CS sample EDX elemental analysis in location 1.

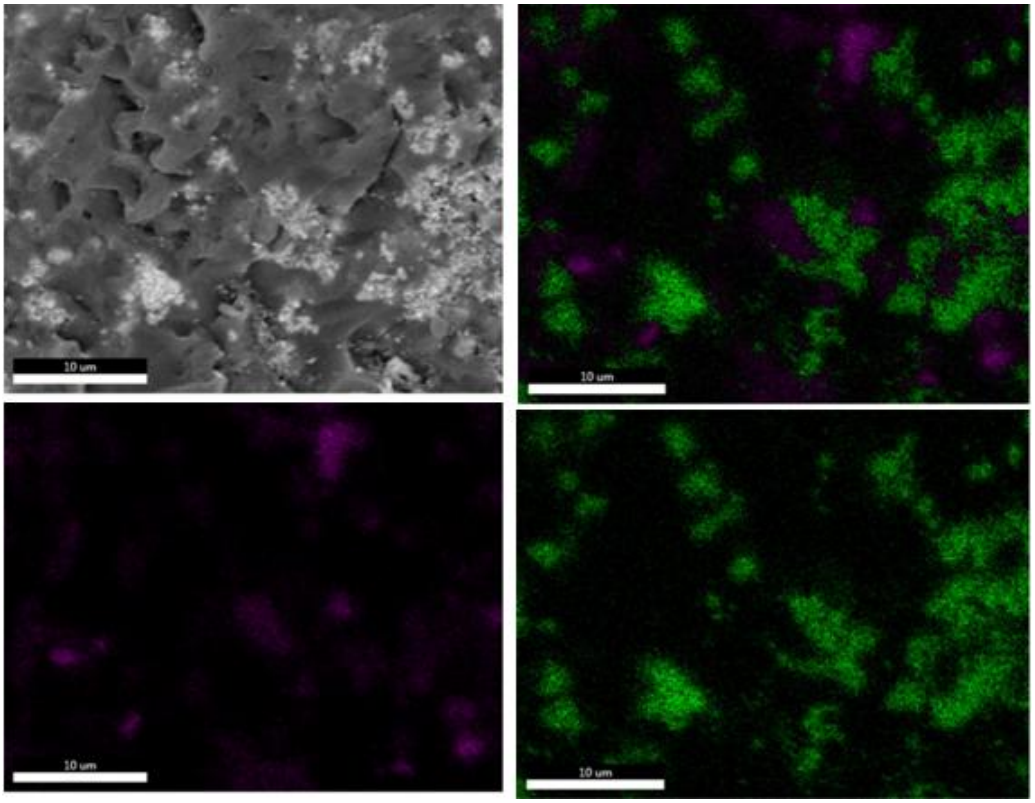

(a)

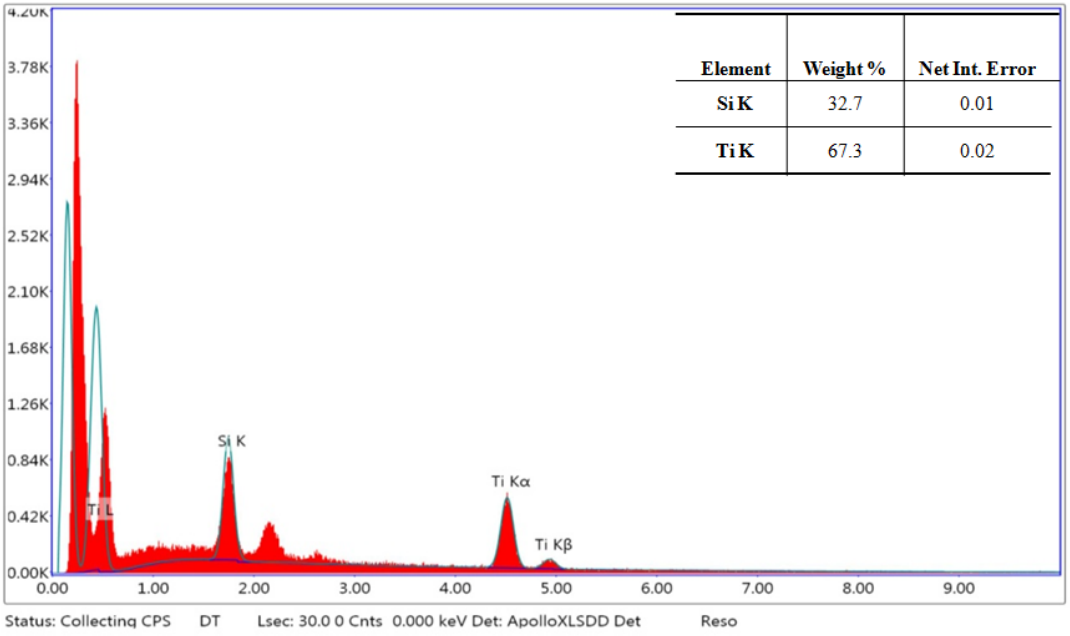

Element	Weight %	Net Int. Error
Si K	32.7	0.01
Ti K	67.3	0.02

(b)

Figure 3.23: EDX-mapping and elemental analysis for the CS sample in location 2, (a) the CS sample EDX-mapping in location 2; top left is the SEM image, bottom left is the Si element mapping, bottom right is the Ti element mapping, top right is the overlap mapping for both the Si and Ti element, and (b) the CS sample EDX elemental analysis in location 2.

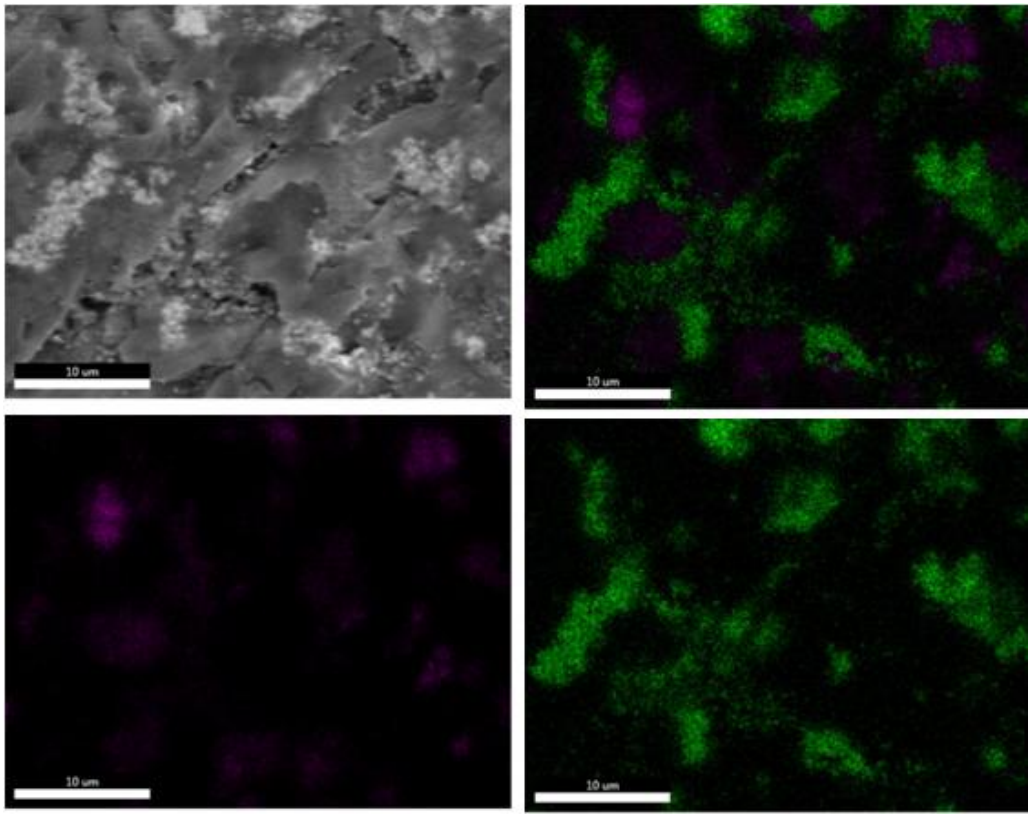

(a)

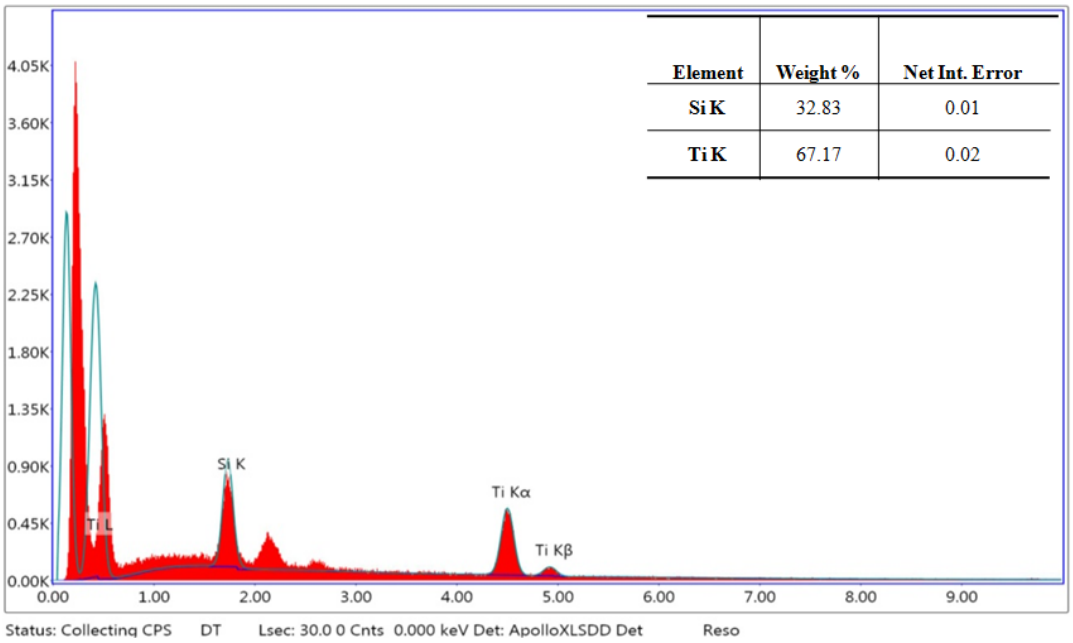

(b)

Figure 3.24: EDX-mapping and elemental analysis for the CS sample in location 3, (a) the CS sample EDX-mapping in location 3; top left is the SEM image, bottom left is the Si element mapping, bottom right is the Ti element mapping, top right is the overlap mapping for both the Si and Ti element, and (b) the CS sample EDX elemental analysis in location 3.

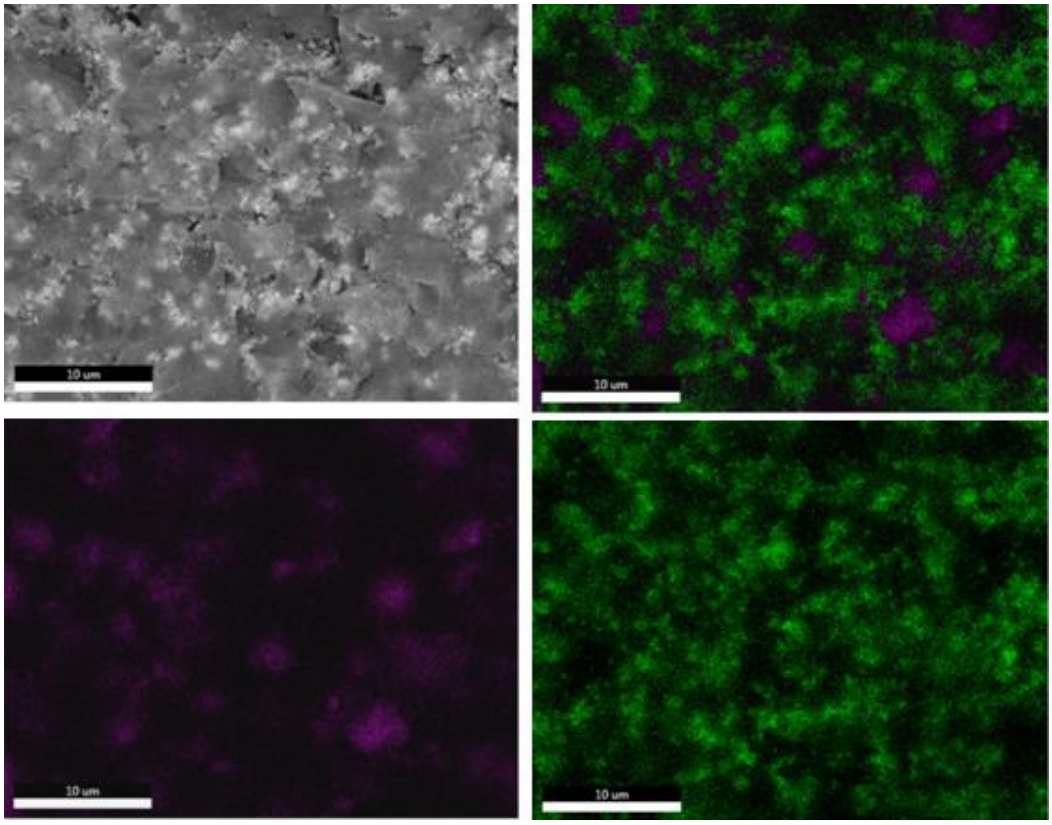

(a)

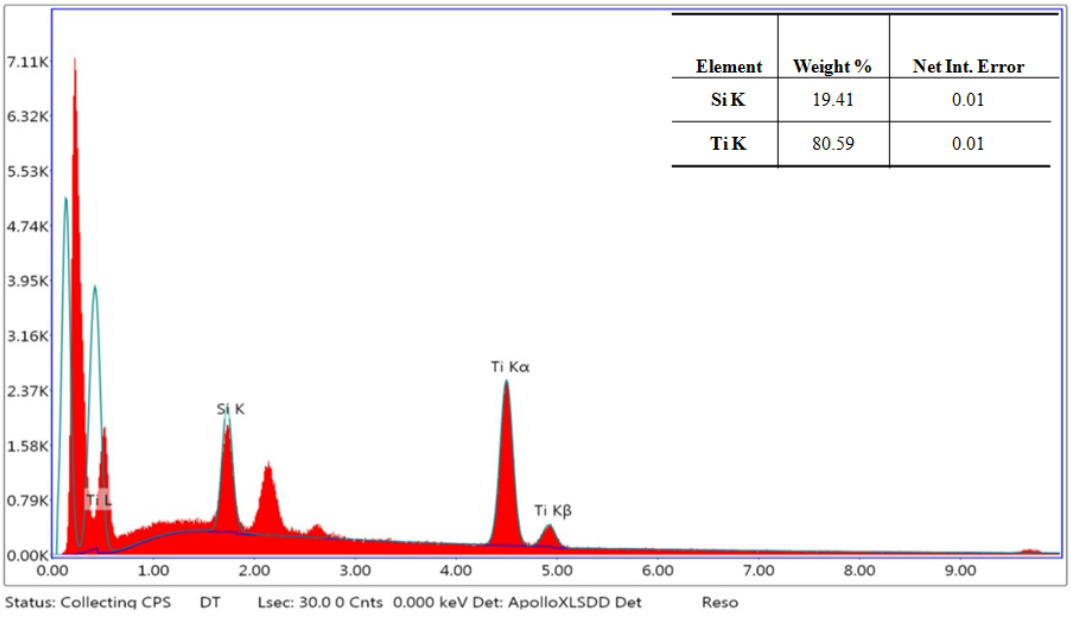

(b)

Figure 3.25: EDX-mapping and elemental analysis for the ES sample in location 1, (a) the ES sample EDX-mapping in location 1; top left is the SEM image, bottom left is the Si element mapping, bottom right is the Ti element mapping, top right is the overlap mapping for both the Si and Ti element, and (b) the ES sample EDX elemental analysis in location 1.

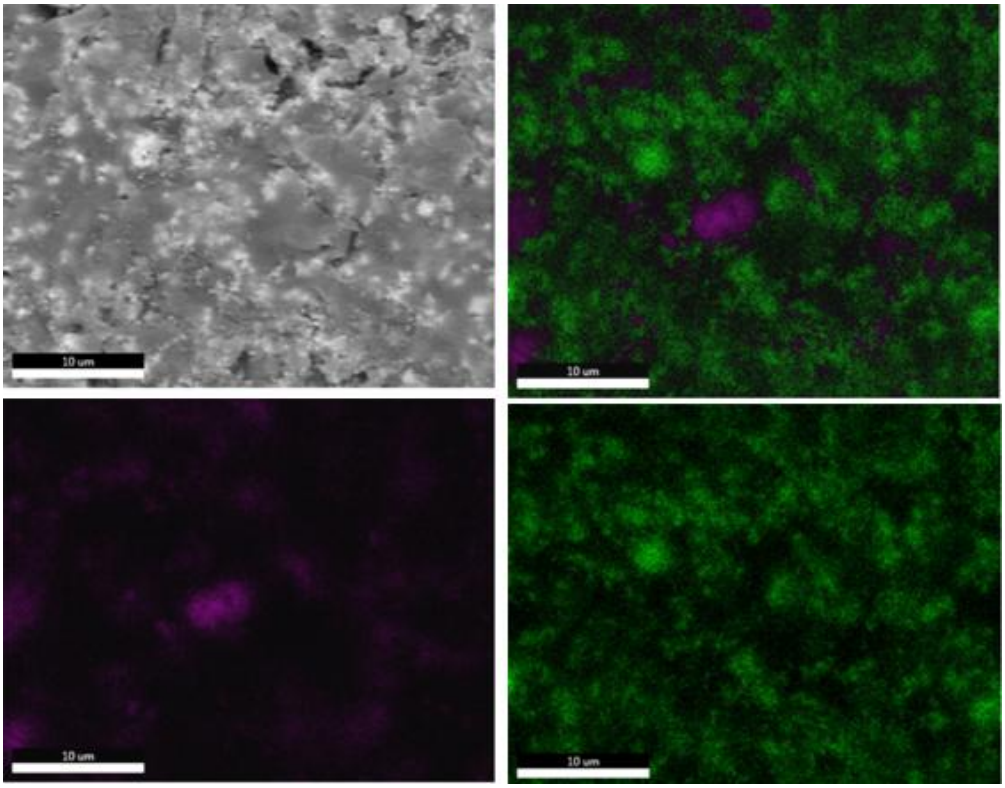

(a)

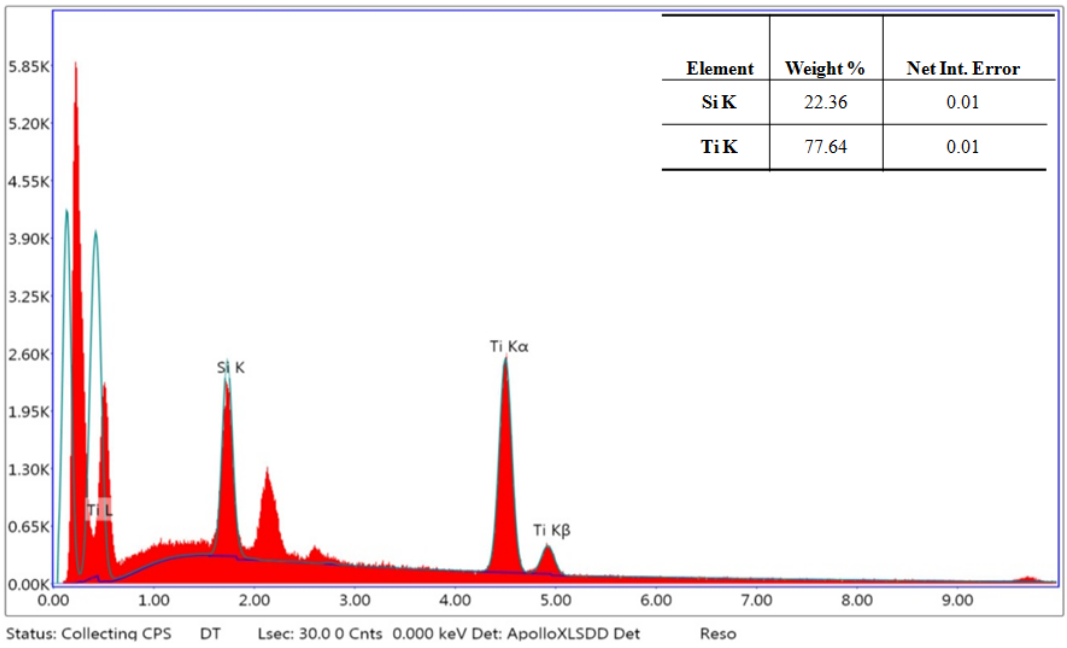

(b)

Figure 3.26: EDX-mapping and elemental analysis for the ES sample in location 2, (a) the ES sample EDX-mapping in location 2; top left is the SEM image, bottom left is the Si element mapping, bottom right is the Ti element mapping, top right is the overlap mapping for both the Si and Ti element, and (b) the ES sample EDX elemental analysis in location 2.

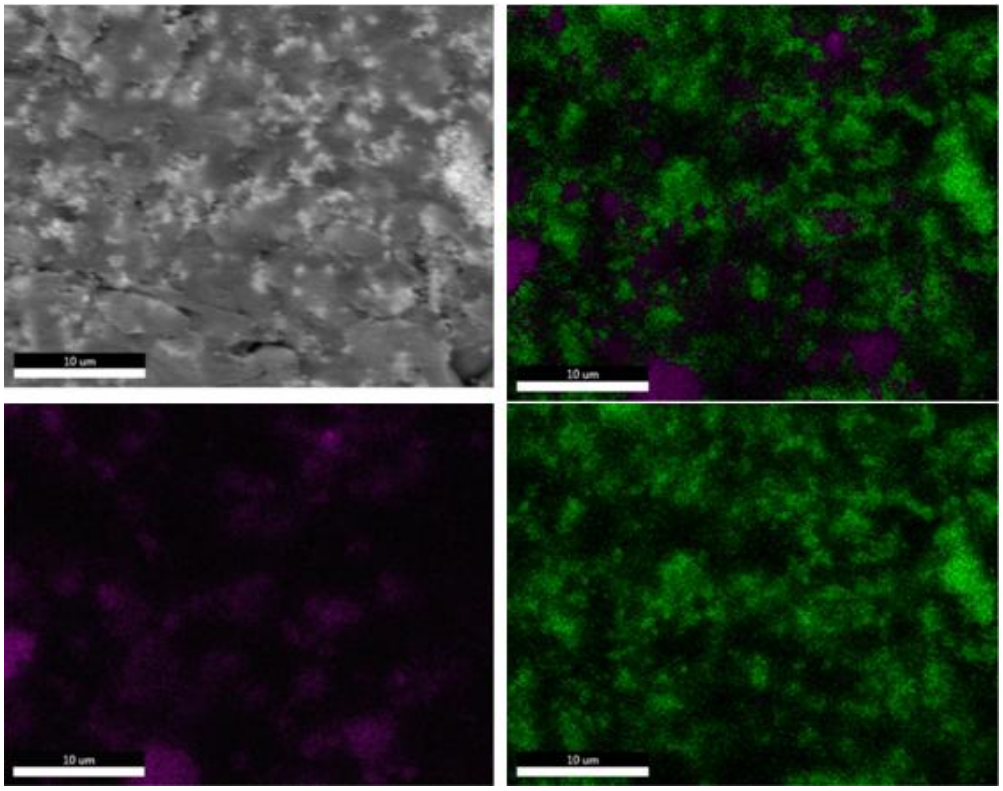

(a)

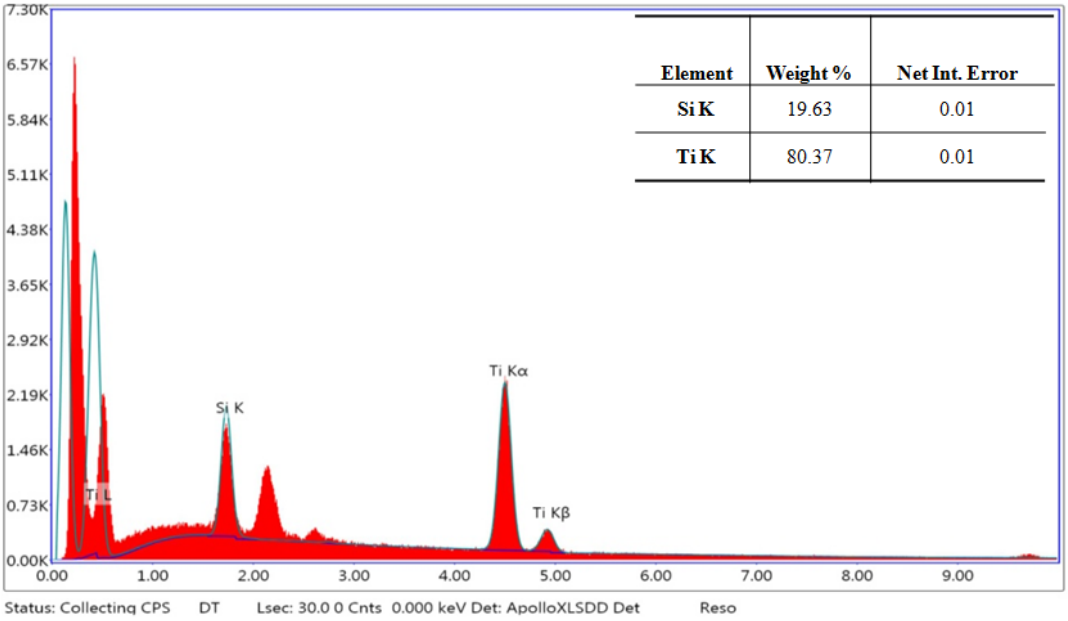

(b)

Figure 3.27: EDX-mapping and elemental analysis for the ES sample in location 3, (a) the ES sample EDX-mapping in location 3; top left is the SEM image, bottom left is the Si element mapping, bottom right is the Ti element mapping, top right is the overlap mapping for both the Si and Ti element, and (b) the ES sample EDX elemental analysis in location 3.

In Figure 3.21, the SEM images portray the filler distribution in both the conventional and electrospun micro and nano-filled samples. The 300X magnification of the SEM images clearly indicates that the fillers are distributed more homogeneously in the electrospun sample than that in the conventional sample, and the 3000X magnification SEM images reveal no large filler clusters in the electrospun samples. However, for the conventional sample, the enlarged local area has some obviously large filler clusters. The filler distribution in the SEM images of nano and micro-filled epoxy is almost similar to the results of the silicone rubber nano and micro-filled composites in Figure 3.19.

For each conventional and electrospun micro and nano-filled sample, the EDX-mapping and elemental analysis is conducted in the three different areas in Figure 3.22 to Figure 3.27. In addition, the elemental analysis in each area is obtained. Here only Si and Ti are chosen to be shown. The EDX-mapping directly presents the distribution of the nano SiO_2 and micro TiO_2 fillers by showing the element distribution. Moreover, the interaction between the nano and micron fillers is obtained by the overlapped element mapping. Not only is nano SiO_2 distributed better by the electrospinning than that by the high shear force mixer in epoxy resin, but also the distribution of the micro TiO_2 in the electrospun sample reveals better uniformity than that of the conventional sample. Because of the 20 wt% TiO_2 plus 5 wt% SiO_2 in the epoxy resin sample, so the weight ratio of TiO_2 to SiO_2 is 4:1. The element weight ratio of Ti and Si in the composite according to the formula can be calculated. Based on the EDX elemental analysis, the element weight percentage in each area for each sample can be acquired. The weight percentage of Ti to Si in the three different areas for the conventional and electrospun sample are represented by the bar graph in Figure 3.28.

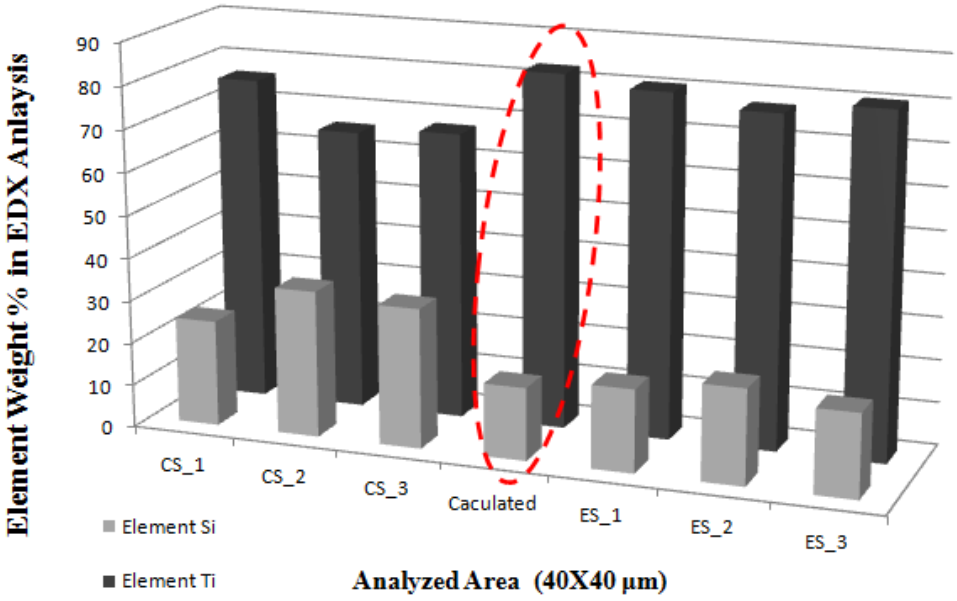

Figure 3.28: The element weight percentage comparison between the CS and the ES samples (the reference represents the calculated element weight ratio of Ti to Si in the formulated epoxy composite).

If both the TiO_2 and SiO_2 fillers are very uniformly distributed in the epoxy resin then in any area, the element weight ratio of Ti to Si should be around the calculated value 83 % : 17 % (the middle reference bar indicates the calculated element weight percentage in the formulated epoxy resin sample). By comparing all the EDX results with the reference values in Figure 3.28, it can be seen that the results in the three different areas for electrospun sample are much closer to the reference ratio than the results of the conventional sample. There is a small variation in the element weight percentage for electrospun sample in that than for the conventional sample.

Also, the good filler interaction and homogeneous distribution are verified again by the EDX-mapping and element weight percentage comparison in addition to the SEM images.

3.3.2 Heat and Erosion Resistance of Epoxy Composites

Both microsilica and nanosilica are also employed to enhance the thermal properties of the epoxy resin. The heat and erosion resistance is tested by the laser

ablation setup without the arcing ignition. Pure epoxy resin, 40 wt% microsilica-filled epoxy resin, 44 wt% microsilica-filled epoxy resin and 40 wt% micro plus 2 to 4 wt% nanosilica-filled epoxy resin samples are compared. The eroded mass trend for the epoxy samples, in Figure 3.29 has a similar trend to that of the silicone rubber samples. It is concluded that the eroded mass is reduced when the filler loading is augmented for the electrospun samples.

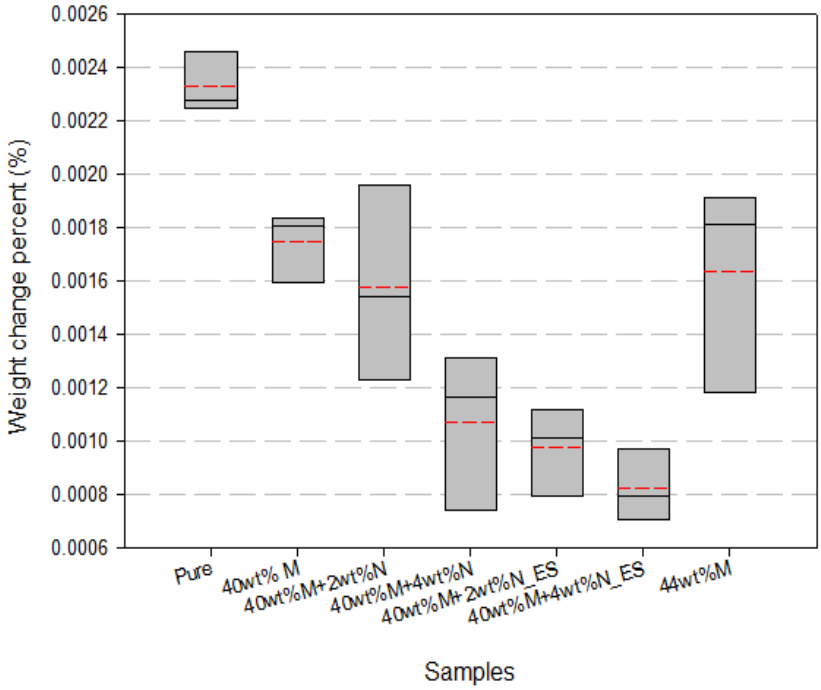

Figure 3.29: The eroded mass for the epoxy formulas with the 40 wt% microsilica plus 2 wt% to 4 wt% nanosilica, pure epoxy resin, 40 wt% microsilica filled epoxy resin and 44 wt% microsilica filled epoxy resin (ES = electrospun sample; CS = conventional sample).

However, there is almost no difference between the unfilled epoxy resin and filled epoxy resin in the IPT test, when the filler loading is lower than 50 wt%. When the filler loading is low, and the tracking on the sample surface is initiated, all the samples begin to flame, and fail in a few seconds. The behaviour of epoxy resin samples differs from that of the silicone rubber samples during the IPT test.

The flammability of the polymers relates to the limiting oxygen index (LOI) which is the minimum concentration of oxygen that sustains the combustion of the polymer. The LOI of the silicone rubber is approximately 26-40 % O_2 [134] and LOI

of cycloaliphatic epoxy resins is 18-20 % O_2 [135], indicating the epoxy resins exhibit a greater tendency to burn. There is a critical filler level for base polymeric dielectrics to completely suppress the tracking. Therefore, much more fillers are required to suppress the tracking and erosion of the epoxy resin than that for the silicone rubber. This is the reason that at least 30 to 50 wt% inorganic fillers are used in the industry in the base polymer to effectively stop tracking and erosion.

Chapter 4

Discussion

Both silicone rubber and epoxy polymeric materials were successfully electrospun. Moreover, nanofillers were uniformly distributed in these polymers. Results of various characterization and analysis confirm that nanofillers in the base polymers were more homogenously mixed by electrospinning than the conventional method. The dispersion of fillers in the polymeric materials was visually analyzed by using SEM and EDX techniques. It is notable that, the results from the inclined plane test and laser ablation showed a good match with the results of thermal degradation and thermal stability in the TGA measurements.

4.1 Advantages of Electrospinning for Filler Dispersion

Compared to conventional mechanical mixing and complicated chemical modification, electrospinning is easier to control and more effective than conventional mixing. Advantages of electrospinning method are summarized as follows:

(a) Improved Dispersion

As shown in Figure 3.3, the contact angles of electrospun nanocomposites increased and their hydrophobicity improved. In addition these results reconfirmed that the dispersion of the electrospun nanofillers was improved compared to conventional samples. EDX-mapping and elemental analysis provide more details about the filler information to a depth of 300-400 nm whereas SEM can provide information only to a around 50 nm depth. The SEM images and EDX-mapping results in Chapter 3 visually presented that the filler dispersion in electrospun samples was much better than that of conventional samples. EDX-mapping in Figures 3.22-3.27 clearly showed that after electrospinning nanofillers were spread all over the polymer, and the size of the filler agglomerations was effectively reduced by the

electrospinning process, the big silica particle that can be detected during SEM , as shown in Figure 4.1.

It was confirmed by using several analysis methods that electrospinning was successfully used to separate nanofillers in two different polymers, silicon rubber and epoxy. Therefore, it is possible to adjust and modify this method for dispersion of nanofiller in other polymers

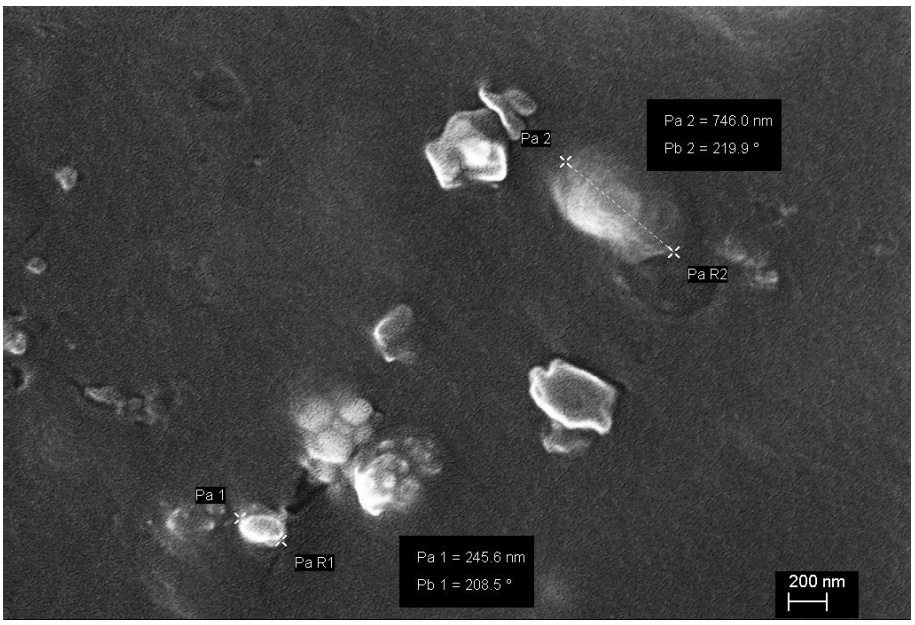

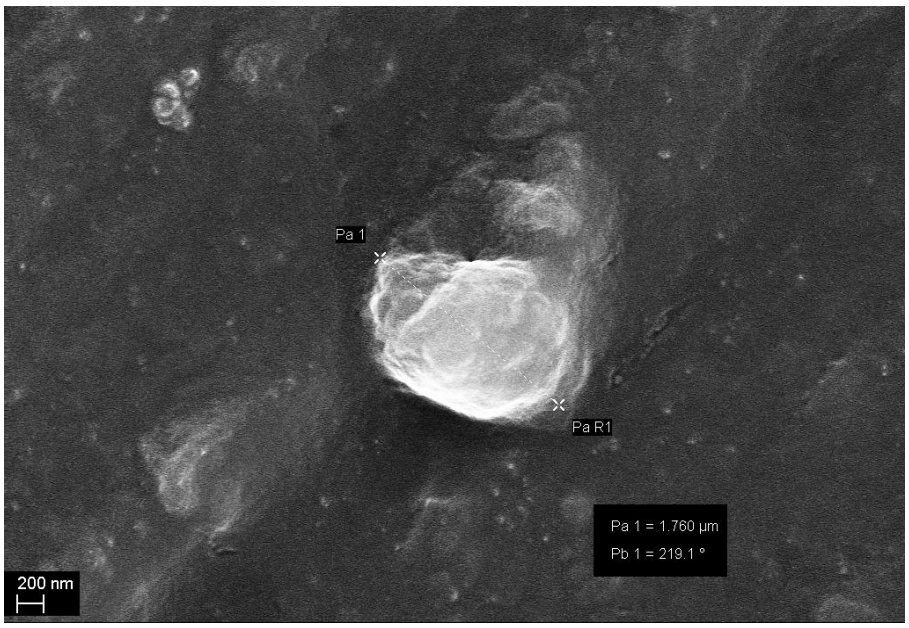

(a)

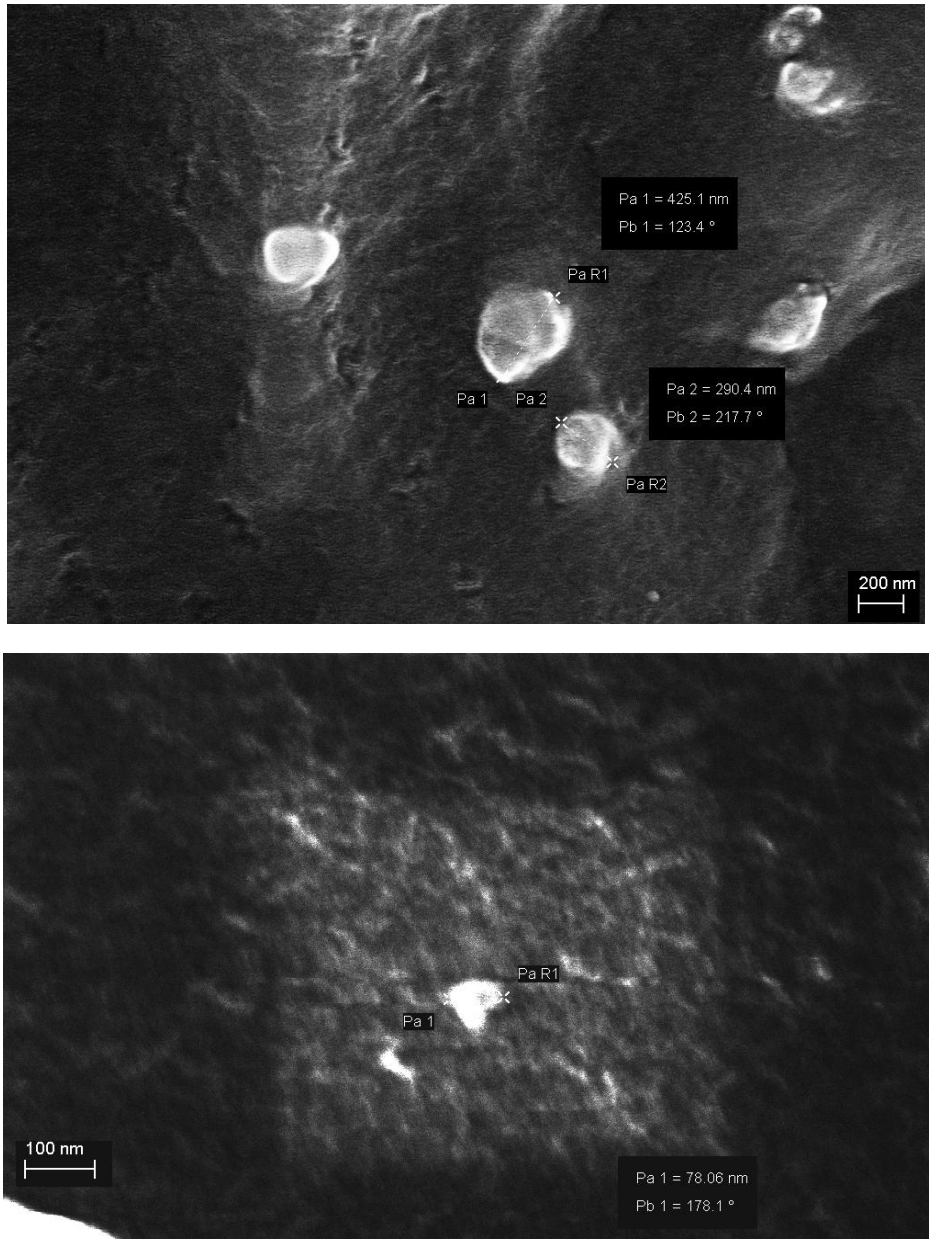

(b)

Figure 4.1: The effect of electrospinning on the agglomeration reduction in silicon rubber composites, (a) nanosilica-filled conventional silicone rubber, and (b) nanosilica-filled electrospun silicone rubber

(b) Reduced Compound Viscosity

A shear capillary rheometer, as mentioned in section 2.3, was used to measure the viscosity of the pure SiR, electrospun pure SiR, 1, 3 and 5 wt% nanosilica-filled conventional and electrospun SiR (without of RTV 615-B). Due to the capability of the set-up, each liquid sample was measured at constant crosshead speed of 100

mm/min three times, see Figure 4.2. The load forces of the pure SiR and 1 wt% SiR of the conventional and electrospun samples had negligible difference. However, when the filling level increases, the load forces for the conventional samples are much higher than those of the electrospun samples, revealing the higher viscosity of conventional samples even at the same filler loading as the electrospun samples.

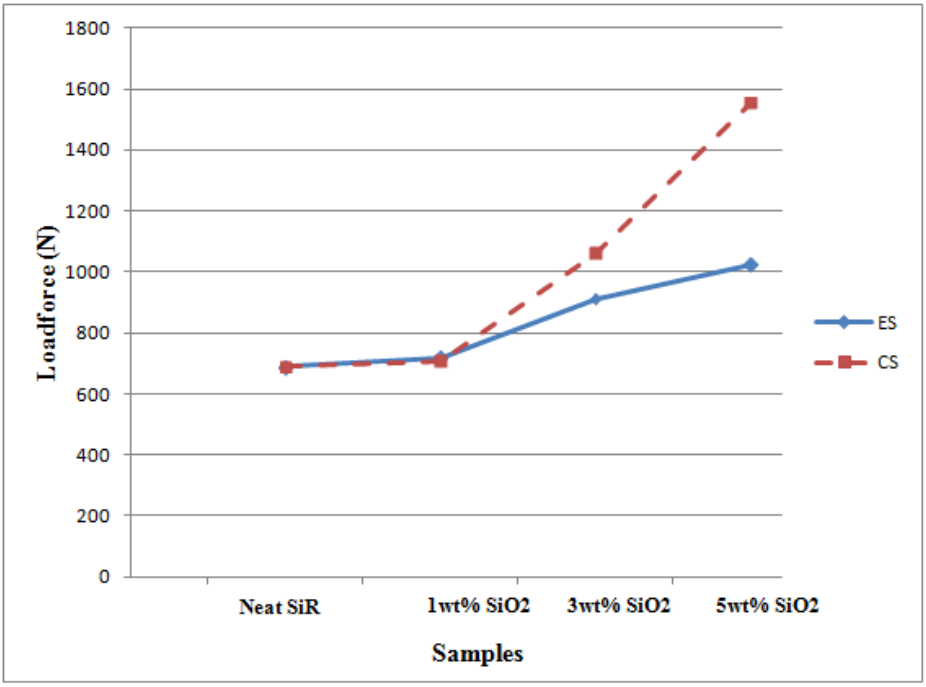

Figure 4.2: The load force vs. different filler loading (blue line represents the electrospun SiR samples; red line represents the conventional SiR samples).

The larger filler volume results in a higher viscosity of the composite due to the hydrodynamic effects. Also, the presence of agglomerates leads to a significant increase in the shear viscosity, strongly affecting the rheological properties of the composites [136]. The agglomerates hinder the flowing of the other primary fillers and immobilize part of the entrapped fluid. The resultant hydrodynamic forces increase the final viscosity [137-138]. The electrospun samples have fewer agglomerates, as shown in the SEM images, consequently these samples have the lower viscosity as shown in Figure 4.2. The reduced viscosity of the electrospun

compound due to the better dispersion makes the processability of the composites is easier.

The relative viscosity of micro aluminum nitride (AIN) filled epoxy samples showed the similar results. The epoxy compounds filled with surfactant modified AIN fillers have the lower viscosity compared to that of epoxy compounds filled AIN without silane treatment at the same filler loading, and filler AIN presented better homogeneity after treatment [139]. As suggested in [136], the rheological response may be a sensitive tool to examine filler dispersion in a polymer than SEM analysis.

(c) Increased Filler Addition

It has been presented in section 3.2 that more filler (nanofillers and microfillers) can be added to the base polymers in the electrospun composites. Using of ethanol diminishes the viscosity of the polymer blends such that more nanofillers can be added at the beginning. In addition, the electrospinning process improves the homogeneity of the nanofillers and reduces the viscosity of the compounds so more microfiller can be infused. Also, the interaction between the nanofiller and microfiller can be improved to form a better network, as shown in Figures 3.22 to 3.27 for the EDX-mapping. The increased filler loading just follows the cost-saving requirement by industry.

(d) Possible Filler Alignment

The SEM images of the silicone rubber composites with 3 and 6 wt% nanosilica after 12 hours of corona aging are depicted in Figure 4.3. From the SEM images, the convention samples appear to be damaged to a greater extent than the electrospun samples. The cracks on the surfaces between the samples in terms of the two mixing methods differ. The cracks on the conventional samples crisscross, but the cracks on the electrospun samples are mostly paralleled. The pattern of cracks on electrospun samples can come from the alignment of nanofillers during electrospinning, and the less degradation of electrospun composites by corona discharge is due to the improved heat and erosion resistance.

The oriented morphology by electrospinning has been studied by different research groups. [140] presented that CNTs tend to oriented along the nylon fiber axis and embedded in the fiber core due to the high electrostatic forces and high shear force experienced by the jet during electrospinning. Dror et al. [141] have suggested a theoretical model to explain the alignment of CNTs in the electrospun fibers due to a hydrodynamic shear mechanism. In the model, the converging streamlines of a sink-like flow (Hamel flow) led to the gradual oriented CNTs in the nanofibers when the flow towards the vertex of Taylor cone. Therefore, there is a possibility to assembly fillers by electrospinning, but how to precisely control the alignment of filler is not clear.

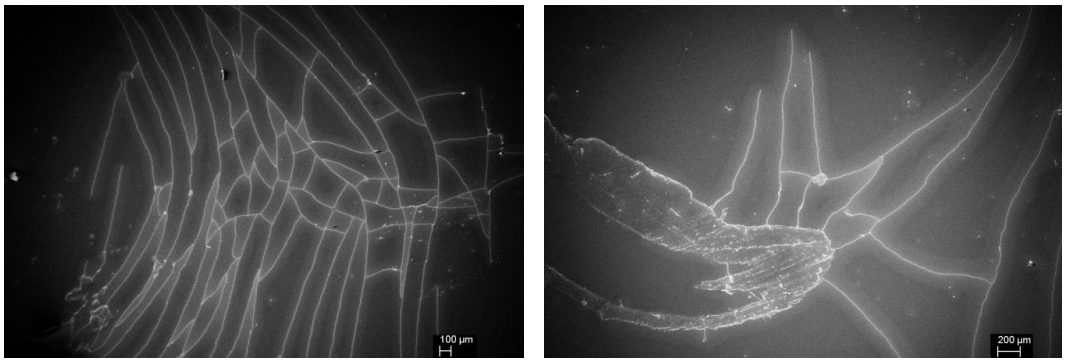

(a)

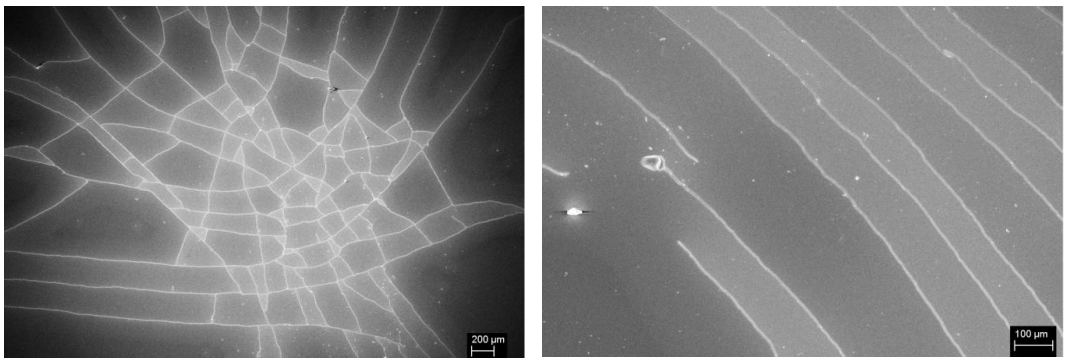

(b)

Figure 4.3: The SEM images of the composite surface after the 12 hours corona aging test at a 12 kV AC voltage: (a) the surface morphology of the 3 wt% aged SiR nanocomposites, and (b) the surface morphology of the 6 wt% aged SiR nanocomposites. The left image shows the conventional samples and the right image shows the electrospun samples.

Besides above several advantages, if the base polymers can satisfy the viscosity, and electrical conductivity requirements or they can be easily modified and electrospun, then there is a wide scope of base polymers can use electrospinning to embed and disperse nanofillers. If the effective surfactants or chemical additives for the surface modification of the targeted fillers are already known then the modified nanofillers plus electrospinning technique should help the further improvement of the filler dispersion in the materials other than using just mechanical mixing. Moreover, as mentioned in Chapter 1 chemical additives sometimes bring side-effects to the final composites, and it is quite difficult to remove it after addition. If the surfactant is liquid and can be evaporated there is also a possibility of removing the surfactant during electrospinning process and reduce the bad effects of additives to the composites.

4.2 Thermal Stability and Thermal Degradation

The present of fillers in the polymers help absorbing thermal energy and protect base polymers from thermal attack, therefore, rising the decomposition temperature of composites [142]. TGA test can monitor this thermal improvement. The lower degradation slope and higher decomposition temperature in the TGA curves, Figure 3.5, for the composites, compared with those for the pure silicone rubber, demonstrate that the addition of the nanofillers caused an impressive improvement in the thermal degradation and thermal stability of the composites. These improvements rise from the fact the nanofillers act as a physical barrier, preventing gas diffusion between the composite and environment [143]. In Figure 3.5, electrospun samples exhibit lower degradation slopes and a little higher decomposition temperature by the position of the peaks of the curves at approximately 450 ^{o}C, than those of conventional samples. The slower weight loss and non-severe decomposed behavior at the beginning of the decomposition were also found for nanosilica and microsilica electrospun SiR composites as illustrated in Figure 3.20. It is concluded that a stronger filler barrier should be formed for the electrospun samples than the conventional samples.

It is noteworthy that in Figure 3.5, the remaining weight of pure silicone rubber after TGA is around 28 %, but the remaining weight of SiR composites after adding 3 and 6 wt% nanosilica are increased far more than the weight of filler loading addition, and this weigh is even more for electrospun samples. The similar results showed in Figure 3.18, in which SiR composite with 20 wt% microsilica was supposed to have remaining weight around 48 wt% after TGA, but instead it has around 60 % remaining weight.

There is usually a significant concentration of hydroxyl (-OH) groups on the surface of the fumed silica due to the formation of silanol functionalities at the time of manufacturing and during storage [144]. Nanofillers, whose surface areas are significantly larger than that of the microfillers [40] have much more –OH groups on their surfaces of nanosilica as compared to microsilica [145]. The higher residue weight for the nanosilica-filled silicone rubber is attributed to the silanol group on the surface of nanosilica [85]. Therefore, a lower residue weight of nanosilica silicone nanocomposite is observed when the fumed silica was calcinated at high temperature. The successful dispersion of the nanosilica through the electrospinning technique produces a larger interfacial area between the nanosilica and the SiR matrix. Therefore, it provides more possibility for the plentiful hydroxyl groups on the surface of nanosilica to bond the polymer matrix, which produces a significant interaction between filler and polymer matrix and strengthens thermal degradation and thermal stability for electrospun composites.

In order to confirm the effect of silanol group, TGA test was conducted onto the aluminum-filled epoxy composites in which the filler and base polymer have no reactive groups with each other. The TGA results of the pure epoxy resin, 4 wt% nano aluminum (Al) epoxy (CS and ES sample) and 20 wt% micro Al plus 4 wt% Al epoxy (CS and ES sample) are illustrated in Figure 4.4.

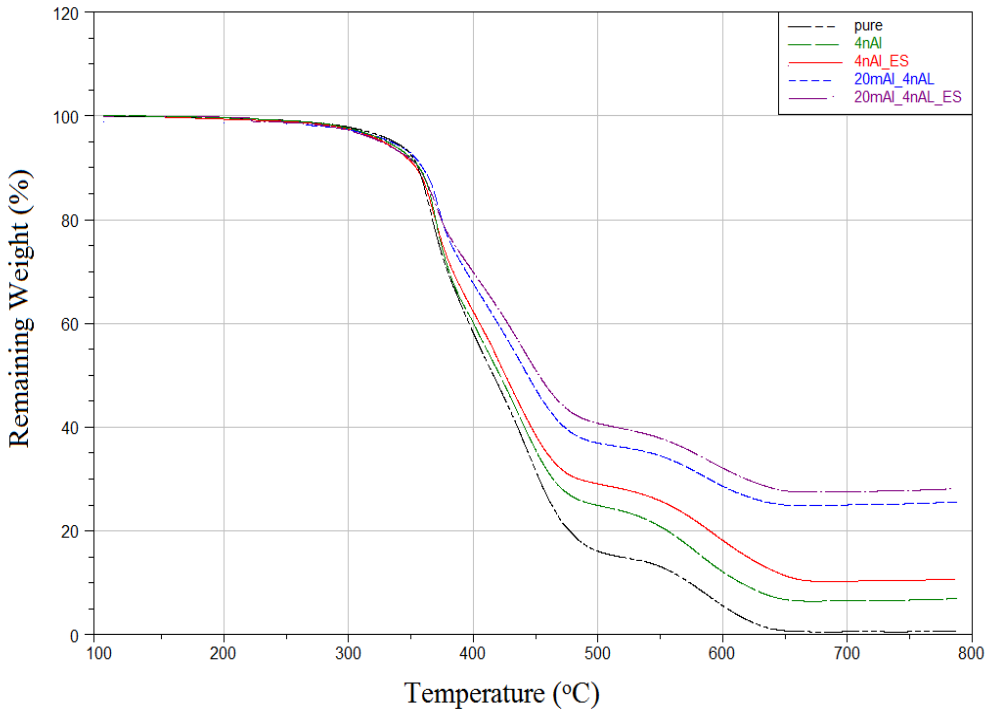

Figure 4.4: The TGA curves for the pure epoxy, epoxy composites with 4 wt% nano Al fillers, and epoxy composites with 20 wt% micro and 4 wt% nano aluminum fillers (CS= conventional sample, ES=electrospun sample).

The TGA measurements are conducted in ambient air with the temperature increasing from 100 to 800 ^{o}C at a rate of 25 ^{o}C/min for the epoxy resin composites .The decomposition time is almost the same for all the epoxy samples, but slight differences are found between the conventional sample and electrospun sample on the TGA slope after passing the $T_{95\%}$ decomposition temperature. The samples with more fillers decompose more slowly than those with less fillers due to the "dilution effect" [146]. Moreover, the electrospun samples demonstrate a relatively better thermal degradation than the conventional samples. It is noted that the remaining weights of epoxy composites are almost matched with the weights of addition filler loading. The thermal degradation of epoxy composites was not improved as much as those of SiR composites compared to their unfilled base polymers. This may imply that the interaction between silica and silicone rubber is stronger than that between silica and epoxy.

4.3 Heat Erosion Performance of SiR Composites

Only nanosilica-filled electrospun SiR composites showed significant improvement in heat erosion resistance in the laser ablation test. Compare to conventional SiR composites with the same filler loading level, electrospun composites showed around 15-40 % improvement in the eroded mass. It is attributed to the improved dispersion of the nanofillers in the materials by electrospinning.

For the electrospun nano and micro silica-filled samples, the eroded mass is linearly reduced at a relatively low filler loading (up to a 30 wt% microfillers). The rate of the reduction in the eroded mass becomes slow and flat at a relatively high filler loading, as indicated by the dotted line in Figure 3.11. This result reveals that the optimum erosion resistance of the SiR composites depends on the optimum combination of the microfiller and nanofiller loading as well. Also, it is unnecessary to increase the complicate of the mixing by adding increased amounts of filler to achieve a very limited improvement. Therefore, from a processing point of view, optimum formula makes the preparation of the samples much simpler. However, for all the formulas of the conventional samples, the rate of change in the eroded mass does not demonstrate as obvious trend as that for the electrospun samples, particularly for the sample filled with a 5 wt% nanosilica and a 30 wt% microsilica. The eroded mass of this sample is not only greater than that of an electrospun sample with the same filler loading but also slightly more than that of a conventional sample filled with a 5wt% nanosilica and 25 wt% microsilica. In addition, the variations in the trend of the eroded mass for the conventional samples arise from the poor dispersion of the nanosilica.

Based on the results in Figures 3.11, and 3.13, and 3.15, it is concluded that for the SiR composites which are filled with nanofillers and microfillers, the improvement in the heat erosion resistance is not always proportional to the filler loading, (whether the filler is a nanofiller or a microfiller). According to the experiments, if the 20 wt% microsilica is kept constant, the erosion behaviour of the SiR

composite does not greatly boost the rate of improvement, once the nanofiller loading exceeds 5 wt% but the erosion resistance is indeed improved with the addition of a small amount of nanofillers. Based on the SEM images, it can be seen that, especially for nanofillers, when the filler loading is excessive, large agglomerations easily form, which can result in an increased number of unfilled spots in the base polymers. Therefore, the erosion resistance is actually weakened in some manner. This inference is supported by the non-identical surface pattern of the conventional IPT samples in Figure 3.15.

Higher filler loading leads to better erosion resistance of SiR samples. Even with electrospinning, which can disperse nanofillers much more effectively than a conventional mechanical mixer, excessive filler loading is very difficult due to the limited unfilled polymer areas that can be eroded. This limitation may explain why the slope of the eroded mass becomes flat and slow with increased filler loadings. An additional observation is that excessive filler loading reduces the flexibility of the polymers. The best formula, which is a combination of nanofiller and microfiller, should be determined through consideration of an appropriate balance of composite processing, cost-saving, and the margin for further improvement in the properties of the materials.

For silica-filled epoxy composites (nano or nano-micro-filled samples), the eroded mass of electrospun samples was less than those of conventional samples but not significant, probably the interaction between silica and epoxy matrix is not as strong as that between silica and silicone rubber. In the industry, ATH is the common filler that is selected to enhance epoxy resin. TGA results in Figure 4.3 somehow explain that if there is no interaction or weak interaction between filler and matrix, the thermal degradation of composites is mainly improved due to the increased filler loading. Therefore, filler dispersion can influence the erosion resistance more if there is interaction between filler and polymer matrix. It did not show improvement for silica-filled composites in the IPT test compared to unfilled epoxy for the filler loading less than 40 wt% due to the low LOI value of epoxy.

The mechanisms of electrospinning for nanofiller dispersion and the effect of dispersion on the improved thermal properties are discussed next.

4.4 Mechanisms of Improved Thermal Performance of Electrospun SiR Composites

First, the addition of inorganic fillers reduces the base polymer portion in the compound, improving the anti-oxidation and thermal degradation. Like a heat sink, silica has a specific heat capacity of 700 J/ kg.K, which is high enough to enhance the thermal stability and thermal degradation of the corresponding composites [143]. As mentioned in the section 3.5, electrospinning allows more fillers to be added into the base polymer due to the enhanced processability, resulting from the well dispersed nanofillers. The combination of nanofillers and microfillers not only takes the advantage of the nanofillers but also satisfies the critical loading requirement for the improvement of the LOI value of polymers. Uniform filler dispersion in the electrospun samples act as a stable and continuous physical shielding for the underlying materials, and protect the underlying base polymer against further decomposition. Better filler dispersion also helps reducing and balancing the local heating when there is not enough fillers in the composites as shown in the thermal profile measurements of Figure 3.6 and simulation results of Figure 3.8 and Figure 3.9. When the percolation threshold of fillers is reached through the combination of micron and nano fillers, good filler dispersion and interaction lead to the formation of better thermal conductive networks in the electrospun samples. It also results in a higher thermal conductivity than that of conventional sample at the same filler loading as mentioned in section 3.2.2.

The improvement in the heat and erosion resistance and thermal degradation for electrospun samples are also due to the enhanced interaction between the filler and polymer matrix. The interactions between the silica and the SiR are principally due to the hydrogen bonding, and more hydroxyl group (-OH) on surface of nanosilica can be exposed when filler agglomerates are reduced by electrospinning. Stronger interaction occurs between hydroxyl group on the nanofiller surface and the siloxane

chain (-Si-O-Si-) of SiR polymer matrix, and further enhances the thermal performances of the final composites [85].

After decomposition, inorganic fillers and oxide residues form a solid layer on the top of the eroded areas during the IPT and laser ablation test. The residues of pure SiR, and nanosilica-filled conventional and electrospun SiR composites after TGA test were examined by EDX elemental analysis. The results for the analysis of residues are shown in Figure 4.5.

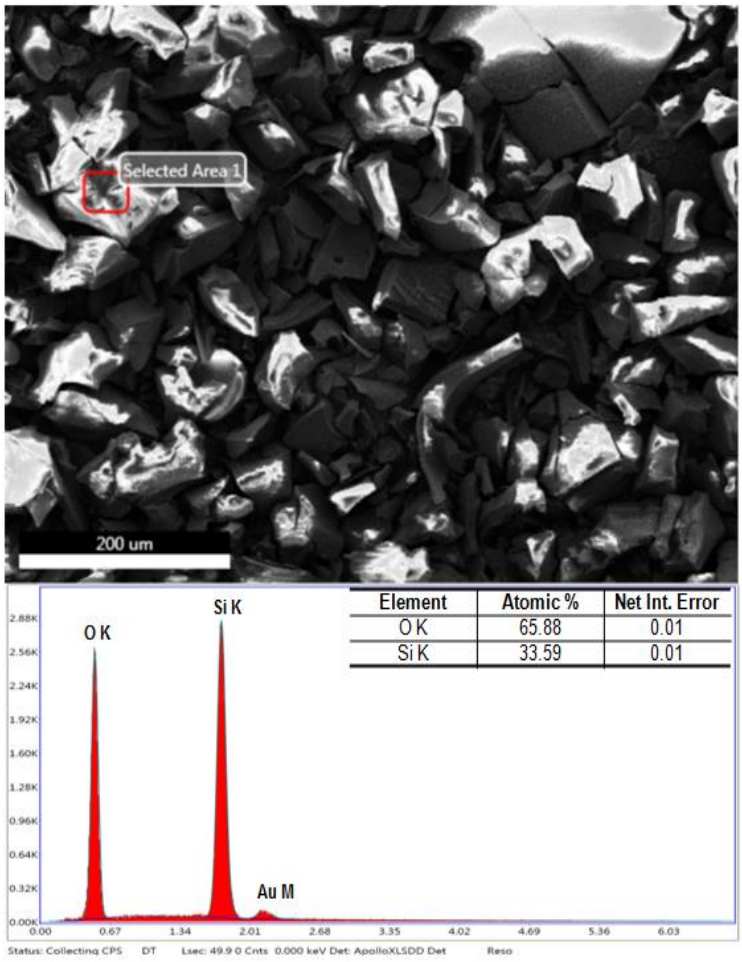

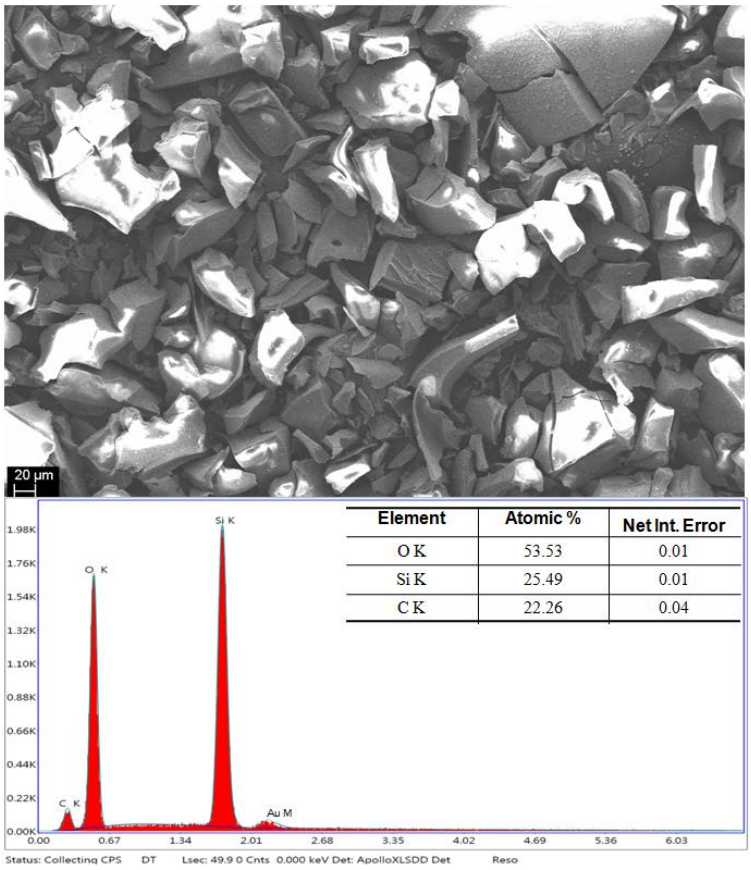

Element	Atomic %	Net Int. Error
O K	53.53	0.01
Si K	25.49	0.01
C K	22.26	0.04

(a)

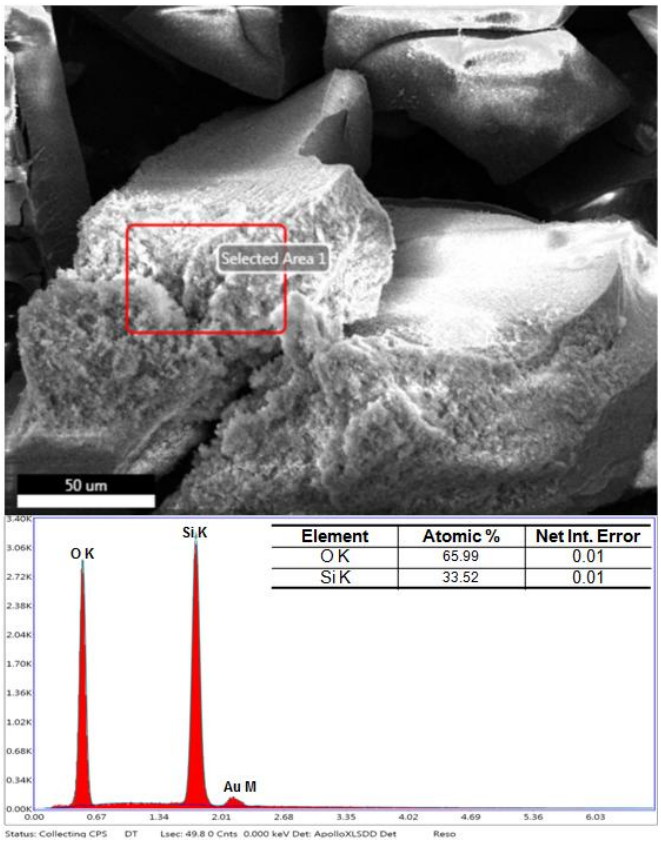

Element	Atomic %	Net Int. Error
O K	65.99	0.01
Si K	33.52	0.01

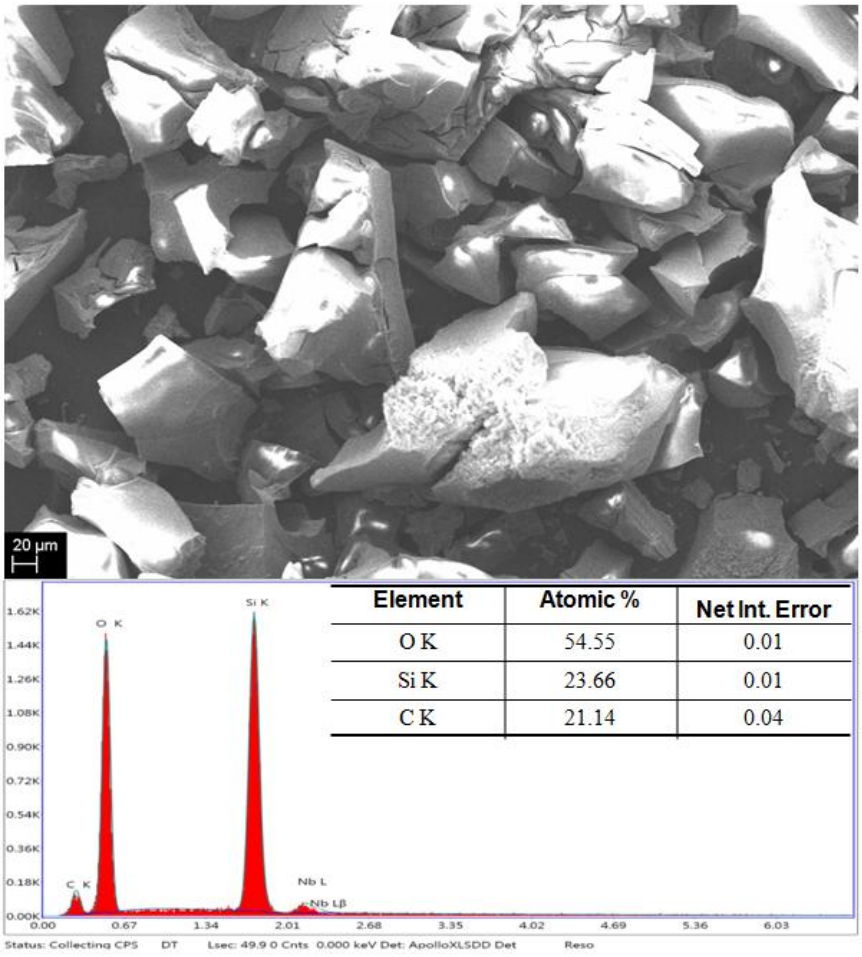

Element	Atomic %	Net Int. Error
O K	54.55	0.01
Si K	23.66	0.01
C K	21.14	0.04

(b)

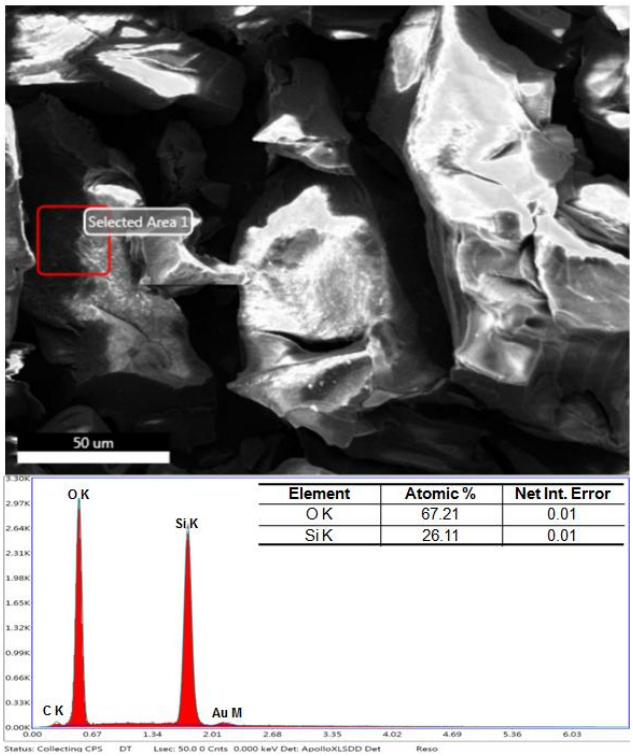

Element	Atomic %	Net Int. Error
O K	67.21	0.01
Si K	26.11	0.01

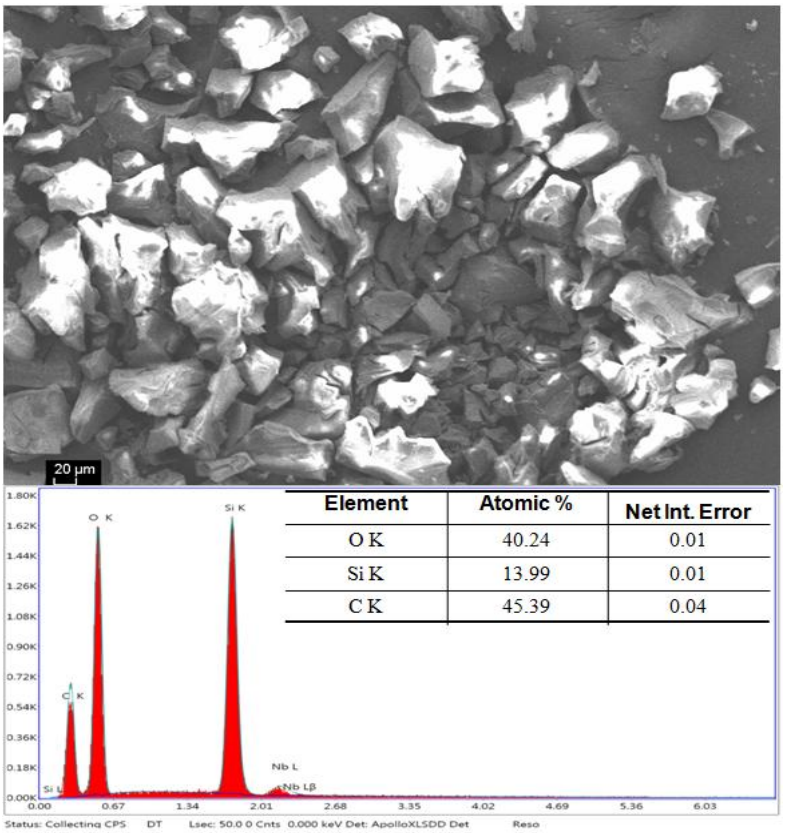

Element	Atomic %	Net Int. Error
O K	40.24	0.01
Si K	13.99	0.01
C K	45.39	0.04

(c)

Figure 4.5: The SEM and EDX analysis for the TGA test residues, and each sample was analyzed from a randomly selected small area and a big area (a) pure silicone rubber residues, (b) conventional nanosilica-filled SiR residues, and (c) electrospun nanosilica-filled SiR residues

It is assumed that after decomposition in the air, the residues will be only silica filler and oxides of SiR matrix. Although there is a difference in the filler dispersion , it is hard to see the detail of nanofiller morphology in the residues. The residues are all look like solid crusts except there is one area in conventional SiR nanocomposite (the selected small area in Figure 4.5 (b)), the residues look like a cluster of fillers. This filler clusters should be the result of the poor dispersion. EDX elemental analysis confirmed that there are only four different principal elements; Si (silicon), O (oxygen), C (carbon) and Au (gold) are detected. The carbon (C) can be from the carbon tape that used for SEM or carbonaceous residues of silicone rubber , and the gold (Au) is the required coating to overcome charging of samples during SEM. It is notable that the ratio of element Si to O in pure silicone rubber is 65.88 % : 33.59 %

and 53.53 % : 25.49 %, which is just around 1:2. Therefore, the residue of pure silicone rubber should be SiO_2 only. The ratio of Si to O in conventional SiR composite is 65.99 % : 33.5 % and 54.55 % : 23.66 %. The ration in the big area is around 1:2 but the ratio in the selected small area is slightly higher than 1:2. For electrospun SiR nanocomposite, the ratio of Si to O is 67.21 % : 26.11 % and 40.24 % : 13.99 % which is around 1:3. The increased oxygen level is probably due to the large amount of (–OH) groups on the surface of nanosilica which were exposed after electrospinning. The sufficient oxygen and the heat during TGA may produce amorphous SiO_2 with (-OH) groups ($SiO_2.xH_2O$) under 900 ^oC [147]. The well dispersed nanosilica and the enhanced bonding between nanosilica and polymer matrix can also lead to the modification of the thermal degradation pathways in the composites. Therefore, more stable carbonaceous residues can remain even at high temperature. The atomic % of carbon element for electrospun sample is around 45 %, but for conventional and pure sample are around 21 % and 22 %, respectively. Therefore, this assumption is confirmed by the high carbon element concentration in the EDX analysis for electrospun sample. The higher carbonaceous residues can be also the reason that electrospun SiR composites always have a higher remaining weight in the TGA tests even at the same filler loading compared to the conventional SiR composites.

More residues mean that electrospun composites can have a thicker layer of crust after erosion. This layer not only acts as a more effective thermal insulation layer to prevent the further erosion or decomposition of underneath materials, but also act as a barrier against the migration of the volatile thermal degradation products to the surface [148].

The using of electrospinning technique enhanced the properties of SiR composites is because of the increased filler loading and enhanced filler-matrix interaction. Ultimately, these benefits are attributed to the better dispersion of fillers in the electrospun SiR composites.

4.5 Possible Mechanisms of Electrospinning for Nanofiller Dispersion

During electrospinning, both the polymer and the nanosilica fillers embedded in it are charged, when the mixture is expelled from the metallic needle that is energized with a high DC voltage. The electrostatic forces and some other forces such as surface tension force, gravity, extrude the compound from the metallic needle form thin nanofibres. These forces may also act on the fillers but it is hard to specify which force dominantly contributes to the filler dispersion. Following forces may all help for the improved dispersion:

Over the extrusion process, a very strong shear force develops during the high elongation of silicone rubber fibres [140]. This large shear force is believed to be responsible for breaking up the nanofiller agglomerations.

The interaction of the electrical charges with the external electric field causes the repulsion of the charged nanofillers and prevents coalescing of fillers is another possible reason for the filler separation.

The permittivity of filled fillers can also have effects to the filler dispersion. Figures 4.6 and 4.7 show both the dispersion morphology of nanosilica (12 nm) and nano titanium dioxide (40 nm) in the electrospun epoxy samples. The distribution of nano titanium dioxide is more homogenous than that of nanosilica in the epoxy matrix. The permittivity of nanosilica is around 3.7, and permittivity of titanium dioxide is greater than 83. It is obvious that there is a big difference in dielectric constant for these two nanofillers. The nano titanium dioxide particle with higher permittivity will be polarized easier than that of the lower permittivity nanosilica, which may somehow help the separation of titanium dioxide fillers.

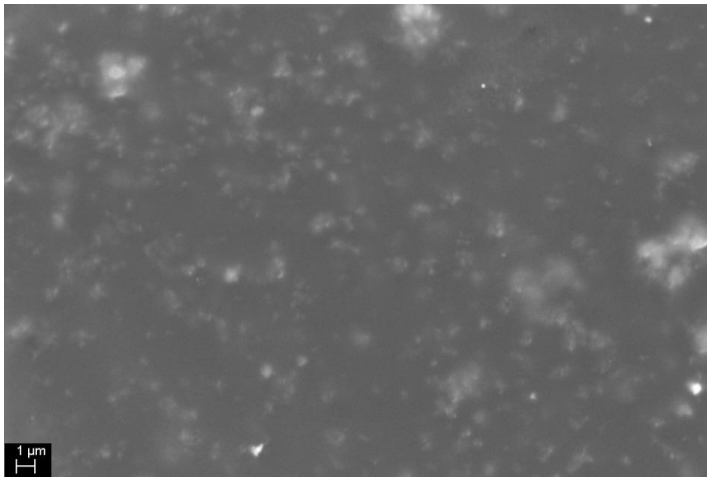

(a)

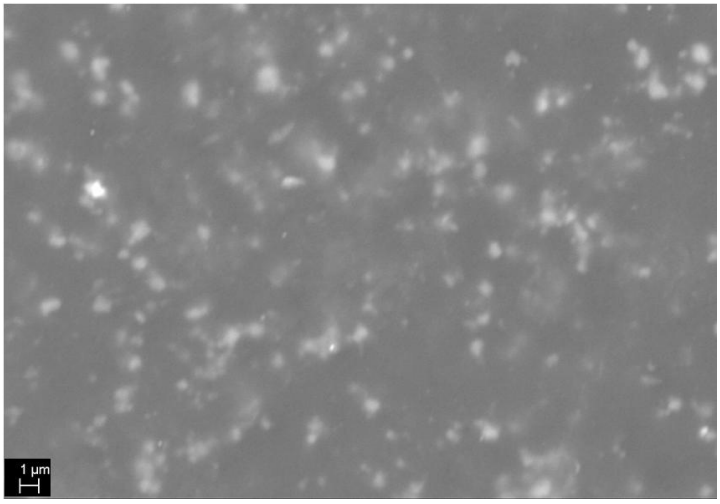

(b)

Figure 4.6: The SEM images of nano silica and nano titanium dioxide filled epoxy composites. (a) nanosilica-filled epoxy, and (b) nano titanium dioxide-filled epoxy.

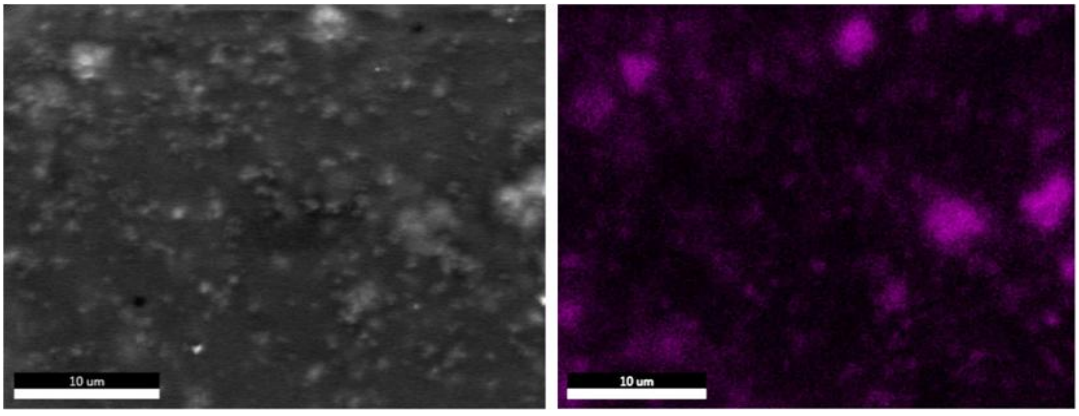

(a)

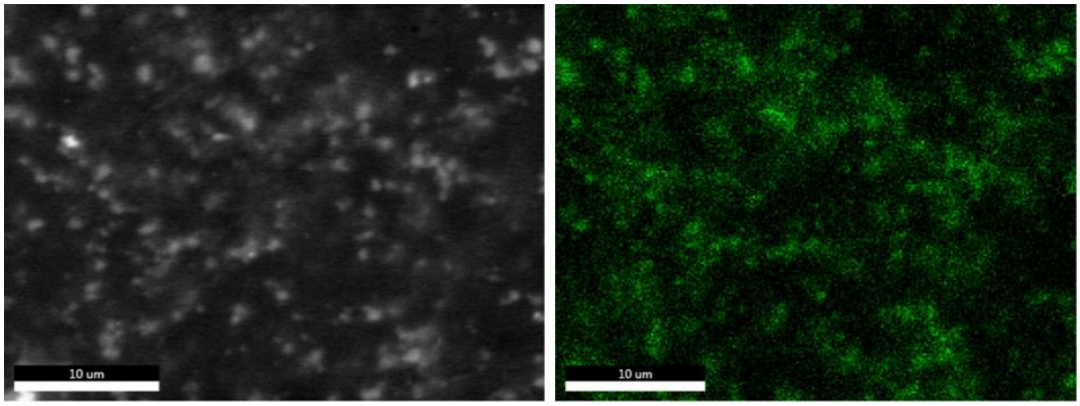

(b)

Figure 4.7: EDX-mapping of of nano silica and nano titanium dioxide filled epoxy composites. (a) nanosilica-filled epoxy, and (b) nano titanium dioxide-filled epoxy.

Chapter5

Conclusions and Suggestions for Future Work

5.1 Conclusions

Polymeric materials with several outstanding properties such as light weight, excellent flexibility, and good surface characteristics are replacing conventional insulation materials such as porcelain and glass materials in a wide range of high voltage insulation applications. However, polymeric materials are usually poor thermal conductors and weak mechanical structures, such that they are prone to fail in terms of electrical tracking and erosion due to the synergism of pollution, moisture, and voltage. To improve the performances of polymeric materials, inorganic fillers are commonly added to base polymers to enhance the desired properties of polymers, and reduce the total cost. Microfillers are extensively used in both research and industry to modify the physical properties of polymers. Conventional polymer composite materials with particular properties can meet the special requirements of electrical applications in the past. However, the incessant compaction of electrical power equipment continues to necessitate new requirements to electrical insulating materials. Consequently, nanofillers, compelled to microfillers, are capable of providing similar or even better properties at considerably lower volume fraction due to the large surface area of nanofillers.

The primary problem of using nanofillers is that they easily agglomerate because of their high surface energy. Conventional mechanical mixing cannot effectively break apart the filler clusters, and existing chemical nanofiller dispersion methods are very complicated. The effective and consistent physical properties of a composite is a function of the physical properties of the constituents, the filler loading, the filler

shape and size, and the filler dispersion, as well as the interfacial properties of the fillers and matrices. Filler dispersion is a critical factor that cannot be ignored in the development of nanocomposites. Due to the limitations of existing mixing methods, an alternative simple mixing method is necessary.

In this thesis, an electrospinning technique has been proposed as an efficient alternative method for nanofiller dispersion. Further reinforcement of pure polymeric materials is successfully achieved with nanofillers and the combination of micro and nano fillers by electrospinning. The scanning electron microscopy images and energy dispersive X-ray analysis confirmed that electrospun nanocomposites have an enhanced filler dispersion and filler interaction than conventional nanocomposites prepared by mechanical mixing. The electrospinning technique also presented the potential to separate various nanofillers in various base polymers such as nanosilica (SiO_2), nano titanium oxide (TiO_2) in silicone rubber (SiR) and epoxy resin. Moreover, more nanofillers and even microfillers were pushed into base polymers by the electrospinning technique due to the better dispersion of nanofillers.

During electrospinning, both the polymer and its nanosilica fillers are charged when the mixture is expelled from a metallic needle energized by a high DC voltage. During the extrusion process, a very strong shear force develops on the silicone rubber fibres, and is believed to mitigate the nanofiller agglomerations. In addition, the interaction of the electrical charges with the external electric field causes the repulsion of the charged nanofillers, which is an additional explanation for the separation of the nanofillers' agglomerates.

The thermal degradation of composites is enhanced since the addition of inorganic fillers reduces the base polymer portion in the compound, improving the anti-oxidation and thermal degradation. Electrospinning has significantly improved the thermal degradation and heat erosion resistance for nanosilica-filled and micron plus nanosilica-filled silicone rubber (SiR) composites without deteriorating the other properties. The static contact angle, tensile strength, hardness, or permittivity is slightly improved or remains unchanged compared to those of conventional SiR

composites. Also, the electrospun SiR composites reflect thermal and economic advantages. Thermo-gravimetric analysis (TGA), an infrared laser-based heat ablation test, and ASTM standard inclined plate test are used to evaluate the enhanced thermal performances of the SiR composites. There is no significant global thermal conductivity improvement at the selected filler loading for both electrospun and conventional nanosilica filled SiR composites, using only nanofillers. This is probably due to the low filler concentration which does not reach the filler percolation threshold. But there is local temperature reduction based on the thermal profile measurement and the simplified thermal simulations showing nanofilled samples yielded a lower and more uniform temperature distribution if the nanofillers were evenly separated. The combination of the microfillers and the nanofillers not only takes advantage of the nanofillers but also can satisfy the high filler loading requirement for the improvement of the LOI of polymers. In addition, the global thermal conductivity was improved when more fillers were added. Electrospun sample showed a thermal conductivity of 0.5 W/ m ŀK as compared to conventional sample of 0.31 W/ m ŀK at a filler loading of 20 wt% microsilica plus 5 wt% nanosilica. The significant thermal conductivity improvement of electrospun sample is contributed to the improved filler-to-filler interaction which leads to the improved thermal conductive pathways for the heat transfer.

Both fillers and oxide residues due to the decomposition of the polymers, act as a physical heat barrier protecting the underlying base polymer against further decomposition. The uniform distributed filler by electrospinning provide a more uniform and continuous physical shielding to the underlying materials. The interactions between silica and SiR impact through hydrogen bonding when the nanofiller are well dispersed, more interaction occurs between the filler and polymer matrix which further enhance the thermal performances of the final composites. This observation is also confirmed by the TGA and EDX analysis and thermal performance tests.

In summary, electrospinning, as a new alternative mixing method, effectively improves the nanofiller dispersion in at least two different polymeric materials. Also, more fillers can be added. The heat and erosion resistance of electrospun SiR nanocomposites improves significantly, but the optimal results come from the micro and nano-filled SiR composites, satisfying the ASTM standard requirements and reducing the cost as well.

5.2 Suggestions for Future Work

Based on the research work of the thesis, nanofiller dispersion is the governing parameter for enhancing composite's properties. SEM images, EDX-mapping and rheological property of compound are used to evaluate the dispersion level of nanofillers in the base polymers. However, a computational methodology is desired to combine with the previous methods to precisely quantify the degree of dispersion of nanofillers.

The production of the single needle electrospinning setup is not very efficient. For commercial applications, an extension of this research should include alternative electrospinning configurations to speed up nanofiller dispersion in polymers.

In this thesis, two polymeric materials are successfully electrospun and only nanosilica is primarily studied. More dielectrics and nanofillers should be investigated to understand how to control the electrospinning technique in the nanofiller dispersion. Besides the heat erosion resistance and thermal degradation, many other properties should be further reinforced if necessary.

The thesis focuses on the heat erosion resistance, but other interesting results should be further investigated, including the surface patterns of SiR composites under corona aging, and the distribution patterns of different permittivity nanofillers in electrospun composites. These extensions might facilitate a better understanding of the mechanism of electrospinning for nanofiller dispersion and define the application range of this mixing method.

Improved thermal modelling should allow for a temperature prediction or develop a modeling of nanocomposite interactions on a molecular level to help better understanding the basic interactions and predict the possible properties of nanocomposites.

References

1. G.C.Stone, R.G. van Heeswijk, and R.Bartnikas, “Investigation of the effect of repetitive voltage surges on epoxy insulation,” Energy Conversion, IEEE Transactions on, vol.7,no.4, pp.754-760, 1992.
2. J.P.Reynders, I.R.Jandrell, “Rubber Insulation for Outdoor Insulation,” Dielectrics and Electrical Insulation, IEEE Transactions on , vol.6,no.5,pp.620-631,1999.
3. J.F.Chailan, G.Boiteux, J.Chauchard, B.Pinel, G.Seytre, “Viscoelastic and dielectric study of thermally aged ethylene-propylene diene monomer (EPDM) compounds,” Polymer Degradation and Stability, vol.47, no.3, pp.397-403, 1995.
4. M.Katz, R.J.Theis , “ New high temperature polyimide insulation for partial discharge resistance in harsh environments,” Electrical Insulation Magazine, vol.13,no.4, pp.24-30, 1997.
5. J.Muccigrosso, P.J. Phillips, “ The Morphology of Cross-Linked polyethylene Insulation,” Electrical Insulation, IEEE Transactions on, vol.EI-13,no.3, pp.172-178,2007.
6. F.N.Lim, R.J. Fleming, R.D. Naybour, “Space charge accumulation in power cable XLPE insulation,” Dielectrics and Electrical Insulation, IEEE Transactions on , vol.6,no.3, pp.273-281, 1999.
7. Mouzheng Fu, Baojun Qu, “ Synergistic flame retardant mechanism of fumed silica in ethylene-vinyl acetate/ magnesium hydroxide blends,” Polymer Degradation and Stability, vol.85,no.1, pp.633-639,2004.
8. Huijun Wu, Jintu Fan, Xiaohong Qin, Sam Mo, Juan P.Hinestroza, “Fabrication and characterization of a novel polypropylene/poly(vinyl alcohol)/aluminum hybrid layered assembly for high-performance fibrous insulation,” Journal of Applied polymer Science, vol.110, no.4, pp.2525-2530, 2008.
9. E.Mihlayanlar, S.Dilmac, A. Güner, “Analysis of the effect of production process parameters and density of expanded polystyrene insulation boards on mechanical properties and thermal conductivity,” Material & Design, vol.29, no.2, pp.344-352, 2008.
10. R.Gorur, “Epoxy formulation for composite polymer insulators,” Insulator News and Market Report,vol.jul/Aug,2000.
11. Luiz Henrique Meyer, “A study of the role of fillers in silicone rubber compounds for outdoor insulation,” PhD thesis, University of Waterloo, 2003.
12. Gui-Hong Chen, Bing Yang, Yu-Zhong Wang, “ A novel flame retardant of spirocyclic pentaerythritol bisphosphorate for epoxy resins," Journal of Applied Polymer Science, vol.102,no.5, pp.4978-4982, 2006.
13. G.M. Tsangaris, N.Kouloumbi, S.Kyvelidis, “Interfacial relaxation phenomena in particulate composites of epoxy resin with copper or iron particles," Materials Chemistry and Physics, vol.44, no.3, pp.245-250, 1996.
14. J.P.Reynders, I.R.Jandrell,” Review of Aging and Recovery of Silicone Rubber Insulation for Outdoor Use," IEEE Transactions on Dielectrics and Electrical Insulation, vol.6, no.5, pp.620-631, 1999.
15. George G.Karady, Minesh Shah, R.L.Brown,” Flashover Mechanism of Silicone Rubber Insulations Used for Outdoor Insulation-I," IEEE Transitions on Power Delivery, vol.10, no.4, pp.1965-1971, 1995.

16. Kumagai S, Yoshimura N, “Hydrophobic transfer of RTV silicone rubber aged in single and multiple environmental stresses and the behavior of LMW silicone fluid,” IEEE Transactions on Power Delivery, vol.18, no.2, pp.506-516, 2003.
17. E.A.Cherney, “Silicone Rubber Dielectrics Modified by Inorganic Fillers for Outdoor High Voltage Insulation Applications," IEEE Transactions on Dielectrics and Electrical Insulation, vol.12, no.6, pp.1108-1115, 2005.
18. T, Zhao and R. A. Bernstorf, "Aging Tests of Polymeric Housing Materials for Non- Ceramic Insulators," IEEE Electrical Insulation Magazine, vol. 14, no. 2, pp. 26-33, 1998.
19. S.Kumagai, N.Yoshimura, "Tracking and Erosion of HTV Silicone Rubber and Suppression Mechanism of ATH," IEEE Transactions on Dielectrics and Electrical Insulation, vol.8, no.2, pp.203-211, 2001.
20. R.Gorur, E.Cherney, R.Hackam and T.Orbeck, "The Electrical Performance of Polymeric Insulating Materials under Accelerated Aging in A fog Chamber," IEEE Transactions on Power Delivery, vol.3, pp.1157-1164, 1988.
21. Luiz Meyer, Shesha.Jayaram and Edward A.Cherney, "Thermal Conductivity of Filled Silicone Rubber and Its Relationship to Erosion Resistance in the Inclined Plane Test, " IEEE Transactions on Dielectrics and Electrical Insulation, vol.11, no.4,pp.620-630,2004.
22. S. Kim, E A. Cherney and R. Hackam, "Effects of filler level in RTV silicone rubber coatings used in HV insulators," IEEE Trans. Elect. Insul., vol. 27, pp. 1065–1072, 1992.
23. L.H.Meyer, E.A.Cherney and S.H.Jayaram, "The Role of Inorganic Fillers in Silicone Rubber for Ourdoor Insulation –Alumina Tri-Hydrate or Silica," IEEE Electr.Insul.Mag., vol.20, pp.13-21, 2004.
24. Ranimol Stephen, A.M.Siddique, Fouran Singh, Lekshmi Kailas, Seno Jeose, Kuruvilla,Sabu Thomas, " Thermal Degradation and Aging Behavior of Microcomposites of Natural Rubber, Carboxylated Styrene Butadiene Rubber Latices, and Their Blends", Journal of Applied Polymer Science ,vol.105, pp.341-351, 2007.
25. H.Z.Ding and B.R.Varlow, "Filler Volume Fraction Effects on the Breakdown Resistance of An Epoxy Microcomposite Dielectric,” 2004 international Conference on Solid Dielectrics, Toulouse, France, vol.2, pp.816-820, July5-9, 2004.
26. Toshikatsu Tanaka, Shin-ichi Kuge, "Nano Effects on PD Endurance of Epoxy Nanocomposites,” Proc.ICEE, No.ME1-01 pp.1-4, 2006.
27. K.Ghosh and S.N. Maiti ", Mechanical Properties of Silver –Powder-Filled Polypropylene Composites,”Journal of Applied Polymer Science, vol.60, pp. 32-331, 1996.
28. Manwar Hussain, Atsushi NakaHira, Shigehiro Nishijima,Koichi Niihara, " Fracture behavior and fracture toughness of particulate filled epoxy composites,” Material Letters, vol.27,pp.21-25,1996.
29. M. F. Fréchette, M. Trudeau, H. D. Alamdari, and S.Boily, "Introductory remarks on Nano Dielectrics,” IEEE Conf. Electr. Insul. Dielectr. Phenomena, pp. 92-99, 2001.
30. W. Peukert, H-C. Schwarzer, M. Gozinger, L. Günther, and F. Stenger, "Control of particle interfaces—the critical issue in nanoparticle technology,”Adv. Powder Tech.,vol. 14, no. 4, pp. 411-426, 2003
31. Joseph H. Koo, Polymer Nanocomposites: processing, characterization and Applications. New York: McGraw-Hill, 2006.

32. T.J.Lewis, "Interfaces are the Dominant Feature of Dielectrics at the Nanometric Level," IEEE Transactions on Dielectrics and Electrical Insulation, vol.11, no.5, pp.739-753, 2004.
33. Christopher Green and Alun Vaughan, "Nanodielectrics- How Much Do We Really Understand?," IEEE Electrical Insulation Magazine, vol.24, no.4, pp.6-16, 2008.
34. M.F. Frechette, M.L. Trudea, H.D. Alamdari and S. Boily, "Introductory Remarks on Nanodielectrics," IEEE Transactions on Dielectrics and Electrical Insulation, vol.11, no.5, pp.808-818, 2004.
35. R.C. Smith, C. Liang, M. Landry, J.K. , Nelson, L.S. Schadler, " The Mechanisms Leading to the Useful Electrical Properties of Polymer Nanodielectrics," IEEE Transactions on Dielectrics and Electrical Insulation, vol.15,no.1,pp.187-196,2008.
36. Lan Lei,Wen Xishan and Cai Dengke, " Corona Aging Tests of RTV and RTV Nanocomposite Materials, " 2004 International Conference on Solid Dielectrics, Toulouse , France,vol.2,pp.804-807,2004.
37. A.H.EI-Hag, L.C.Simon, S.H.Jayaram and E.A.Cherney, "Erosion Resistance of Nano-filled Silicone Rubber," IEEE Transactions on Dielectrics and Electrical Insulation, vol.13, no.1, pp.122-128, 2006.
38. L.H.Meyer, E.A.Cherney and S.H.Jayaram, "The Role of Inorganic Fillers in Silicone Rubber for Ourdoor Insulation –Alumina Tri-Hydrate or Silica," IEEE Electr.Insul.Mag., vol.20, pp.13-21, 2004.
39. Stephanie Ratzke and Josef Kindersberger, "Erosion Behaviour of Nano Filled Silicone Elastomers," Proceeding of the XIVth International Symposium on High Voltage Engineering Tsinghua University, Beijing, China, 2005.
40. R.Kochetov, T.Andritsch, P.H.F.Morshuis,J.J.Smit, "Effect of iller size on Complex Permittivity and Thermal Conductivity of Epoxy-based Composites Filled with BN particles," CEIDP 2010, Purdue University, West Lafayette, Indiana, CEIDP symposium, vol.1, pp.534-537,2010.
41. Frormann L, Iqbal A, Abdullah S.A, "Thermo-Viscoelastic Behavior of PCNF-Filled Polypropylene Nanocomposites," J Appl Polym Sci, vol.107, no.4, pp.2695-2703, 2008.
42. Zhang MY, Zeng SJ, Dong TQ, Fan Y, and Lei QQ, "Synthesis and Characterization of Polyimide/Silica Nanocomposite Films," IEEE International Conference on Solid Dielectrics ICSD, pp.357-359, 2007.
43. Zhou H, Fan Y, Lei QQ, "Synthesis and Characterization of Corona-Resistant Polyimide/Alumina Hybrid Films, "8th International Conference on Properties and Applications of Dielectric Materials, pp.736-738, 2006.
44. P.C.Irwin, Y.Cao,A.Bansal and L.S.Schadler, "Thermal and Mechanical Properties of Polymide Nanocomposites," 2003 Annual Report Conference on Electrical Insulation and Dielectric Phenomena, pp.120-123,2003.
45. Zhanhu Guo, Xiaofeng Liang, Toney Pereira, Roberto Scffaro,H.Thomas Hahn, "CuO nanoparticle filled vinyl-ester resin nanocomposites: Fabriccation , characterization and property analysis," Composites Science and Technology, vol.67, pp.2036-2044, 2007.
46. Qi Zahng, Ming Tian, Youping Wu, Gui Lin, Liqun Zhang, " Effect of particle size on the properties of $Mg(OH_2)$ –Filled rubber Cmpsoites," Journal of Applied Polymer Science ,vol.94, pp.2341-2346,2004.

47. M.W.Beatty, M.L.Swartz, B.K.Moore, R.W.Philips, T.A.Roberts, "Effect of Microfiller faction and silane treatment on resion composite properties," J Biomed Mater Res., vol.40, no.1, pp. 12-23, 1998.
48. G.Weymans and U.Esiele, "Influence of the Filler on the Reinforcing Mechanism of Styrene-butadiene Rubbers," Progress in Colloid & Polymer Science, vol.75, pp.231-233, 1987.
49. Alfred J.Crosby and Jong-Yong Lee, " Polymer Nanocomposites: The "Nano" Effect on mechanical Properties, " Polymer Reviews, vol.47, pp.217-229, 2007.
50. Maurizio Avella, Maria Emanuela Errico, Gennaro Gentile, "PMMA Based Nanocomposites Filled with Modified $CaCO_3$ Nanoparticles," Macromol, Symp, pp. 140-146, 2007.
51. Weisenberger MC, Grulke EA, Jacques D, Rantell T,Andrews R., "Enhanced mechanical properties of polyacrylonitrile/multiwall carbon nanotube composite fibers, " J Nanosci Nanotech, vol.3,no.6, pp.535-539,2003.
52. Dalton AB, Collins S, Munoz E, Razal JM, Ebron VH, Ferraris JP, et al. "Super-tough carbon-nanotube fibres, " Nature, pp. 423-703, 2003.
53. R.Andrews, M.C. Weisenberger, "Carbon nanotubes polymer composites, "Current Opinion in Solid State and Materials Science ,vol.8, pp.31-37,2004
54. M. Kozako, R. Kido, N. Fuse, Y. Ohki, T. Okamoto, and T. Tanaka, "Difference in Surface Degradation due to Partial Discharges between Polyamide Nanocomposite and Microcomposite, " IEEE Conf. Electr. Insul. Dielectr. Phenomena, pp. 398-401, 2004.
55. B. J. Ash, L. S. Schadler, R. W. Siegel, T. Apple, B. C. Benicewicz, D. F. Roger, and C. J. Wiegand, "Mechanical Properties of Al2O3 / Polymethylmethacrylate Nanocomposites, " Polymer Composites, vol. 23, pp.1014-25, 2002.
56. Tuncer Enis, Industrial Applications Perspective of Nanodielectrics, Springer, New York, 2011.
57. Kozako Masahiro, Kuge Shin-Ichi, Imai Takahiro, Ozaki Tamon, Shimizu Toshio and Tanaka Toshikatsu, "Surface erosion due to partial discharges on several kinds of epoxy nanocomposites," Conference on Electrical Insulation and Dielectric Phenomena 2005, pp.162-165,2005.
58. J.Keith Nelson, John C.Fothergill, L.A. Dissado and W.Peasgood, " Towards an understanding of nanomeric dielectrics," Electrical Insulation and Dielectric Phenomena, 2002 Annual Report Conference on, CEIDP, pp. 295 – 298,20-24 Oct. 2002.
59. J.Keith Nelson, John C.Fothergill, "Internal Charge Behavior in Nanocomposites," Nanotechnology, vol. 15, pp. 586-595, 2004.
60. Roy M, Nelson JK, MacCrone RK, Schadler LS, Reed CW Keefe R and Zenger W," Polymer Nanocomposite Dielectrics-The role of the Interface," IEEE Transactions on Dielectrics and Electrical Insulation, vol.12, no.4, pp.629-643, 2005
61. S.Alapati and M.Joy Thomas, "Influence of nano-fillers on electrical treeing in epoxy insulation," IET Sci.Meas.Techol., vol.6, no.1, pp.21-28, 2012.
62. Peter Barber, Shiva Balasubramanian, Yogesh Auguchamy, Shushan Gong,"Polymer Composite and Nanocomposite Dielectric Materials for Pulse Power Energy Storage," Materials, vol.2,pp.1697-1733,2009.
63. Philseok Kimt, Natalie M. Dosst, John P.Tillotsont,"High Energy Density Nanocomposites Based on Surface-Modified $BaTiO_3$ and a Ferroelectric Polymer," ACS Nano, vol.3,no.9,pp.2581-2592,2009.
64. Li L, Takahashi A, Hao JJ, Kikuchi R, Hayakawa T, Tsurumi TA, Kakimoto MA, "Novel polymer-ceramic nanocomposite Based on New Concepts for Embedded Capacitor Application

(I),” IEEE Transactions on Components and Packaging Technologies, vol.28, no.4, pp.754-759, 2005.
65. Ying Shen, Cherney, E.A., Jayaram, S.H. “Electric Stress Grading of composite Bushing using High Dielectric Constant Silicone Compositions,” IEEE International Symposium on Electrical Insulation 2004, pp.19-22.
66. Yang Cao, Qin Chen, Daniel Qi Tan, and Patricia C Irwin, "Nanostructured Dielectric Materials," 2010 International Conference on Solid Dielectrics, Potsdam, Germany, pp.1-4 ,2010.
67. Santanu Singha and M.Joy Thomas, "Dielectric Properties of Epoxy Nanocomposites," IEEE Transactions on Dielectrics and Electrical Insulation, vol.15, no.1, pp.12-23, 2008.
68. C.Albano, M.Ichazo, J. Gonz áez, M. Delgado and R. Poleo,"Effects of filler treatments on the mechanical and morphological behavior of PP+wood flour and PP+sisal fiber," Materials Research Innovations, vol.4,no.5-6,pp.284-293,2001.
69. Ko F, Gogotsi Y, Ali A, Naguib N, Ye H, Yang G, et al.,"Electrospinning of continuous carbon nanotube-filled nanofiber yarns," Adv Mater; vol.15, no.14, pp. 1161–5, 2003.
70. X. Chen and K.E. Gonsalves, "Synthesis and Properties of an Aluminum Nitride/Polyimide Nanocomposite Prepared by A Nonaqueous Process," J. Mater. Res. vol.12, pp. 1274–1286, 1997.
71. M.Z.Rong, M.Q.Zhang and W.H.Ruan, "Surface Modification of Nanoscale Fillers for Improving Properties of Polymer Nanocomposite: a review, " Materials Science and Technology, vol.26, no.7, pp.787-796, 2006.
72. A.W.Pacek,P.Ding and A.T.Utomo, " Effect of Energy Density , pH and Temperature on De-aggregation in Nano-particles/Water Suspensions in High Shear Mixer," Power Technology,vol.173,pp.203-210,2007.
73. Rajesh Dave,Ram Gupta and Robert Pfeffer, "Deagglomeration and Mixing of Nanoparticles, " NSF Science and Engineering Grantees Conference,2006.
74. Deuk Yong Lee, Kwang Jin Kim, Seok heo, Myung Hyun Lee, and Bae Yeon Kim, “Application of an Equivalent Circuit Model for Ionic Polymer-Metal Composite (IPMC) Bending Actuator Loaded With Multiwalled Carbon Nanotube (M-CNT),” Key Engineering Materials , vol.309-311, pp.593-596, 2006.
75. Dongguang Wei, Rajesh Dave and Robert Pfeffer, "Mixing and Characterization of Nanosized Powders: An Assessment of Different Techniques, "Journal of Nanoparticle Research, vol.4, pp.21-41, 2002.
76. V.V.Klimov and A.Lambrecht, "Van der Waals Forces between Plasmonic Nanoparticles," Plasmonics, vol.4, pp.31-36, 2009.
77. I.Ramirez, E.A.Cherney, S.Jayaram and M.Gauthier, "Nanofilled Silicone Dielectrics Prepared with Surfactant for Outdoor Insulation Applications," IEEE Transactions on Dielectrics and Electrical Insulation, vol.15, no.1, pp.228-235, 2008.
78. Sahhan C. Jana and Sachin Jain, "Dispersion of Nanofillers in High Performance Polymers Using Reactive Solvents as Processing Aids," Polymer, vol.42, pp.6897-6905, 2001.
79. Santanu Singha and M.Joy Thomas, "Polymer Composite/Nanocomposite Processing and Its Effect on the Electrical Properties," 2006 Annual Report Conference on Electrical Insulation and Dielectric Phenomena, pp.557-560.
80. S.Mende,F. Stenger,W. Peukert, J. Schweder, "Mechanical Production and Stabilization of Submicron Particles in Stirred Media, " Powder Technol. vol.132,pp. 64-73,2003.

81. Pukanszky. B and Fekete .E, "Aggregation tendency of particulate fillers: determination and consequences, " Polym. Polym. Compos, vol.6, pp.313-322, 1998.
82. A.H.EI-Hag, L.C.Simon, S.H.Jayaram and E.A.Cherney, "Erosion Resistance of Nano-filled Silicone Rubber," IEEE Transactions on Dielectrics and Electrical Insulation, vol.13, no.1, pp.122-128, 2006.
83. Karol Bula,Teofil Jesionowski, "The effect of filler surface modification and processing conditions on distribution behavior of silica nanofillers in polyesters," Colloid Polym Sci, vol.285, pp.1267-1273,2007.
84. P.Y.Chow and L.M.Gan, "Microemulsion Processing of Silica-Polymer Nanocomposites," Journal of Nanoscience and Nanotechnology, vol.4, pp.197-202, 2004.
85. M.S.P.Shaffer, X.Fan and A.H.Windle, "Dispersion and Packing of Carbon Nanotubes," Carbon, vol.36, no.11, pp.1603-1612, 1998.
86. Isaias Ramirez,Shesha Jayaram, Edward.A.Cherney and Mario Gauthier, " Ersion Resistance and Mechanical Properties of Silicone Nanocomposite Insulation, " IEEE Transactions on Dielectrics and Electrical Insulation, vol.16,no,1,pp.52-59,2009.
87. B.Vincent, "The Effect of Adsorded Polymers on Dispersion Stability," Advances in Colloid and Interface Science, vol.4, pp.193-277, 1974.
88. Yangyang,Sun, Zhuqing Zhang and C.P.Wong, "Influence of Nanosilica on Composite Underfill Properties in Flip Chip Packaging," 9th International Symposium on Advanced Packaging Materials,pp.253-259, 2004.
89. Zongwei Li and Yongfa Zhu, "Surface-modification of SiO_2 Nanoparticles with Oleic Acid," Applied Surface Science, vol.211, pp.315-320, 2003.
90. D.I.Tee, M.Mariatti, A.Azizan,C.H.See and K.F.Chong, "Effect of Silane-based Coupling Agent on the Properties of Silver Nanoparticles filled Epoxy Composites," Composites Science and Technology, vol.67,pp.2584-2591,2007.
91. Formhals, "Process and Apparatus for Preparing Artificial Threads," U.S. Patent No. 1975504.
92. Angammana, Chitral Jayasanka," A Study of the Effects of Solution and Process Parameters on the Electrospinning Process and Nanofibre Morphology", PhD Thesis, University of Waterloo, 2011.
93. S. Ramakrishna, K. Fujihara, W.E. Teo, T.C. Lim, and Z. Ma, An Introduction to electrospinning and nanofibers. Singapore: World Scientific Publishing Co. Pte. Ltd., 2005.
94. G. Taylor,"Electrically Driven Jets,"Proceedings of the Royal Society of London, Series A, Mathematical and Physical Sciences, vol. 313, No. 1515, pp. 453-475, Dec. 1969.
95. C. Burger, B. S. Hsiao, and B. Chu, "Nanofibrous Materials and Their Applications," Annu. Rev. Mater. Res., vol. 36, pp. 333–368, 2006.
96. X.M. Mo, C.Y. Xu, M. Kotaki, and S. Ramakrishna, "Electrospun P (LLA-CL) nanofiber: A Biomimetic Extracellular Matrix for Smooth Muscle Cell and Endothelial Cell Proliferation," Biomaterials, vol. 25, pp. 1883–1890, 2004.
97. D.H. Reneker, A.L. Yarin, H. Fong, and S. Koombhongse, "Bending Instability of Electrically Charged Liquid Jets of Polymer Solutions in Electrospinning," J. Appl. Phys., vol. 87, 4531–4547, 2000.
98. R.S.Gorur, E.A.Cherney and J.T. Burnham, Outdoor Insulators.USA: Ravi S.Gorur, Inc, 1999.
99. Audrey Frenot and Ioannis S.Chronakis, "Polymer Nanofibers Assembled by Electrospinning," Current Opinion in Colloid and Interface Science, vol.8, pp.64-75, 2003.

100. Yu-Hsun Nien,Po-Jung Lin,Lih-Yun Wu,Tzy-Harn Liou and Pey-I Wey, " Preparation of Poly (vinyl alcohol)/TiO_2 Nanofibers by electrospinning," 4th Topical Conference on Nanoscale Science and Engineering Forum, AlChE Fall 2004,pp.1-4,2004.
101. Shunsuke Yagi, Tomoki Nakagawa and Eiichiro Matsubara, et al, "Formation of Tin Nanoparticdles Embedded in Poly (L-Lactic Acid) Fiber by Electrospinning," Electrochemical and Solid-State letters, vol.11, pp.E25-E27, 2008.
102. Di Zhang, Amar B.Karki and Dan rutman, et al, "Electrospun Polyacrylonitrile Nanocomposite Fibers Reinforced with Fe_3O_4 Nanoparticles: Fabrication and Property Analysis, " Polymer, vol.50, pp.4189-4198, 2009.
103. Leslie Y.Yeo and James R.Friend, "Electrospinning Carbon Nanotube Polymer Composite Nanofibers," Journal of Experimental Nanoscience, vol.1, no.2, pp.177-209, 2006.
104. Meei-Jiun Chen, "Carbon Nanotube Dispersion Using Electrospraying," M.S.Thesis, The Florida State University, Florida, United States, 2007.
105. G.M. Kim, G.H. Michler and P. Potschke, "Deformation Processes of Ultrahigh Porous Multiwalled Carbon Nanotubes/Polycarbonate Composite Fibers Prepared by Electrospinning," Polymer, vol.46, pp.7346-7351, 2005.
106. Y.Dror, W. Salalha,R.L. Khalfin, and et al, "Carbon Nanotubes Embedded in Oriented Polymer Nanofibers by Electrospinning," Langmuir, vol.19, pp.7012-7020 ,2003.
107. C.Seoul, Y.T.Kim andC.K.Baek, "Electrospinning of Poly (vinylidene fluoride)/ Dimethylformamide Solutions with Carbon Nanotubes," Journal of Polymer Science Part B: Polymer Physicsv, vol.41, pp.1572-1577, 2003.
108. Ge.JJ, Hou.H, Li.Q, M.J and et al, "Assembly of Well-aligned Multiwalled Carbon Nanotubes in Confined Polyacrylonitrile Environments: Electrospun Composite Nanofiber Sheets, " J. Am. Chem. Soc., vol.126, pp.15754 -15761, 2004.
109. Saeedeh Mazinani, Abdellah Ajji and Charles Dubois, "Morphology, Structure and Properties of Conductive PS/CNT Nanocomposite Electrospun Mat," Polymer, vol.50, pp.3329-3342, 2009.
110. Frank K.Ko,Sakina Khan,Ashraf Ali and et al, "Structure and Properties of Carbon Nanotube Reinforced Nanocomposites," American Institute of Aeronautics and Astronautics, pp.1-9.
111. Prabhakaran Kannan, Stephen J.Eichorn and Robert J.Young, "Deformation of Isolated Single-wall Carbon Nanotubes in Electrospun Polymer Nanofibers," Nanotechnology, vol.18, pp.1-8, 2007.
112. Junbo Gao, Aiping Yu, Mikhail E.Itkis and et al, "Large-scale Fabrication of Aligned Single-walled Carbon Nanotube Array and Hierarchical Single-walled Carbon Nanotube Assembly," J.AM.CHEM.SOC, vol.126, pp.16698-16699, 2004.
113. Isaias Ramirez, Edward A.Cherney, Shesha Jayaram and Mario Gauthier “Nanofilled Silicone Dielectrics Prepared with Surfactant for Outdoor Insulation Applications,” IEEE Transactions on Dielectrics and Electrical Insulation, vol.15, no.1, pp.228-235, 2008.
114. M.F. Frechette and C.W. Reed, “The Emerging Field of Nanodielectrics: an Annotated Appreciation," Conference Record of the 2006 IEEE International Symposium on Electrical Insulation, pp.458-465, 2006.
115. J.F.Dexter , P.C.Servais, “Silicone rubber as cable insulation”, Dow Corning Coporation, Midland, Michigan,pp.1-28,1967.

116. Michele Preghenella, Alessandro Pegoretti, and Claudio Migliaresi, “Thermo-mechanical characterization of fumed silica-epoxy nanocomposites," Polymer, vol.46, pp.12065-12072, 2005.
117. Shahzada Ahmad, H.B.Bohidar, Sharif Ahmad, and S.A.Agnihotry,” Role of fumed silica on ion conduction and rheology in nanocomposite polymeric electrolytes," Polymer, vol.47, pp.3583-3590, 2006.
118. H.Cochrane, C.S. Lin, “Influence of fumed silica properties on the processing, curing, and reinforcement of properties of silicone rubber,” Rubber Chem Technol, vol.66, pp.48-60, 1993.
119. M.J. Wang, “Effect of polymer-filled and filler-filler interactions on dynamic properties of filled vulcanizates,” Rubber Chem Technol, pp.520-520, 1998.
120. Maria Nargiello-Tetreault, Applications Manager/ Degussa Corp. "Successful Use of Fumed Silica in Liquid Systems," October 1, 2001.
121. Chidchanok Mituppatham, Manit Nithitanakul, Pitt Supaphol,” Ultrafine Electrospun Polyamide-6 Fibers: Effect of Solution Conditions on Morphology and Average Fiber Diameter," Macromolecular Chemistry and Physics, vol.205, no.17, pp.2327-2338, 2004.
122. Silke Megelski, Jean S. Stephens, D.Bruce Chase, and John F.Rabolt, “Micro-and nanostructured Surface Morphology on Eletrospun Polymer Fibers”, Macromolecules, vo.35, pp.8456-8466, 2002.
123. Seeram Ramakrishna, Kazutoshi Fujihara, Wee-Eong Teo, Teik-Cheng Lim, Zuwei Ma, “An Introduction to Electrospinning and Nanofibers," World Scientific Publishing Company, 2005.
124. ASTM D2240-05, "Standard test method for rubber property – durometer hardness," 2005.
125. ASTM D1708-6a, "Standard test method for tensile properties of plastics by use of microtensile specimens," 2006.
126. R.S.Gorur, E.A.Cherney, R.Hackam, “The AC and DC Performance of Polymeric Insulating Materials under Accelerated Aging in A Fog Chamber,” IEEE Transactions on Power Delivery, vol.3, no.4,1988..
127. J.Culham, P.Teertstra, I. Savija, and M. M. Yovanovich, "Design, assembly and commissioning of a test apparatus for characterizing thermal interface materials," Thermal and Thermomechanical Phenomena in Electronic Systems, 2002. ITHERM 2002. The Eighth Intersociety Conference, pp. 128-135, 2002.
128. Luiz H.Meyer, Shesha Jayaram, and Edward Cherney, " A Novel Technique to Evaluate the Erosion Resistance of Silicone Rubber Composites for High Voltage Outdoor Insulation Using Infrared laser Erosion," IEEE Transactions on Dielectrics and Electrical insulation, vol.12, no.6,2005.
129. ASTM D2302-97, “Standard Test Methods for Liquid-Contaminant, Inclined-Plane Tracking and Erosion of Insulating Materials”, 1997.
130. IEC 60343 “Recommended test methods for determining the relative resistance of insulating materials to breakdown by surface discharges," 1991-01.
131. P.Karayacoubian, M.M. Yovanovich, J.R.Culham, “Thermal Resistance-Based Bounds for the Effective Conductivity of Composite Thermal Interface Materials," 2006 Semiconductor Thermal Measurement and Management Symposium, pp.28-36, 2006.
132. N.Araki, D.W.Tang, A.Makino, M.Hashimoto, and T.Sano, “Transient Characteristics of Thermal Conduction in Dispersed Composites," International journal of Thermophysics, vol.19, no.4, pp. 1239-1251, 1998.

133. M. Barmar, M. Barikani, and M. Fereidounnia, “Study of Polyurethane / Clay Nanocomposites Produced via Melt Intercalation Method”, Iranian Polymer J., Vol.15, Vol. 9, pp.709-714, 2006.
134. Silicones for Textile Coating Product Overview, Wacker Chemie AG.
135. Ian Molynesux, Sina Ebnesajad, “Environmental Aspects of PTFE Based Laminates inRelation to “Halogen-Free”," pp.1-15, 2003.
136. Maged A.Osman, Ayman Atallah, Thomas Schweizer and Hans, “Particle-particle and particle-matrix interactions in calcite filled high-density polyethylene-steady shear,” Journal of Rheology, vol.48, no.5, pp.1167-1184, 2004.
137. T. B. Lewis, L. E. Nielsen “Viscosity of Dispersed and aggregated suspension of sphere," Journal of Rheology, vol.12, no.3, pp.421-443, 1968.
138. Lawrence E. Nielsen “Dynamic mechanical properties of polymers filled with agglomerated particles,” Journal of Polymer Science: Polymer Physics Edition, vol.17, no.11, pp.1897-1901, 1979.
139. Eun-Sung Lee, Sang-Mock Lee, “ Enhanced Thermal Conductivity of Polymer Materix Composite via High Solids Loading of Aluminum Nitride in Epoxy Resin,” Journal of the American Ceramic Society, vol.91,no.4, pp.1169-1174, 2008.
140. Avinash Baji, Yiu-Wing Mai, Shing-Chung Wong, Mojtaba Abtahi, Pei Chen, “ Electrospinning of polymer nanofibers: effects on oriented morphology, structures and tensile properties,” Composites Science and Technology, vol.70,pp.703-718,2010.
141. Y.Dror, W.Salalha, R.L.Khalfin, Y.Cohen,A.L.Yarin, E.Zussman, “Carbon nanotubes embedded in oriented polymer nanofibers by electrospinning,” Langmuir, vol.19,no.1, pp.7012–7020, 2003
142. Shouliang Yi, Yi Su, Yinhua Wan, “Preparation and characterization of vinyltriethoxysilane (VTES) modified silicate-1/PDMS hybrid pervaporation membrane and its application in ethanol separation from dilute aqueous solution,” Journal of Membrane Science, vol.360, pp.341-351,2010.
143. Anusuya Choudhury, Anil K. Bhowmick, Christopher Ong, Matthias Soddemann “Effect of Various Nanofillers on Thermal Stability and Degradation Kinetics of Polymer Nanocomposites," Journal of Nanoscience and Nanotechnology, vol.10, pp.5056-501, 2010.
144. Salhan C.Jana, Sachin Jain, “Dispersion of nanofillers in high performance polymers using reactive solvents as processing aids,” Polymer, vol.42, pp.6897-6905, 2001.
145. Isaias Ramirez Vázquez, “A Study of Nanofilled Silicone Dielectrics for Outdoor Insulation,” PhD Thesis, University of Waterloo, 2009.
146. T.K.Jayasree, P.Predeep, “ Effect of fillers on Mechanical Properties of Dynamically Crosslinked Styrene Butadiene Rubber/High Density Polyethylene Blends,” Journal of Elastomers and Plastics, vol.40, pp.127-146,2008.
147. S.Kumagai,Xinsheng Wang and N.Yoshimura, “ Solid Residue Formation of RTV Silicone Rubber due to Dry-band Arcing and Thermal Decomposition,” IEEE Transactions on Dielectrics and Electrical Insulation, vol.5, no.2, pp.281-289,1998.
148. A Krivda, F.Greuter, J.Rocks, X.Kornmann, P.Meier, “Chemical analysis of outdoor silicone materials after electrical and environmental testing,” 2006 Annual report conference on electrical insulation and dielectric phenomena, pp.389-392,2006.

Appendix A

Table A 1: Characteristics of Some Commonly Used Nanofillers in the Literature.

Filler	Commercial available Nanofiller Size (nm)	Shape	Permittivity	Thermal Conductivity (W/mK)	Features	Expected property improvements in the Composites
Silica (SiO_2)	Natural Nanosilica: 10 Fumed Nanosilica: 5-50	Sphere	3.7-5.4	1.5-1.6 3	Good abrasion resistance, electrical insulation and high thermal stability	Heat resistance, partial discharge & corona, electrical field grading
Barium Titanate ($BaTiO_3$)	25-110	Sphere	1250-10000	6.2	High relative permittivity	Dielectric properties, electrical field grading, storage capacity
Titanium Dioxide (TiO_2)	5-250	Sphere	83-173	1.8-11.7	High relative permittivity	Dielectric properties, electrical field grading, Storage capacity
Aluminum (Al)	10-100	Sphere	--	237-250	Good corrosion resistance, high relative permittivity, high thermal conductivity	Dielectric properties, thermal properties
Boron Nitride (BN)	Diameter × Length: 40-50nm × 0.5 μm 10-100	Tube Sphere	4.1	29-33	Super hard, superior thermal and chemical stability ,high electric breakdown strength, low relative permittivity, high thermal conductivity	Thermal conductivity, thermal stability, hardness
Aluminum oxide/ Alumina (Al_2O_3)	40nm-254nm	Sphere	9.3-11.5	30	High thermal conductivity resistance to weathering	Thermal properties
Carbon Nanotubes (CNTs)	Diameter × Length: 1.1-50nm × 0.5-100 μm	Tube	13.2-14.7	1800 - 6000	Strong tensile strength and hardness, flexibility and best heat-conducting material	Thermal and electric conductivity, reinforcement of polymers

Table A2: Characteristics of Some Commonly Used Dielectric Materials.

Base Polymer	Classification	Permittivity (Room Temperature)	Thermal Conductivity (W/mK)	Characteristics
Silicone rubber (SiR)	Elastomers	2.7-3.1	0.17-0.26	Good dielectric properties, maintaining their properties in a very wide temperature range, excellent resistance to ozone and corona discharge, good chemical and oil resistance
Epoxy resin (ER)	Thermoset	3.5-3.9	0.17-0.21	Good chemical and heat resistance, excellent mechanical properties, very good electrical insulating properties
Poly(methyl methacrylate) (PMMA)	Thermoplastic	3-3.5	0.18-0.2	Good impact strength, good environmental stability ,high coefficient of thermal expansion, good dimensional stability
Polypropylene (PP)	Thermoplastic	2.2-2.28	0.12 -0.22	High stiffness, good resistance to fatigue, good tensile strength

Appendix B

The dispersed composites are considered to be the stacking of many 3D cubes with spheres in the centre to represent the filler, based on the model, suggested by Karayacoubian et al. [131], and Araki et al. [132] , as shown in Figure B.1.

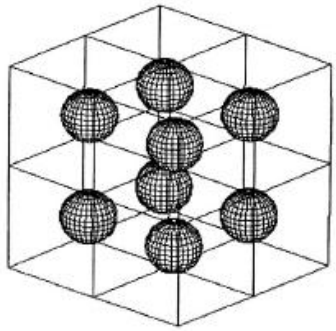

Figure B.1: The 3D cell model of the dispersed composites [131].

To analyze the effect of the filler size and filler dispersion on the local temperature distribution of the composites, a simple thermal model is employed under stationary condition. The simulated filler size is 5 μm and 500 nm in diameter, respectively, to reduce the calculation time by the computer. For the 5 μm SiO_2 (density 2.65 g/cm^3) filler, assuming it is spherical the volume is 65.45 μm^3. For 30 wt% (16.3 % by volume fraction) of microsilica-filled composite, each square cell's side is 7.4 μm, as show in Figure 2.10 (a). For the 500 nm SiO_2 (density 2.2 g/cm^3) filler, each filler sphere has a volume of 0.06545 μm^3, 5 wt% (2.79 % by volume fraction) of nanosilica-filled composite, and each square cell has 1.3 μm sides. Therefore, the volume of 6x6x6 cubic cells of nanosilica that stacked together is approximately equal to that volume of one square cell of microsilica. The 2D cross-sections of the two models which are obtained from the middle of the 3D models are as shown in Figure B.2 (b). In order to save the computational time, those simple 2D models are used just for a comparison purpose.

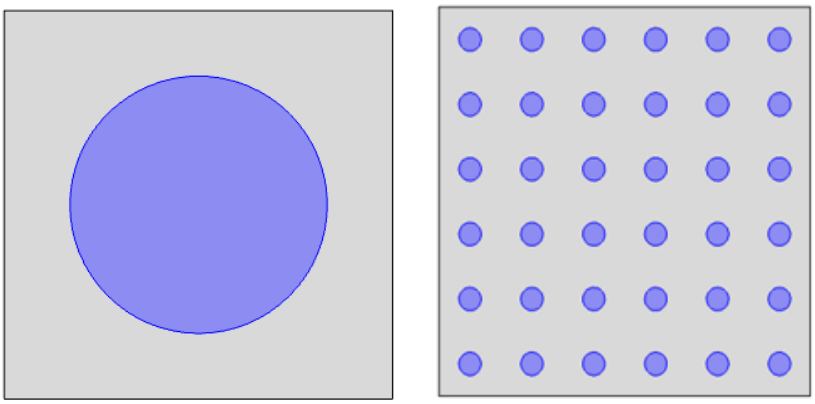

(a) (b)

Figure B.2: The simple 2D model of the dispersed composites: (a) the middle cross-section one cubic cell of the microsilica filler, and (b) the middle cross-section of 6 × 6 × 6 cubic cells of the nanosilica filler in the same volume size as in (a).

If the filler and polymer matrix are isotropic, the boundaries, parallel to the "Y" axis, are thermally insulated, and the other two boundaries are isothermal. Heat travels from the top to the bottom. The boundary conditions can be set easily in the heat transfer module of COMSOL. Figure B.3 shows the temperature distribution in the unfilled SiR square cell, 30 wt% microsilica-filled square cell and 5 wt% nanosilica-filled square cell. All of the squares have the same size in terms of the size of 30 wt% microsilica-filled cell. As shown in Figure B.3 (b) and (c), the temperature is more uniform when the filler size is small and distributed evenly.

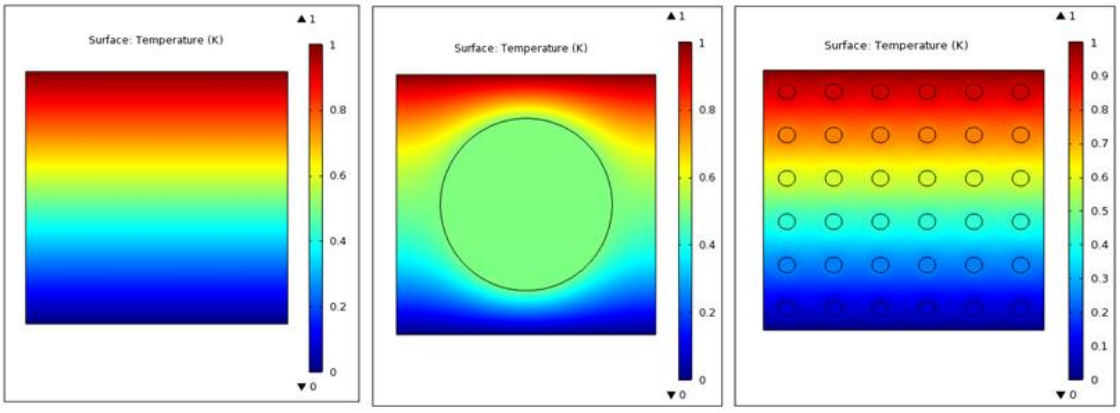

(a) (b) (c)

Figure B.3: The temperature distribution in the 2D square cell (a) unfilled SiR cell, (b) 30 wt% microsilica-filled SiR cell , and (c) 5 wt% nanosilica-filled SiR cell.

Above different square cells of dispersed composites are stacked separately to construct a 50 × 100 μm 2D sample. The boundaries that parallel to the "Y" axis are thermally insulated, and the other two boundaries are open boundaries. A point heat source was used to simulate the laser source and applied in the same position for all models.

A contact power 2 W is applied to the model to simulate as a laser power and COMSOL can calculate the heat flux that passes through the defined area. The temperature on the surface is found by calculating:

$$\rho C_p \nabla T + \nabla \cdot (-k\nabla T) = Q/A \quad \text{(B.1)}$$

where ρ is the material density, C_p is the heat capacity, k is the thermal conductivity, and Q is the heat source, A is the heat area. The equation is solved by using the FEM technique with COMSOL software. The results were shown in Figure 3.8 and Figure 3.9.